Final Report for AOARD Grant 114008

Fabrication Processes and Mechanical Properties of CNT/Metal Nanocomposites

Dec. 1, 2013

Name of Principal Investigators (PI and Co-PIs): Soon H. Hong

- e-mail address : shhong@kaist.ac.kr
- Institution : Korea Advanced Institute of Science and Technology
- Mailing Address : 291 Daehak-ro, Yuseong-gu, Daejeon 305-701, Republic of Korea
- Phone : +82-42-350-3327
- Fax : +82-42-350-3310

Period of Performance : 12/6/2010 – 12/5/2013

Report Documentation Page

Form Approved
OMB No. 0704-0188

1. REPORT DATE	2. REPORT TYPE	3. DATES COVERED
16 DEC 2013	**Final**	**12-12-2010 to 05-12-2013**

4. TITLE AND SUBTITLE
Fabrication Processes and Mechanical Behavior of CNT/Metal Nanocomposites

5a. CONTRACT NUMBER
FA23861114008

5b. GRANT NUMBER

5c. PROGRAM ELEMENT NUMBER

6. AUTHOR(S)
Soon Hyung Hong

5d. PROJECT NUMBER

5e. TASK NUMBER

5f. WORK UNIT NUMBER

7. PERFORMING ORGANIZATION NAME(S) AND ADDRESS(ES)
Korean Advanced Institute of Science and Technology,335 Gwahangro, Yusung-Gu,Daejeon 305-701,Korea,KR,305-701

8. PERFORMING ORGANIZATION REPORT NUMBER
N/A

9. SPONSORING/MONITORING AGENCY NAME(S) AND ADDRESS(ES)
AOARD, UNIT 45002, APO, AP, 96338-5002

10. SPONSOR/MONITOR'S ACRONYM(S)
AOARD

11. SPONSOR/MONITOR'S REPORT NUMBER(S)
AOARD-114008

12. DISTRIBUTION/AVAILABILITY STATEMENT
Approved for public release; distribution unlimited

13. SUPPLEMENTARY NOTES

14. ABSTRACT

A novel process for fabrication of CNT/Metal nanocomposites, named as ?molecular level mixing process?, was developed and applied to various metallic matrices of Cu, Ni, NiTi and Al-Cu. Mechanical properties of CNT/Metal nanocomposites were characterized to understand the relationships between microstructure and mechanical behavior, and to analyse the strengthening mechanisms of CNT/Metal nanocomposites. The molecular level mixing process is based on accurately controlled molecular chemistry in order to solve key issues of the homogeneous dispersion of carbon nanotubes with strong interfacial bonding with the matrices.

15. SUBJECT TERMS
composite materials, CNT/metal nanocomposites

16. SECURITY CLASSIFICATION OF:			17. LIMITATION OF ABSTRACT	18. NUMBER OF PAGES	19a. NAME OF RESPONSIBLE PERSON
a. REPORT	b. ABSTRACT	c. THIS PAGE			
unclassified	**unclassified**	**unclassified**	**Same as Report (SAR)**	**111**	

Abstract

A novel process for fabrication of CNT/Metal nanocomposites, named as "molecular level mixing process", was developed and applied to various metallic matrices of Cu, Ni, NiTi and Al-Cu. Mechanical properties of CNT/Metal nanocomposites were characterized to understand the relationships between microstructure and mechanical behavior, and to analyse the strengthening mechanisms of CNT/Metal nanocomposites. The molecular level mixing process is based on accurately controlled molecular chemistry in order to solve key issues of the homogeneous dispersion of carbon nanotubes with strong interfacial bonding with the matrices.

In the 1st & 2nd year, a novel fabrication process, i.e. the molecular level mixing process, were investigated and applied for fabrication of CNT/Cu and CNT/Ni nanocomposite powders. The spark plasma sintering process was applied to consolidate the powders and to fabricate the CNT/Cu and CNT/Ni nanocomposites. It is observed that the CNTs were homogenously dispersed in Cu or Ni matrices of the CNT/Metal nanocomposites fabricated by the molecular level mixing process. The mechanical properties and microstructures of the CNT/Cu and CNT/Ni nanocomposites were investigated. CNT/Cu and CNT/Ni nanocomposites showed outstanding mechanical properties of 200-300% increase of yield strength and 50-70% increase of Young's modulus, compared to unreinforced Cu or Ni. Then, the effect of CNTs on the mechanical behavior and strengthening mechanisms was analyzed.

In the 3rd year, a new fabrication processes combining molecular level mixing process and high energy milling process had been investigated for the fabrication of CNT/NiTi and CNT/Al-Cu nanocomposites. The CNT/NiTi and CNT/Al-Cu nanocomposite powders were fabricated by the molecular level mixing process and followed by the high energy milling process. Then, the nanocomposite powders were consolidated by spark plasma sintering process to fabricate CNT/NiTi and CNT/Al-Cu nanocomposites. It is confirmed that the CNTs were homogeneously dispersed in NiTi and Al-Cu alloy matrices of CNT/NiTi and CNT/Al-Cu nanocomposites. The CNT/NiTi and CNT/Al-Cu nanocomposites showed good mechanical properties of 30-100 % increase of yield strength and 15-30% increase of Young's modulus, compared to unreinforced NiTi and Al-Cu. The effects of CNTs on the mechanical behavior and their strengthening mechanisms have been analyzed for the CNT/NiTi and CNT/Al-Cu nanocomposites.

1. Introduction

1-1. Background of Research

The carbon nanotube (CNT), which was discovered by S. Ijima in 1991, has been subjected to significant attention to many researchers due to promising properties as composite reinforcement. Among the many attractive properties of CNTs, the mechanical properties are superior to any other types of known conventional reinforcements. The high aspect ratio of CNTs is suitable for reinforcement of composite, because of large surface area and enhanced load transfer efficiency. Although various approaches were made to fabricate high strength CNT/Metal nanocomposites, most of the results were below expectations due to strong agglomeration of CNTs and poor interfacial bonding between CNTs and metal matrices.

In the 1st year of research, a novel fabrication process, named molecular level mixing process, and consolidation processes of CNT/Cu and CNT/Ni nanocomposite powders were investigated. The phases, morphologies, distribution and interfaces were characterized for the CNT/Cu and CNT/Ni nanocomposite powders and sintered nanocomposites. The CNT/Metal nanocomposite powders were successfully fabricated and sintered into the nanocomposites in which CNTs were homogeneously dispersed throughout the metal matrix.

In the 2nd year of research, the mechanical properties of CNT/Cu and CNT/Ni nanocomposites were characterized. The CNTs in the nanocomposites showed an outstanding reinforcing effect in CNT/Cu and CNT/Ni nanocomposites. The strengthening mechanisms of CNTs in the metal matrix had been quantitatively analyzed. CNT/NiTi nanocomposite powder had been fabricated to expand the properties and applications of CNT/Metal nanocomposites. Fabrication processes, microstructures and fundamental properties of CNT/NiTi nanocomposite powders had been characterized.

In the 3rd year of research, a new fabrication process, i.e. molecular level mixing and high energy milling process, for fabrication of CNT/NiTi and CNT/Al-Cu nanocomposites were investigated. The microstructure and mechanical properties were characterized for the nanocomposite powders and sintered CNT/NiTi and CNT/Al-Cu nanocomposites. It has been identified that CNT also shows strong reinforcing effect in NiTi and Al-Cu alloy matrices. This final report is focused on the research contents of the 3rd year of research.

1-2. Objectives and Contents of Research

The final objective of research is to develop fabrication processes of CNT/Metal nanocomposites, in which carbon nanotubes are homogeneously dispersed in metal matrices, and to investigate the mechanical behavior and strengthening mechanisms. This research is expected to establish a fundamental technology for the development of multi-functional CNT/Metal nanocomposites having high strength/modulus/conductivity for advanced aerospace structural & functional materials.

In the 3rd year of research, the objective is focused on development of a new fabrication process, i.e. molecular level mixing and high energy milling process, and understanding of mechanical properties of CNT/NiTi and CNT/Al-Cu nanocomposites. Detail contents of research for the 3rd year contract are summarized as follows.

- Fabrication processes of CNT/NiTi nanocomposite
  - Fabrication process and characterization of CNT/NiTi nanocomposite by using CNT/Ni nanocomposite powder
  - Fabrication process and characterization of CNT/NiTi nanocomposite by using CNT/SiO_2 nanocomposite powder
  - Fabrication process and characterization of CNT/NiTi nanocomposite by using CNT/TiO_2 nanocomposite powder
  - Fabrication process and characterization of CNT/NiTi nanocomposite by using pristine CNTs
  - Analysis of mechanical behavior and strengthening mechanism of CNT/NiTi nanocomposite

- Fabrication processes and characterization of CNT/Al-Cu nanocomposites
  - Fabrication processes and characterization of CNT/Al-Cu nanocomposite powder
  - Consolidation processes and characterization of CNT/Al-Cu nanocomposite
  - Characterization of microstructures and mechanical properties of CNT/Al-Cu nanocomposite
  - Analysis of mechanical behavior and strengthening mechanism of CNT/Al-Cu nanocomposite

3. Results of 3rd Year Research

As a result of 1st year and 2nd year researches, the molecular level mixing process for CNT/Cu and CNT/Ni nanocomposites was developed and accomplished optimized nanocomposite microstructures which show a homogeneous distribution of nano-sized reinforcement in metal matrix. Additionally, the effect of CNTs as reinforcement on metal matrix composites has been analyzed based on the characterization of microstructures and mechanical properties. It had been concluded that CNT acted as excellent reinforcement in the Cu and Ni matrix, forming strong interfacial bonding with metal matrix. In the 3rd year research, metal matrix was extended to alloy matrices which are NiTi and Al-Cu matrix. The new fabrication processes, which is molecular level mixing process combined with high energy milling process, were investigated to fabricate CNT/NiTi and CNT/Al-Cu nanocomposites. The microstructures and mechanical properties of CNT/NiTi and CNT/Al-Cu nanocomposites were characterized.

3-1. Fabrication processes and characterization of CNT/NiTi nanocomposite

In fabricating CNT/NiTi nanocomposite, CNTs need to remain undamaged during the fabrication process for effective strengthening effect as reinforcement in nanocomposite. However, CNTs consisting of carbon atoms could react with Ti, and results in a formation of TiC phase. The effect of CNT coating has been investigated to control the unwanted severe reaction between CNT and Ti. In this research, three different materials of Ni, SiO_2 and TiO_2 were coated on the CNTs for fabrication of CNT/NiTi nanocomposites, and their properties were compared with the uncoated pristine CNT/NiTi nanocomposite.

3-1-1. CNT/NiTi nanocomposite fabricated by using CNT/Ni nanocomposite powders

3-1-1-1. Fabrication process of CNT/NiTi nanocomposite by using CNT/Ni nanocomposite powder

CNT/NiTi nanocomposite powders were fabricated by mixing of Ti powders, NiTi powders and CNT/Ni nanocomposite powders which were prepared by molecular level mixing process in the 2nd year research as can be seen in Figure 1-1. The CNT/NiTi composite powders were consolidated by spark plasma sintering (SPS, Dr. Sinter Lab., Sumitomo). The CNT/NiTi nanocomposite powders were heated up to 1000°C and maintained for 5 mins in a vacuum of 10^{-3} torr under a pressure of 50 MPa. The heating rate was 100°C/min to sintering

temperature. Figure 1-2 shows the sintering behavior of CNT/NiTi nanocomposite powders by spark plasma sintering process. With increasing temperature, displacement increases and increase of displacement was stopped over 850^{o}C. Subsequently, displacement starts to decrease because of full densification and thermal expansion of consolidated nanocomposite. Photograph in Figure 1-2 shows button type of CNT/NiTi nanocomposite consolidated by spark plasma sintering process. The relative density of CNT/NiTi nanocomposite is 99.3 %.

3-1-1-2. Phase analysis of CNT/NiTi nanocomposite fabricated by using CNT/Ni nanocomposite powder

XRD result of CNT/NiTi nanocomposite fabricated by using CNT/Ni nanocomposite powders is shown in Figure 1-3. As can be seen in Figure 1-3, phases in the CNT/NiTi nanocomposite consist of NiTi, Ti_2Ni, Ni_4Ti_3 and TiC. In order for CNTs to show their reinforcing effect, CNTs shouldn't react with other elements. So, the CNT/Ni nanocomposite powder in which Ni layer was coated on the CNTs was used to fabricate CNT/NiTi nanocomposite. However, although nickel was coated onto CNT in the CNT/Ni nanocomposite powder, the TiC was formed. It indicates that Ni layer on the CNTs can't act as a barrier for the reaction between CNTs and Ti. In addition, Ni_4Ti_3 phase which doesn't exist in the NiTi was formed in the CNT/NiTi nanocomposite. Surrounding of CNT is Ni-rich region due to Ni coating layer. Ni_4Ti_3 phase is a Ni-rich phase to be generated from reaction between Ni layer on CNTs and Ti. Ni_4Ti_3 phase is a brittle phase, so it is expected that brittleness of CNT/NiTi nanocomposite is increased.

3-1-1-3. Mechanical properties of CNT/NiTi nanocomposite fabricated by using CNT/Ni nanocomposite powder

Figure 1-4 shows the stress-strain curves of NiTi and 1vol.% CNT/NiTi fabricated by using CNT/Ni nanocomposite powder. The mechanical properties such as elastic modulus, yield strength, ultimate tensile strength and elongation to fracture are presented in the Table 1-1. The elastic modulus and yield strength were improved. The elastic modulus of 1vol.% CNT/NiTi nanocomposite is 76 GPa, which is 25 % higher than that of NiTi. In addition, the 1 vol.% CNT/NiTi nanocomposite shows 259 MPa, which is 71.5 % higher than that of NiTi. On the other hand, ultimate tensile strength and elongation were decreased. The ultimate tensile strength of 1vol.% CNT/NiTi nanocomposite is decreased by 42 %, compared than that of NiTi. Also, elongation is decreased from 11.2 % to 2.5 %. In general, commercialized

NiTi shape memory alloy is deformed and then return to original shape by heating up to 6 % of strain. Therefore, elongation of CNT/NiTi nanocomposite should be higher than 6 % in order to characterize shape memory properties.

The reduction of elongation is mainly from Ni_4Ti_3 phase formed by reaction between Ni layers on CNT in CNT/Ni nanocomposite powders. Although CNTs were homogeneously dispersed in the CNT/NiTi nanocomposite powders by adding CNT/Ni nanocomposite powder in the NiTi matrix instead of pristine CNTs, reaction between Ni layer on CNT and Ti formed Ni_4Ti_3 phase, which is brittle phase. Additionally, Ni layer on CNT can't prevent CNT from reacting with Ti, resulting in decrement of reinforcing effect of CNTs.

Therefore, coating layer on CNT is needed to change into other layer such as ceramic layer. CNTs were coated by SiO_2 and TiO_2. Fabrication process of SiO_2-coated CNT and TiO_2-coated CNT was studied and CNT/NiTi nanocomposite was produced by adding SiO_2-coated CNT and TiO_2-coated CNT. Then, properties of CNT/NiTi nanocomposite were characterized.

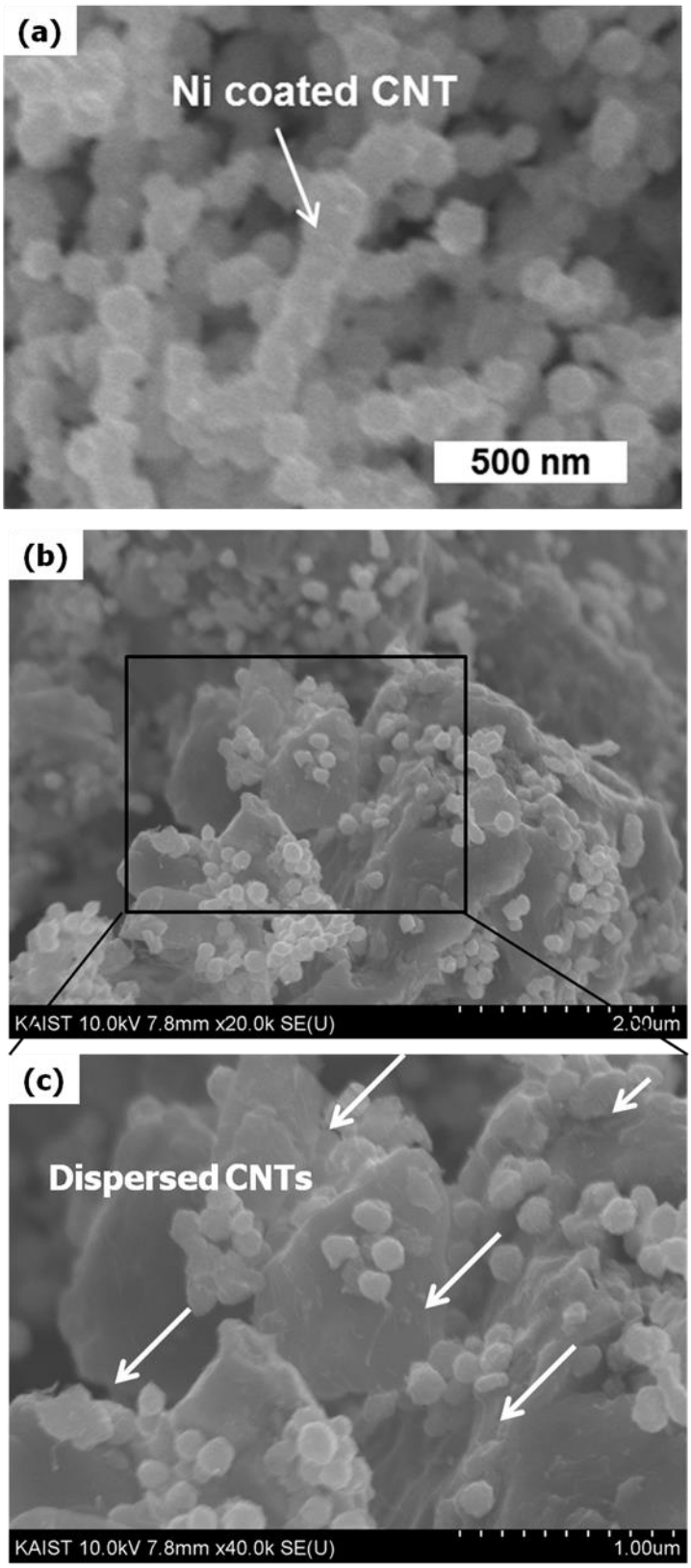

Figure 1-1. Microstructures of CNT/Ni and CNT/NiTi nanocomposite powders by molecular level mixing and high energy milling. (a) CNT/Ni, (b) CNT/NiTi at low magnification, (c) high magnification

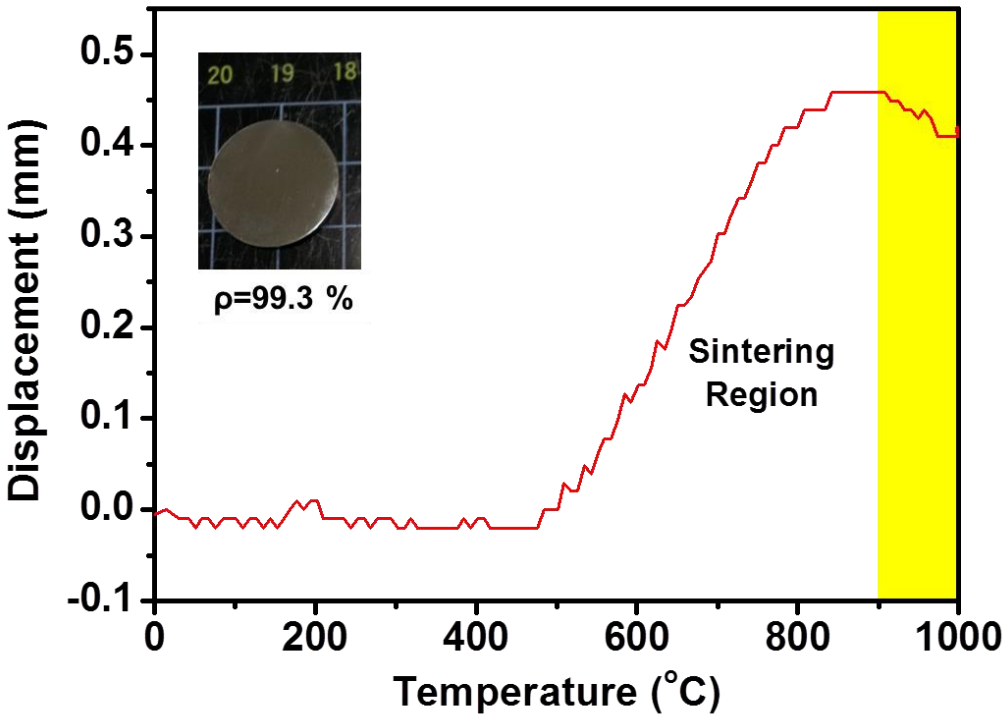

Figure 1-2. Sintering behavior of CNT/NiTi nanocomposite powders fabricated by using CNT/Ni nanocomposite powders by spark plasma sintering process

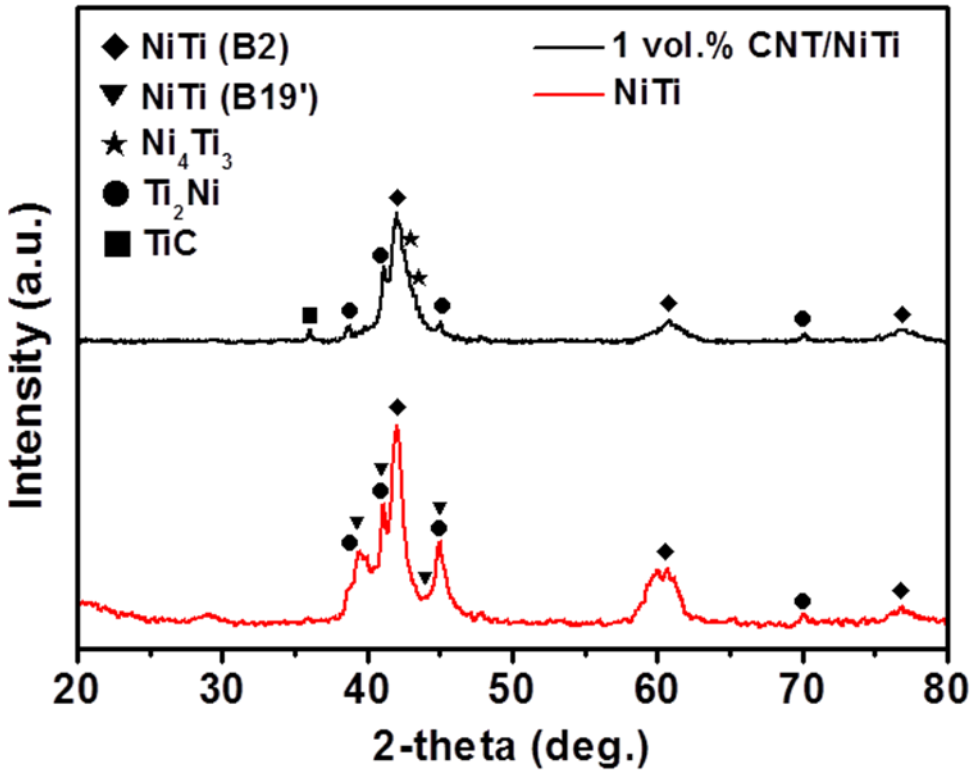

Figure 1-3. XRD pattern of CNT/NiTi nanocomposite fabricated by using CNT/Ni nanocomposite powders

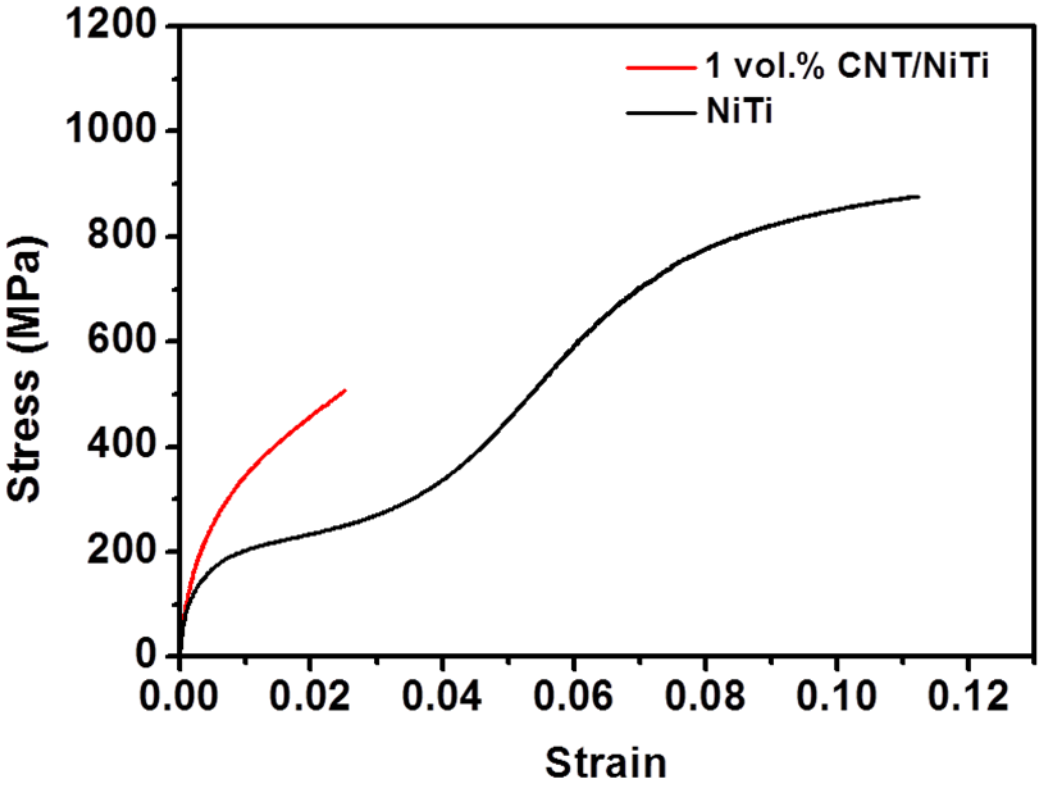

Figure 1-4. Stress-strain curve of NiTi and CNT/NiTi nanocomposite fabricated by using CNT/Ni nanocomposite powders

	E.M. (GPa)	Y.S. (MPa)	U.T.S (MPa)	Elongation (%)
NiTi	61	151	876	11.2
1 vol.% CNT/NiTi	76 (25 %↑)	259 (71.5 %↑)	506 (42 %↓)	2.5 (77 %↓)

Table 1-1. Mechanical properties of NiTi and CNT/NiTi fabricated by using CNT/Ni nanocomposite powder

3-1-2. CNT/NiTi nanocomposite fabricated by using CNT/SiO_2 nanocomposite powder

3-1-2-1. Fabrication process of CNT/SiO_2 nanocomposite powder by sol-gel process

1) Functionalization of CNTs by acid treatment

Multi-walled carbon nanotubes (Hanwha Nanotech Corporation.), with diameters of 10-15 nm, length of 10-20 μm (Figure 1-7 (a)), and fabricated by thermal chemical vapor deposition, were functionalized by acid treatment. The CNTs were sonicated for 5 hours in a HCl for purification CNTs from metal catalyst and vacuum filtered. The purified CNTs were sonicated for 10 hours in a mixed solution of H_2SO_4 (95 %, Junsei extra pure grade)/HNO_3 (60 %, Junsei extra pure grade) in a 3:1 ratio for in achieving functionalization mainly with carboxylic groups. The functionalized CNTs were centrifuged and filtered with distilled water until the pH reached 7 and then they were finally dried in vacuum at 100 ℃. Figure shows the morphology of CNTs after functionalization by acid treatment. The length of CNTs was reduced to 1-2 μm due to damage during acid treatment. The schematic diagram for functionalization of CNTs by acid treatment is shown in Figure 1-5.

2) Fabrication process and microstructure of CNT/SiO_2 nanocomposite powder

Functionalized CNTs were dispersed in ethanol by sonication. With magnetic stirring (500 rpm), TEOS (Tetraethyl orthosilicate – $Si(OR)_4$, R=C_2H_5) was added in drops in the CNT dispersed ethanol solution. Then, water and then NH_4OH was dropped. The solution was heated to 70°C and maintained for 6 hrs. The SiO_2 layer was formed on CNTs by the reaction as follows:

$$Si(OR)_4 + 2H_2O \rightarrow SiO_2 + 4\ ROH,\ (R=C_2H_5)$$

After that, the solution was washed and dried, followed by heat treatment at 300°C for 1 hr. The schematic diagram for coating of CNTs by SiO_2 is shown in Figure 1-6. Microstructure of CNT/SiO_2 nanocomposite powder was presented in Figure 1-7 (b) and (c). CNTs are uniformly coated by SiO_2. The thickness of SiO_2 coating layer on CNTs is 15-20 nm.

3-1-2-2. Fabrication process of CNT/NiTi nanocomposite by using CNT/SiO_2 nanocomposite powder

The CNT/NiTi nanocomposite was prepared by using CNT/SiO_2 nanocomposite powders, nickel powder (Kojundo chemical Laboratory Co. Ltd., 99.9 % purity) with average particle size of 2-3 μm and titanium powder (Kojundo chemical Laboratory Co. Ltd., 99.9 % purity)

with average particle size of 38 μm as starting materials (Figure 1-8). These powders are high-energy ball-milled to fabricate CNT/NiTi nanocomposite powder by using a planetary ball mill (Fritsch GmbH, Pulverisette 5) under Ar atmosphere for 2 hours with 100 rpm of rotation speed. The ball to powder ratio was 12:1 and balls with 8 mm of diameter were used. Chemical compositions (at.%) were designed as 50Ni-50Ti. Subsequently, the CNT/NiTi nanocomposite powder was consolidated by spark plasma sintering process. The spark plasma sintering process was conducted at 900°C for 5 min with a pressure of 50 MPa in a vacuum of 10^{-3} torr. Heating rate was 100°C/min. Sintering behavior of CNT/NiTi nanocomposite fabricated by using CNT/SiO_2 nanocomposite powder is shown in Figure 1-9. With increasing temperature, the displacement increases and is stopped over 800°C due to full densification. An inset of Figure 1-9 is a photograph of button type of CNT/NiTi nanocomposite, showing 99.1 % of relative density.

3-1-2-3. Phase analysis of CNT/NiTi nanocomposite by using CNT/SiO_2 nanocomposite powder

XRD result of CNT/NiTi nanocomposite fabricated by using CNT/SiO_2 nanocomposite powder is shown in Figure 1-10. Phases in the CNT/NiTi nanocomposite fabricated by using CNT/SiO_2 nanocomposite powder are composed of $Ni_{16}Ti_6Si_7$ and TiC as well as NiTi. In particular, $Ni_{16}Ti_6Si_7$ is formed by reaction between SiO_2 and NiTi. In addition, TiC phase was formed by reaction of CNTs with Ti although SiO_2 layer was coated on CNTs. This indicates that the reaction of CNTs with Ti can't be blocked by SiO_2 layer.

3-1-2-4. Mechanical properties of CNT/NiTi nanocomposite fabricated by using CNT/SiO_2 nanocomposite powder

Figure 1-11 shows stress-strain curve of CNT/NiTi nanocomposite fabricated by using CNT/SiO_2 nanocomposite powder. As expected in the phase analysis (Figure 1-10), elongation of CNT/NiTi nanocomposite was 0.14 %, whereas NiTi shows 11.2 % of elongation. This is mainly caused by silicide phase ($Ni_{16}Ti_6Si_7$) which is a brittle phase. Because of brittle behavior, shape memory effect can't be characterized. Thus, another coating layer is needed not to degrade mechanical properties of CNT/NiTi nanocomposite. Required property of coating layer is not to react with NiTi matrix. TiO_2 coating layer is a candidate for the requirement. In following chapter, fabrication process of CNT/TiO_2 nanocomposite powder is studied and properties of CNT/NiTi nanocomposite fabricated by

using CNT/TiO_2 nanocomposite powder are investigated.

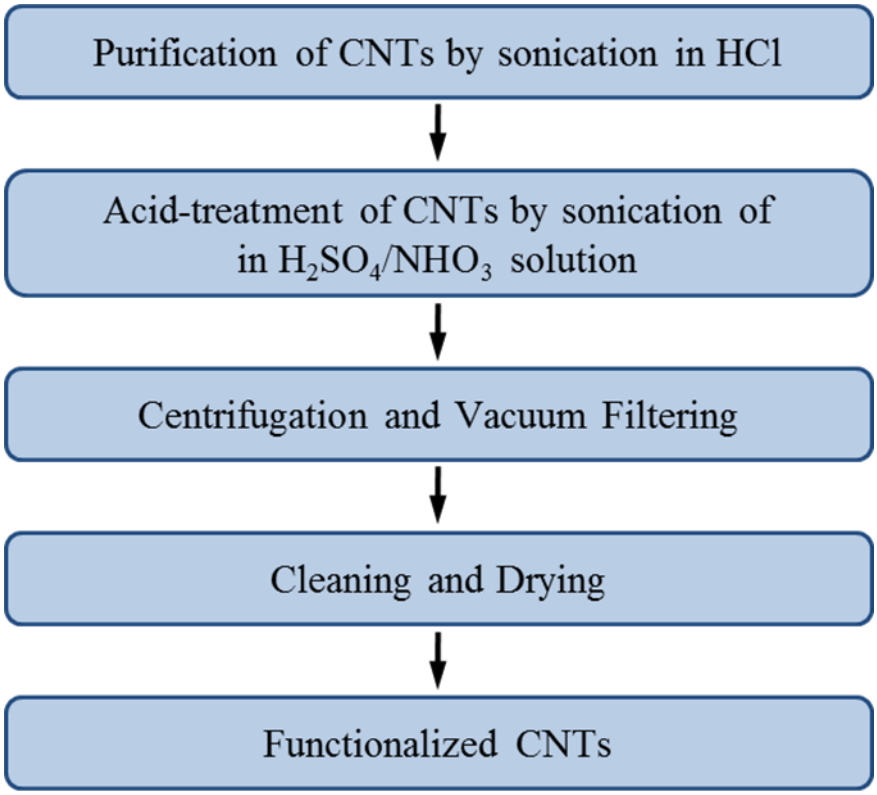

Figure 1-5. Schematic diagram for functionalization of CNTs by acid treatment.

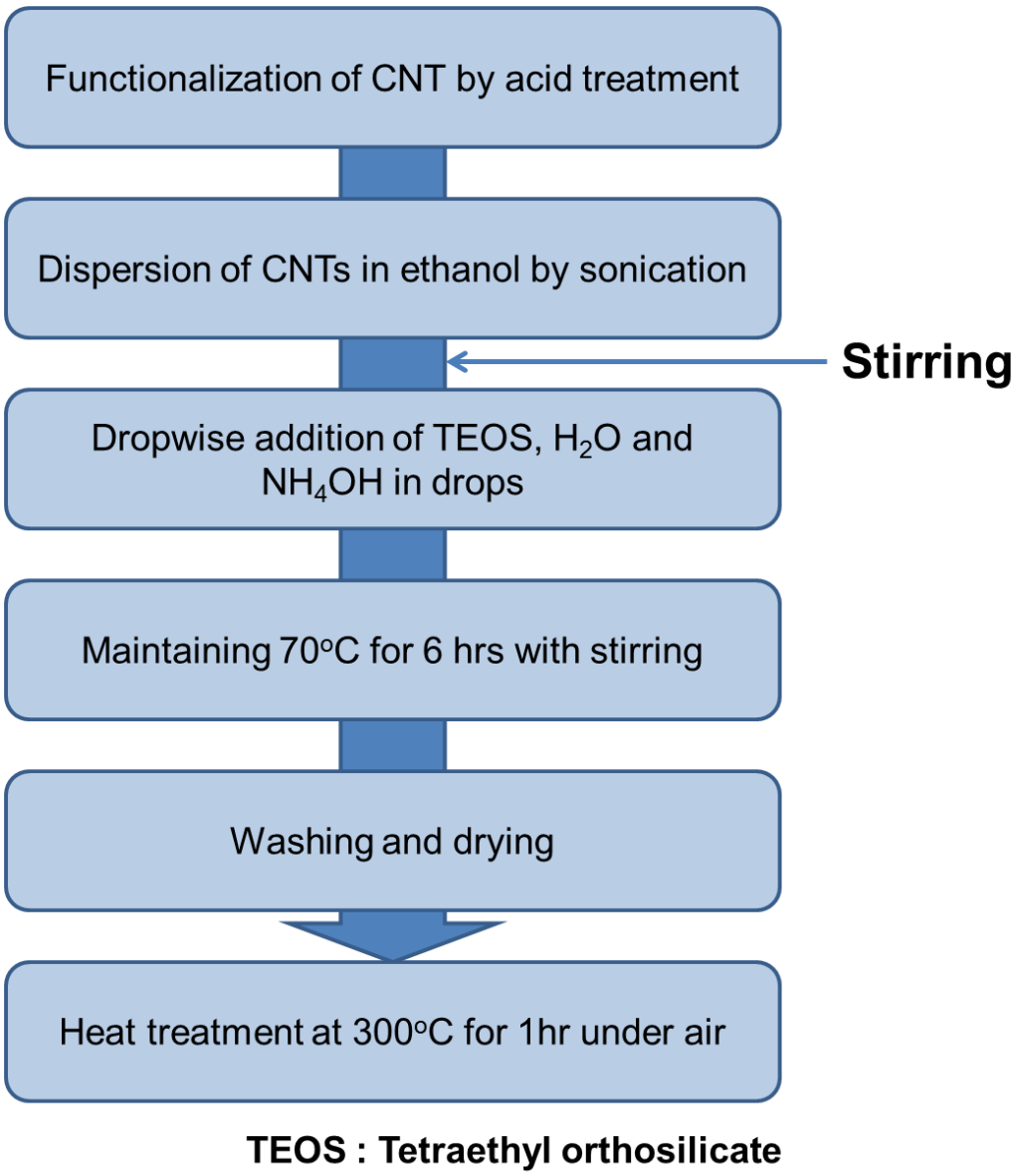

Figure 1-6. Schematic diagram for fabrication process of CNT/SiO_2 nanocomposite powder

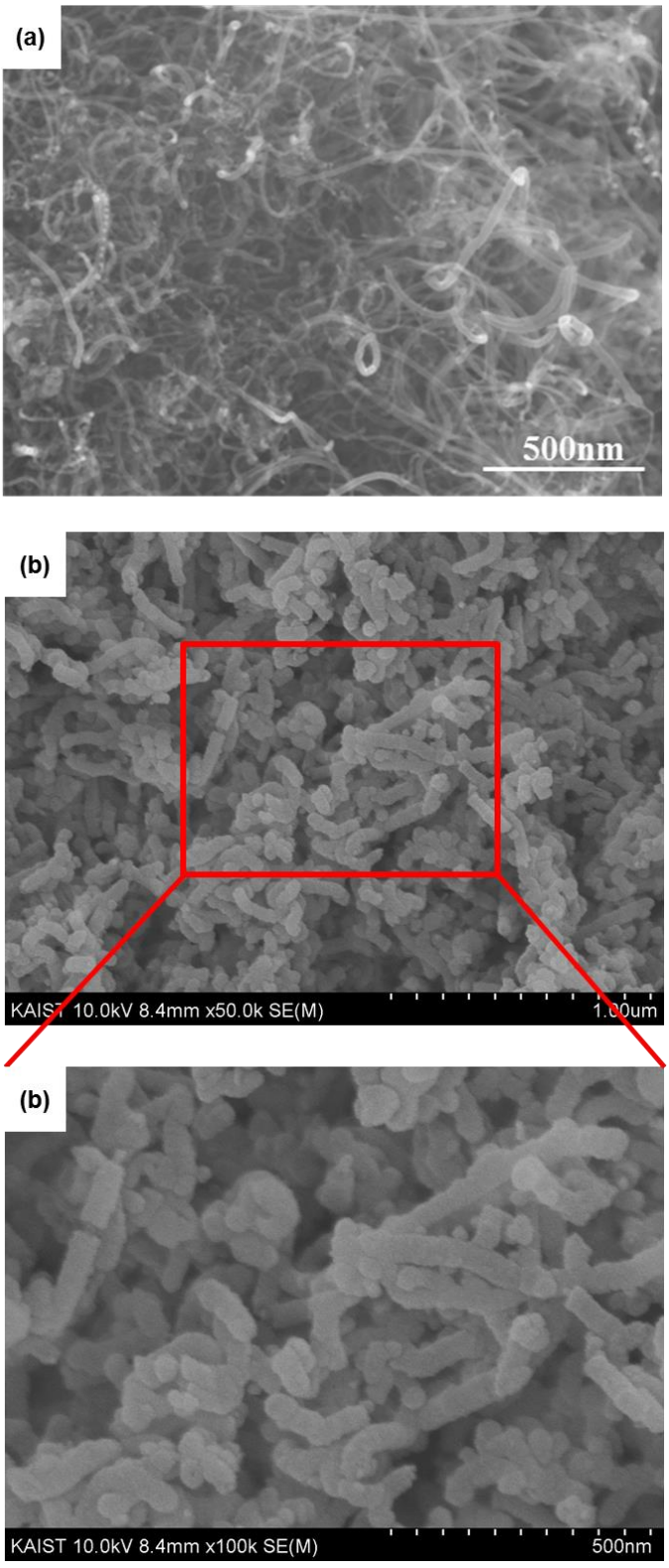

Figure 1-7. SEM micrographs of (a) pristine CNTs, (b) CNT/SiO_2 nanocomposite powder at low magnification and (c) high magnification

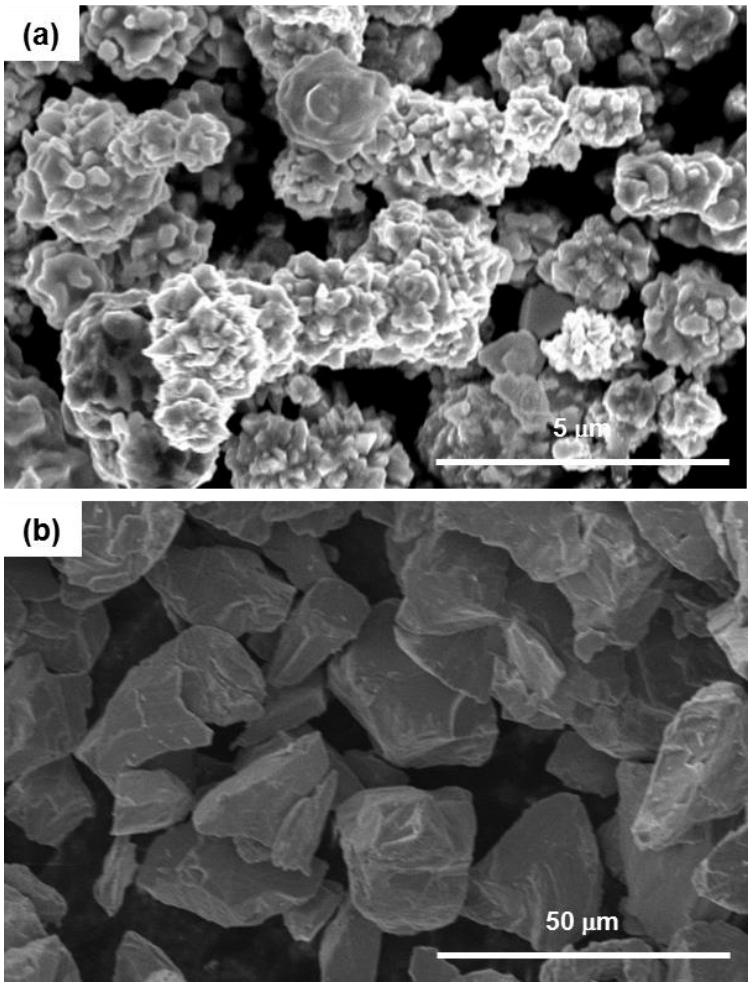

Figure 1-8. SEM micrographs of (a) Ni powder, (b) Ti powder

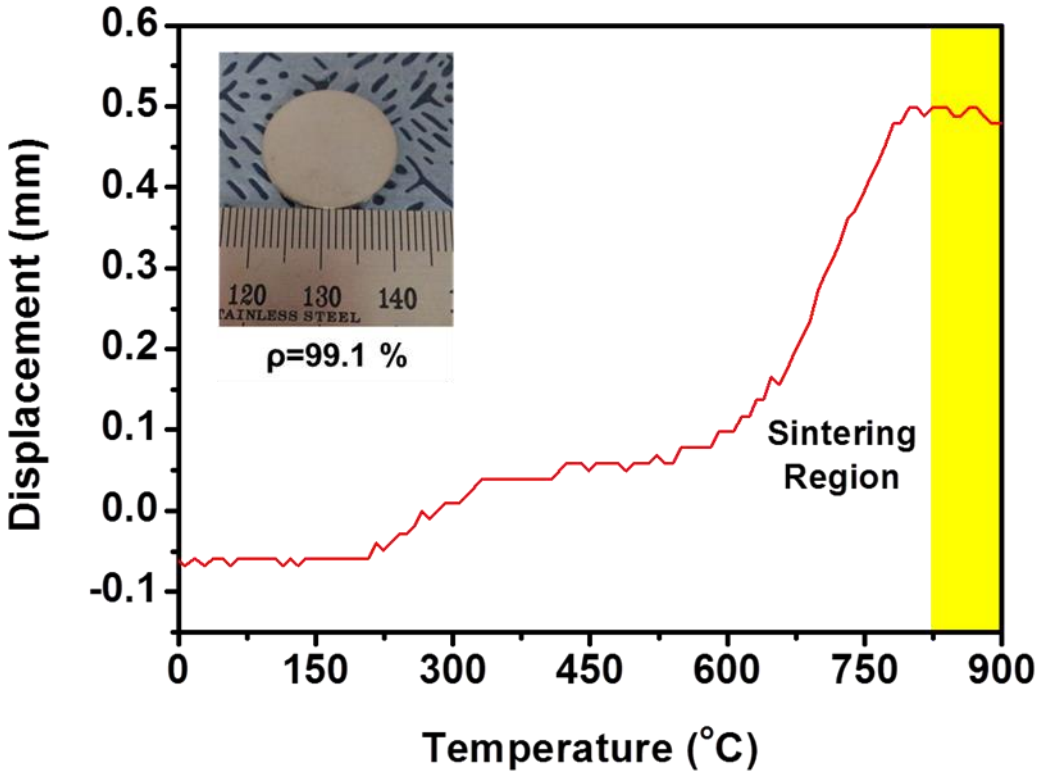

Figure 1-9. Sintering behavior of CNT/NiTi nanocomposite powders fabricated by using CNT/SiO_2 nanocomposite powder by spark plasma sintering process

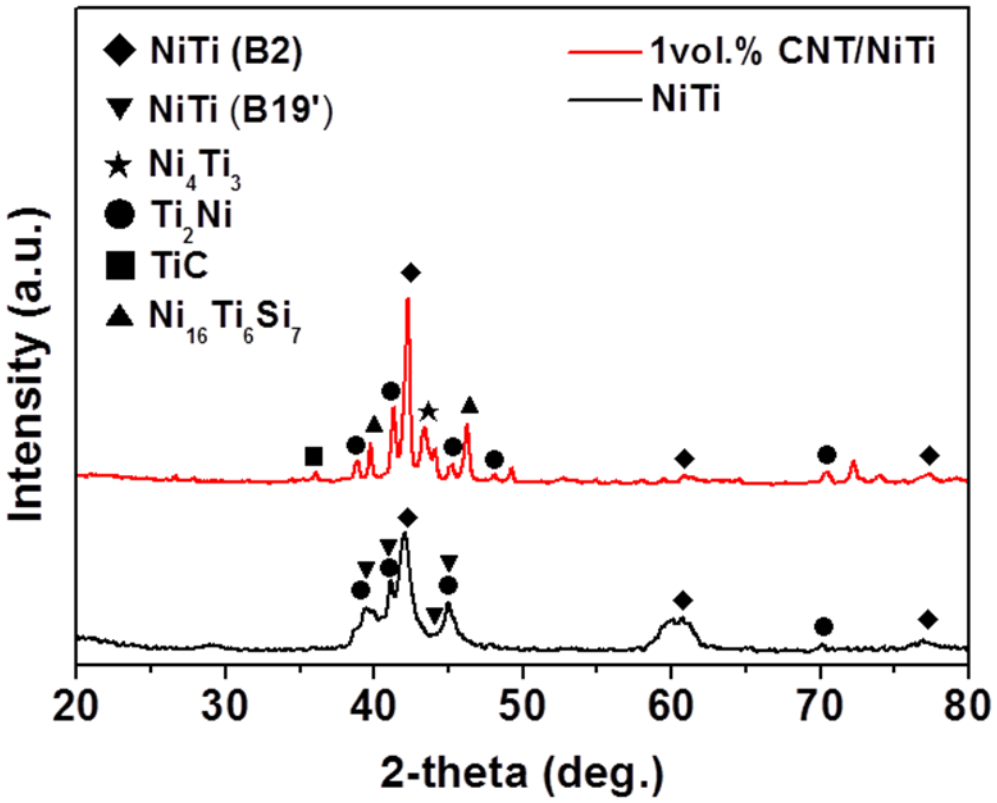

Figure 1-10. XRD pattern of CNT/NiTi nanocomposite fabricated by using CNT/SiO_2 nanocomposite powder

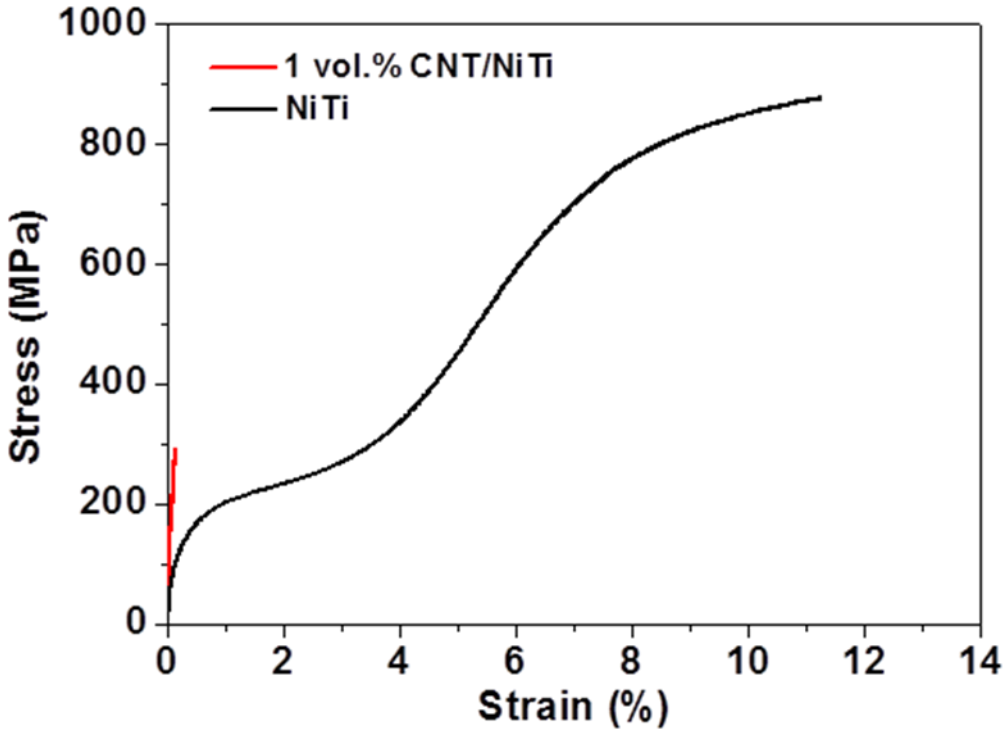

Figure 1-11. Stress-strain curve of CNT/NiTi nanocomposite fabricated by using CNT/SiO_2 nanocomposite powder

3-1-3. CNT/NiTi nanocomposite fabricated by using CNT/TiO_2 nanocomposite powder

3-1-3-1. Fabrication process of CNT/TiO_2 nanocomposite powder by sol-gel process

Functionalized CNTs by acid treatment were dispersed in ethanol by sonication. With magnetic stirring (500 rpm), TTIP (Titanium isopropoxide – $Ti\{OCH(CH_3)_2\}_4$) was added in drops in the CNT dispersed ethanol solution. Then, water was dropped in the solution. The solution was kept at room temperature for 6 hrs. The TiO2 layer was formed on CNTs by the reaction as follows:

$$Ti\{OCH(CH_3)_2\}_4 + 2\ H_2O \rightarrow TiO_2 + 4\ (CH_3)_2CHOH$$

After that, the solution was washed and dried, followed by heat treatment at 400°C for 1 hr under air. The schematic diagram for coating of CNTs by TiO_2 is shown in Figure 1-12. Microstructure of CNT/TiO_2 nanocomposite powder was presented in Figure 1-13 (a) and (b). CNTs are uniformly coated by TiO_2 with thickness of 10-15 nm. TiO_2 was well synthesized by coating process as can be seen in XRD result of CNT/TiO_2 nanocomposite powder of Figure 1-13 (c).

3-1-3-2. Fabrication process of CNT/NiTi nanocomposite by using CNT/TiO_2 nanocomposite powder

The CNT/NiTi nanocomposite was prepared by using CNT/TiO_2 nanocomposite powders, nickel powder (Kojundo chemical Laboratory Co. Ltd., 99.9 % purity) with average particle size of 2-3 μm and titanium powder (Kojundo chemical Laboratory Co. Ltd., 99.9 % purity) with average particle size of 38 μm as starting materials (Figure 1-8). These powders are high-energy ball-milled to fabricate CNT/NiTi nanocomposite powder by using a planetary ball mill (Fritsch GmbH, Pulverisette 5). The ball to powder ratio was 12:1 and balls with 8 mm of diameter were used. High energy milling process was performed under Ar atmosphere for 2 hours with 100 rpm of rotation speed. Chemical compositions (at.%) were designed as 50Ni-50Ti. Subsequently, the CNT/NiTi nanocomposite powder was consolidated by spark plasma sintering process. The spark plasma sintering process was conducted at 900°C for 5 min with a pressure of 50 MPa in a vacuum of 10^{-3} torr. Heating rate was 100°C/min. Sintering behavior of CNT/NiTi nanocomposite fabricated by using CNT/TiO2 is shown in Figure 1-14. With increasing temperature, the displacement increases and is stopped over 750°C due to full densification. Then, the displacement decreases because of thermal expansion. An inset of Figure 1-14 is a photograph of button type of CNT/NiTi

nanocomposite, showing 99.2 % of relative density.

3-1-3-3. Phase analysis of CNT/NiTi nanocomposite fabricated by using CNT/TiO_2 nanocomposite powder

Figure 1-15 shows XRD result of CNT/NiTi nanocomposite by using CNT/TiO_2 nanocomposite powder. Similar to XRD result of NiTi, phases in CNT/NiTi nanocomposite include NiTi and Ti_2Ni. In addition, reaction of CNT with Ti occurred, resulting in formation of TiC. Objective to coat TiO_2 layer on CNT was to prevent CNT from reacting with Ti. However, TiO_2 layer didn't inhibit the reaction of CNT with Ti.

3-1-3-4. Mechanical properties of CNT/NiTi nanocomposite fabricated by using CNT/TiO_2 nanocomposite powder

Stress-strain curve of CNT/NiTi nanocomposite fabricated by using CNT/TiO_2 nanocomposite powder is presented in Figure 1-16. The yield strength, elastic modulus and ultimate tensile strength of CNT/NiTi nanocomposite are shown in Table 1-2. The elastic modulus and yield strength of CNT/NiTi nanocomposite are enhanced by 52 % and 45 % respectively, compared to those of NiTi. On the other hand, ultimate tensile strength was decreased by 11 % and elongation was reduced from 11.2 % to 4.9 % by adding CNT/TiO_2 nanocomposite powder in NiTi. Elongation was highly reduced since TiO_2 in CNT/TiO_2 nanocomposite was added in the NiTi.

In summary, when coated CNTs were applied in fabrication of CNT/NiTi nanocomposite, the elongation was highly decreased due to reaction of coating layer and NiTi matrix, so characterization of shape memory properties were not possible. Ni-rich phase (Ni_4Ti_3) and silicide ($Ni_{16}Ti_6Si_7$) phase were formed when CNT/Ni and CNT/SiO_2 nanocomposite powders were used, respectively. Thus, TiO_2 coated CNTs were applied to fabricate CNT/NiTi nanocomposite. However, TiO2 layer couldn't prevent CNTs from reacting with Ti and reduced the elongation of CNT/NiTi nanocomposite to 4.9 %, which is lower than 6 %. As a result, pristine CNTs without any coating layer are appropriate for reinforcement in NiTi matrix. In next chapter, CNT/NiTi nanocomposite fabricated by using pristine CNT was prepared and then microstructure, phases, phase transformation behavior and mechanical properties of CNT/NiTi nanocomposite were characterized.

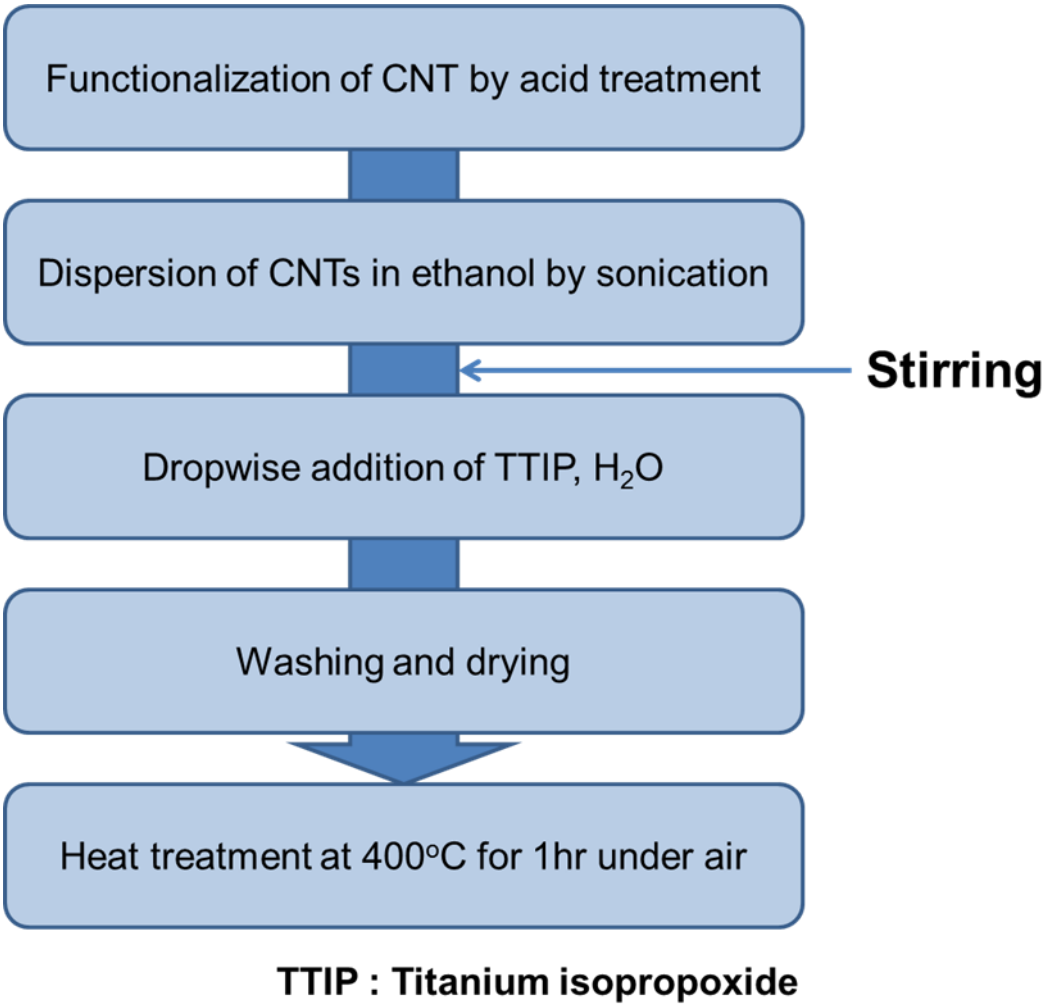

Figure 1-12. Schematic diagram for fabrication process of CNT/TiO_2 nanocomposite powder

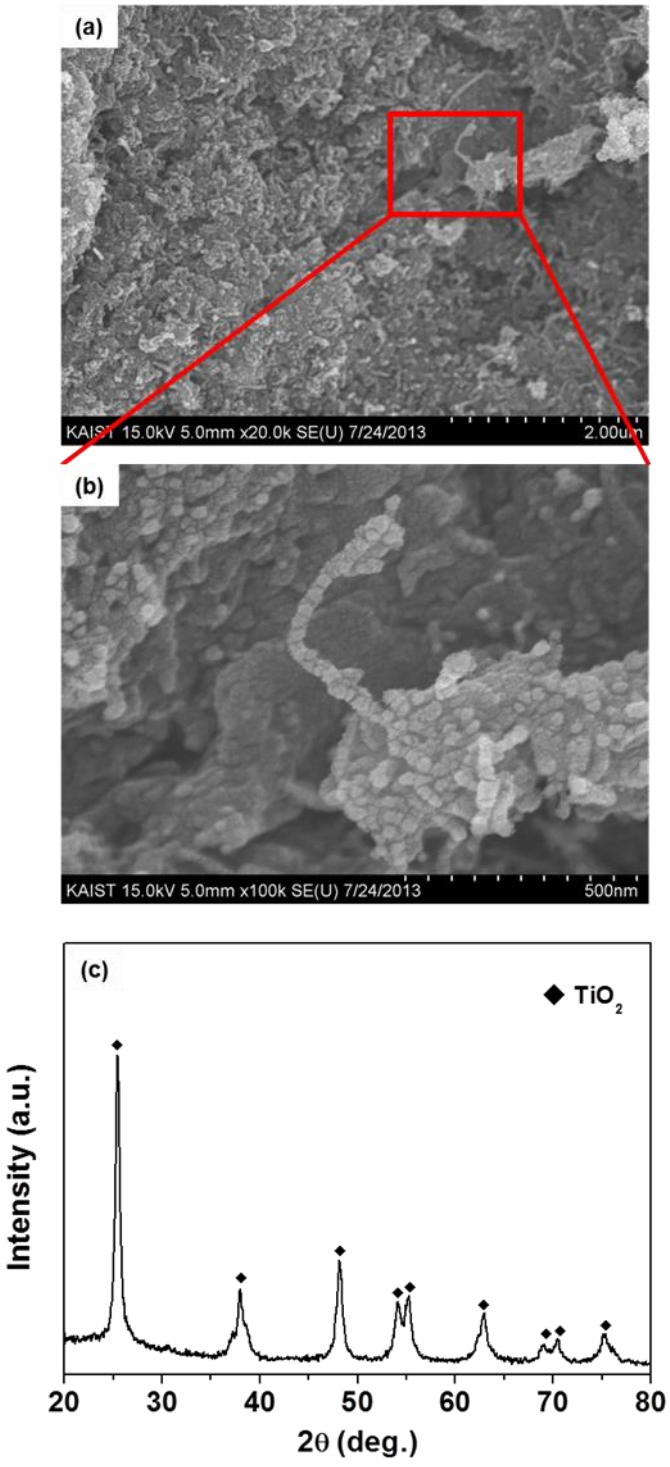

Figure 1-13. SEM micrographs of CNT/TiO_2 nanocomposite powder at (a) low magnification, (b) high magnification and (c) XRD result of CNT/TiO_2 nanocomposite powder

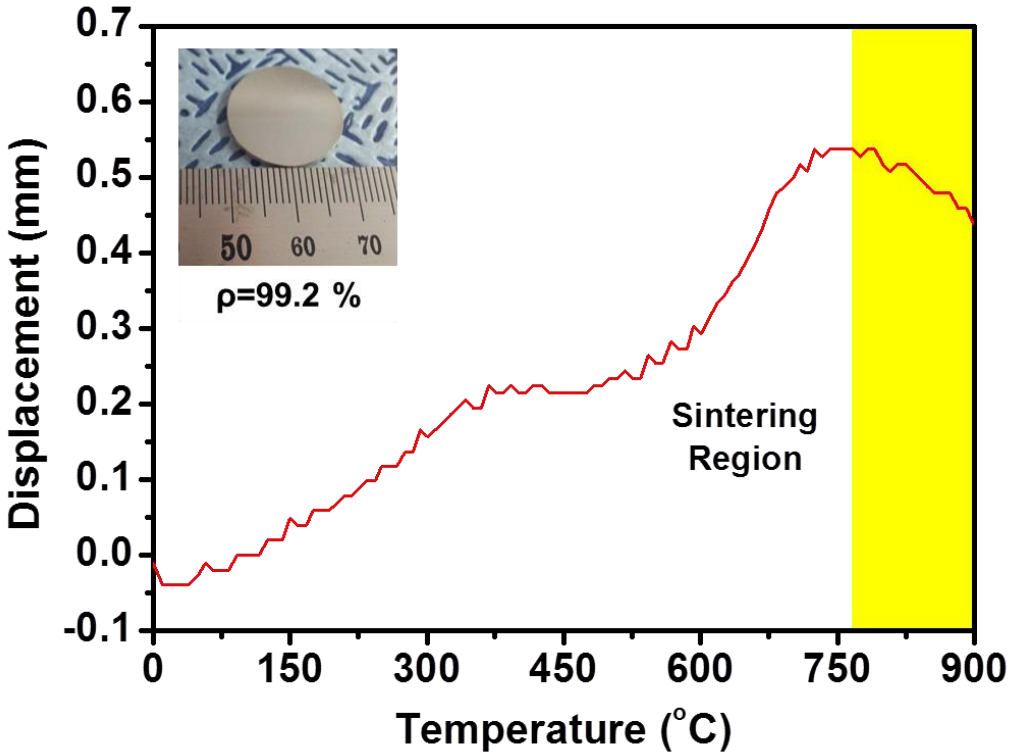

Figure 1-14. Sintering behavior of CNT/NiTi nanocomposite powders fabricated by using CNT/TiO_2 nanocomposite powder by spark plasma sintering process

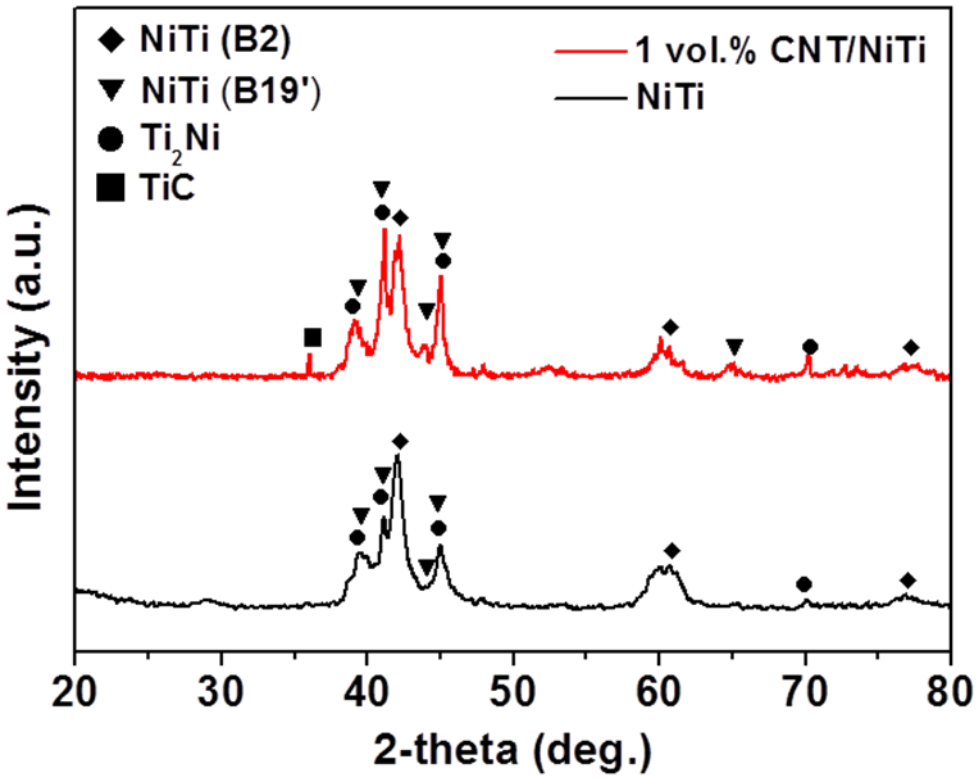

Figure 1-15. XRD pattern of CNT/NiTi nanocomposite fabricated by using CNT/TiO_2 nanocomposite powder

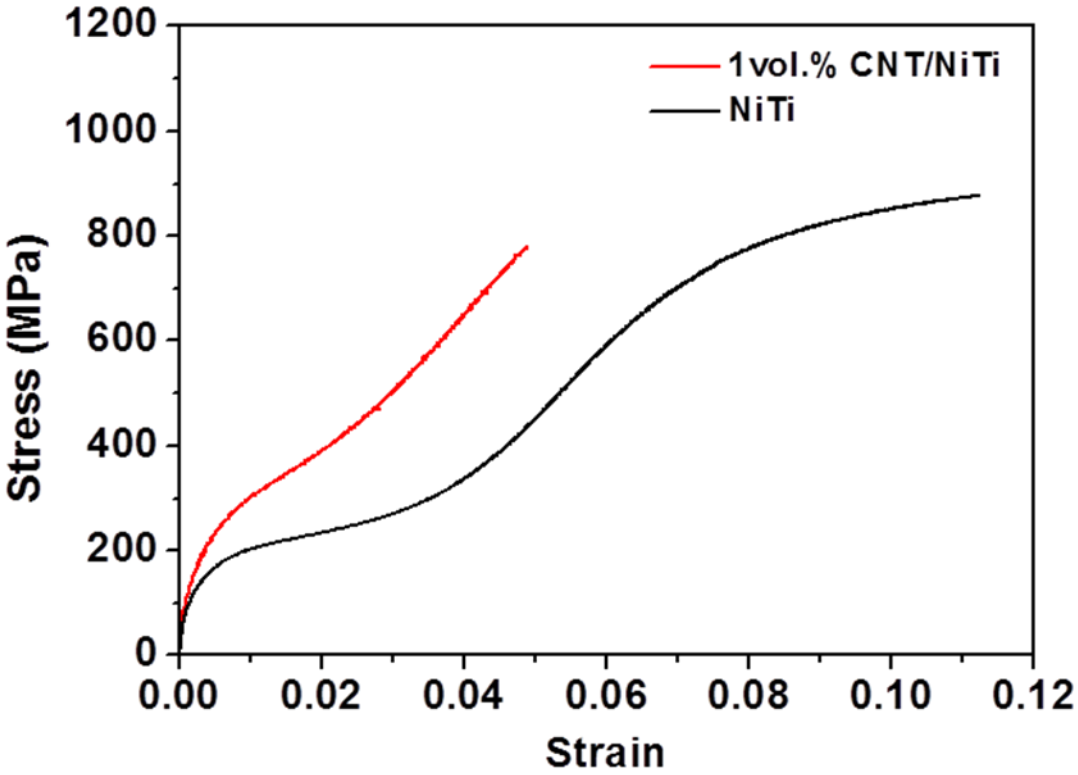

Figure 1-16. Stress-strain curves of NiTi and 1vol.% CNT/NiTi nanocomposite fabricated by using CNT/TiO_2 nanocomposite powder

	E.M. (GPa)	Y.S. (MPa)	U.T.S (MPa)	Elongation (%)
NiTi	61	151	876	11.2
1 vol.% CNT/NiTi	93 (52 %↑)	219 (45 %↑)	778 (11 %↓)	4.9 (56 %↓)

Table 1-2. Mechanical properties of NiTi and CNT/NiTi fabricated by using CNT/TiO_2 nanocomposite powder

3-1-4. CNT/NiTi nanocomposite fabricated by using pristine CNT

3-1-4-1. Fabrication process of CNT/NiTi nanocomposite powder by using pristine CNT

CNT/NiTi nanocomposites powders were fabricated by high energy ball milling process. Nickel powder with average particle size of 2-3 um, titanium powder with particle size under 38 um, CNT with diameter of 10-15 nm and length of 10-20 um were used as starting materials (Figure 1-17). The Ni, Ti powders and CNT powders were high-energy ball-milled to prepare CNT/NiTi nanocomposite powder by using a planetary ball mill (Fritsch GmbH, Pulverisette 5) for 2 hours with 100 rpm of rotation speed and 12:1 of ball to powder ratio under Ar atmosphere. Chemical compositions (at.%) were designed as 50Ni-50Ti. For the high-energy ball milling, steel balls with 8 mm of diameter were used. For comparison with properties of CNT/NiTi nanocomposite, TiC/NiTi composite was also fabricated by using TiC powder with average particle size of 2-3 μm (Figure 1-17 (d)) instead of CNT through same processes above mentioned.

Figure 1-18 shows morphology of CNT/NiTi nanocomposite powder and TiC/NiTi composite powder. As can be seen in the Figure 1-18(a), CNTs in 0.5 vol.% CNT/NiTi nanocomposite powders are homogeneously dispersed in the NiTi powders. When volume ratio of CNTs increases to one, some agglomerated CNTs in NiTi powder were found as shown in Figure 1-18 (b). In TiC/NiTi composite powder, TiC particles were uniformly dispersed as indicated in Figure 1-18 (c)

3-1-4-2. Fabrication process and microstructure of CNT/NiTi nanocomposite by spark plasma sintering

The CNT/NiTi nanocomposite powders were consolidated by spark plasma sintering at 900^{o}C for 5 min with a pressure of 50 MPa in a vacuum of 10^{-3} torr. Heating rate up to sintering temperature was 100^{o}C/min. Figure 1-19 (a) shows the sintering behavior of CNT/NiTi nanocomposite powders by spark plasma sintering process. As temperature increases, displacement increases which means that powders are being sintered in the mold and over 680^{o}C increase of displacement is stopped and displacement start to decrease because of full densification and thermal expansion of nanocomposites. The sintering behavior of TiC/NiTi composite powders was the same as that of CNT/NiTi nanocomposite powders as can be seen in Figure 1-19 (b). Figure 1-20 shows button type of NiTi, CNT/NiTi nanocomposite and TiC/NiTi nanocomposite consolidated by spark plasma sintering. The

relative density of CNT/NiTi nanocomposite and TiC/NiTi nanocomposite with contents is shown in Table 1-3. Relative density of all the specimens is above 99 %. Figure 1-21 shows microstructure of 0.5 vol.% CNT/NiTi nanocomposite. CNTs are survived and dispersed in the NiTi matrix as can be seen in Figure 1-21.

3-1-4-3. Phase analysis of CNT/NiTi nanocomposite fabricated by using pristine CNT

XRD patterns of NiTi, CNT/NiTi nanocomposite and TiC/NiTi composite are shown in Figure 1-22 (a). It can be seen that phases in NiTi, CNT/NiTi nanocomposite and TiC/NiTi composite include NiTi and Ti_2Ni. Ti_2Ni phase is thermodynamically favorable phase at the sintering temperature compared than NiTi as follows.

$Ni + 2Ti \rightarrow Ti_2Ni, \ \Delta G=-67$ kJ/mol

$Ni + Ti \rightarrow NiTi, \ \Delta G=-55.9$ kJ/mol

As a result, Ti_2Ni phase was formed during sintering process. Additionally, the diffraction peaks of TiC phase appeared in the XRD pattern of CNT/NiTi nanocomposite. This is originated from reaction of CNT with Ti powders during sintering process. It is considered that CNTs are carbon sources for the formation of TiC. As reaction of CNTs with Ti happened, CNT could be lost in the NiTi matrix, resulting in decrement of reinforcing effect of CNT. Figure 1-22 (b) shows intensity ratio of diffraction peak of TiC to that of NiTi. If 0.5 vol.% CNT reacts completely with Ti, 1vol.% TiC will be formed in NiTi matrix. As shown in the Figure 1-22 (b), intensity ratio of TiC to NiTi in the XRD pattern is lower in 0.5 vol.% CNT/NiTi nanocomposite than in 1 vol.% TiC/NiTi composite. Therefore, it is considered that CNTs was not completely reacted with Ti and CNTs exist in the NiTi matrix. Survived CNTs are expected to show reinforcing effect in the NiTi matrix.

3-1-4-4. Phase transformation behavior of CNT/NiTi nanocomposite fabricated by using pristine CNT

Figure 1-23 indicates the differential scanning calorimetry (DSC) curves of NiTi, CNT/NiTi nanocomposite and TiC/NiTi composite on heating and cooling. Phase transformation occurred in the NiTi, CNT/NiTi nanocomposite and TiC/NiTi composite on cooling and heating, so it is expected that they have shape memory effect which is caused by phase transformation. There is only one transformation peak in DSC curves of the NiTi, CNT/NiTi nanocomposite and TiC/NiTi composite on cooling and heating, i.e., B2→B19’ and

B19'→B2, respectively. The phase transformation temperatures and thermal hysteresis of NiTi and the composites are listed in Table 1-4. The thermal hysteresis is defined as difference between austenitic finish temperature (A_f) and martensitic start (M_s) temperature. The thermal hysteresis increases with the increase of CNT content and addition of TiC. It is considered that reinforcements in NiTi matrix act as barrier for the phase transformation, resulting in the increase of thermal hysteresis. This implies that recovery ratio of the composites will be decreased with the increase of reinforcements content.

3-1-4-5. Shape memory effect of CNT/NiTi nanocomposite fabricated by using pristine CNT

Shape memory tests were conducted by loading and unloading during tensile tests under M_f temperature, followed by heating above A_f temperature. The results of shape memory tests are presented in the Figure 1-24 and Table 1-5. The NiTi showed complete shape recovery when deformed by 3.5 % and then heated above A_f. In case of 0.5 vol.% CNT/NiTi nanocomposite, shape recovery ratio was 94 % when deformed by 3.6 % and then heated. Also, shape recovery ratio of 1 vol.% CNT/NiTi nanocomposite after deformation of 3.6 % was 90 %. With increase of CNT content, the shape recovery ratio was decreased. This reveals that CNTs act as barrier for the phase transformation, resulting in decrement of shape recovery ratio of CNT/NiTi nanocomposite. However, shape recovery ratio of CNT/NiTi nanocomposite was superior to that of TiC/NiTi nanocomposite. It can be said that larger reinforcement is a larger obstacle to phase transformation. Thus, in order to minimize decrement of shape recovery ratio, small size of reinforcement is preferred.

3-1-4-6. Mechanical properties of CNT/NiTi nanocomposite fabricated by using pristine CNT

Figure 1-25 shows the stress-strain curves of NiTi, CNT/NiTi nanocomposite and TiC/NiTi composite with content. The yield strength, elastic modulus and ultimate tensile strength of NiTi, CNT/NiTi nanocomposite and TiC/NiTi composite from the stress-strain curves are summarized in Table 1-6. The strength of composites was improved and elongation of them was decreased, compared to that of NiTi. The 0.5 vol.% CNT/NiTi nanocomposite shows yield strength of 192 MPa, which is 27 % higher than that of NiTi. Also, elastic modulus increases by 29 % (from 61 GPa to 79 GPa) and ultimate tensile strength increases from 876 MPa to 975 MPa. In the case of 1 vol.% CNT/NiTi nanocomposite, the yield strength is 185

MPa, which is 22.5 % higher than that of NiTi. Although content of CNT increases from 0.5 vol.% to 1 vol.%, the yield strength was decreased, which was originated from agglomerated CNTs observed in the 1vol.% CNT/NiTi nanocomposite powders as shown in Figure 1-18 (b). Due to the agglomerated CNTs, increase ratio of elastic modulus and ultimate tensile strength of the 1vol.% CNT/NiTi nanocomposite is less than those of 0.5 vol.% CNT/NiTi nanocomposite. The yield strength of 1 vol.% TiC/NiTi composite shows 177 MPa, which is 17 % higher than that of NiTi and the ultimate tensile strength increases from 876 MPa to 891 MPa. As a result, although CNTs were changed into TiC by reacting with Ti, enhancement of mechanical properties is much larger when the CNT was added in the NiTi matrix, compared than when the TiC was added in the NiTi matrix. This is due to survived CNT in the NiTi matrix as can be seen in the Figure 1-26, demonstrating that CNTs show superior reinforcing effect in the NiTi matrix.

Additionally, mechanical properties of uncoated pristine CNT/NiTi and coated CNT/NiTi nanocomposites were compared as shown in Table 1-7. When coated CNTs were applied in CNT/NiTi nanocomposite, yield strength and Young's modulus were much improved, compared to when uncoated pristine CNT were applied in CNT/NiTi nanocomposite. However, the elongation was severely reduced because the coating layers reacted with matrix and formed brittle phase such as Ni_4Ti_3 or silicide ($Ni_{16}Ti_6Si_7$) while the coating layers couldn't prevent CNTs from reacting with Ti. In order to characterize shape memory effect, elongation must be more than 6 %. As a result, uncoated pristine CNTs were appropriate to fabricate CNT/NiTi nanocomposite.

3-1-4-7. Analysis of mechanical behavior of CNT/NiTi nanocomposite fabricated by using pristine CNT

In the stress-strain curves of NiTi, CNT/NiTi nanocomposite and TiC/NiTi composite as shown in the Figure 1-25, all the samples show typical stress-strain curves of shape memory alloy showing double yield points on the curve. Typical stress-strain curve of shape memory alloy is separated by four parts as indicated in Figure 1-27. First part is elastic deformation of twinned martensite. After elastic deformation of twinned martensite, an initial plateau appears because twinned martensite change into detwinned martensite. Then, in the third part there is elastic deformation of detwinned martensite followed by a second yielding point. After second yielding point, plastic deformation of detwinned martensite occurs and the samples are fractured finally. As first yield strength is higher, it is more difficult for twinned

martensite to change into detwinned martensite. According to Table 1-6 showing yield strength of the NiTi, CNT/NiTi nanocomposite and TiC/NiTi composite, detwinning process of the 0.5 vol% CNT/NiTi nanocomposite begins at highest stress among them since the yield strength of the 0.5 vol.% CNT/NiTi nanocomposite shows highest value, compared than that of others. This indicates that dispersed CNTs suppress detwinning process of twinned martensite.

On the other hand, 0.5 vol.% CNT/NiTi nanocomposite showed highest ultimate tensile strength. This is due to reinforcing effect of CNTs. If the 0.5 vol.% CNTs react with Ti completely, 1 vol.% TiC will be formed in the NiTi matrix. However, in the XRD pattern of Figure 1-21, intensity ratio of diffraction peak of TiC to that of NiTi was lower in the 0.5 vol.% CNT/NiTi nanocomposite than in the 1 vol.% TiC/NiTi composite, which means that some CNTs were survived, not reacting with Ti. Actually, survived CNT was observed in 0.5 vol.% CNT/NiTi nanocomposite as shown in Figure 1-21 and 1-26. The survived CNTs improved tensile strength. Therefore, CNTs showed an excellent reinforcing effect in the NiTi matrix, influencing little on shape recovery ratio.

In summary, three different materials of Ni, SiO_2 and TiO_2 were coated to control reaction of CNTs with Ti for fabrication of CNT/NiTi nanocomposite. However, the elongation of the coated-CNT/NiTi nanocomposites was severely reduced due to reaction between coating layer and matrix while the coating layer can’t prevent reaction of CNTs with Ti. Thus, pristine CNTs were applied to fabricate CNT/NiTi nanocomposite. Mechanical properties were enhanced by adding CNTs in NiTi matrix and shape recovery ratio of CNT/NiTi nanocomposite maintained higher than 90 %. The CNT/NiTi nanocomposite can be applied in pipe coupling and antenna. Additionally, it can be applied in hinges of solar panel array.

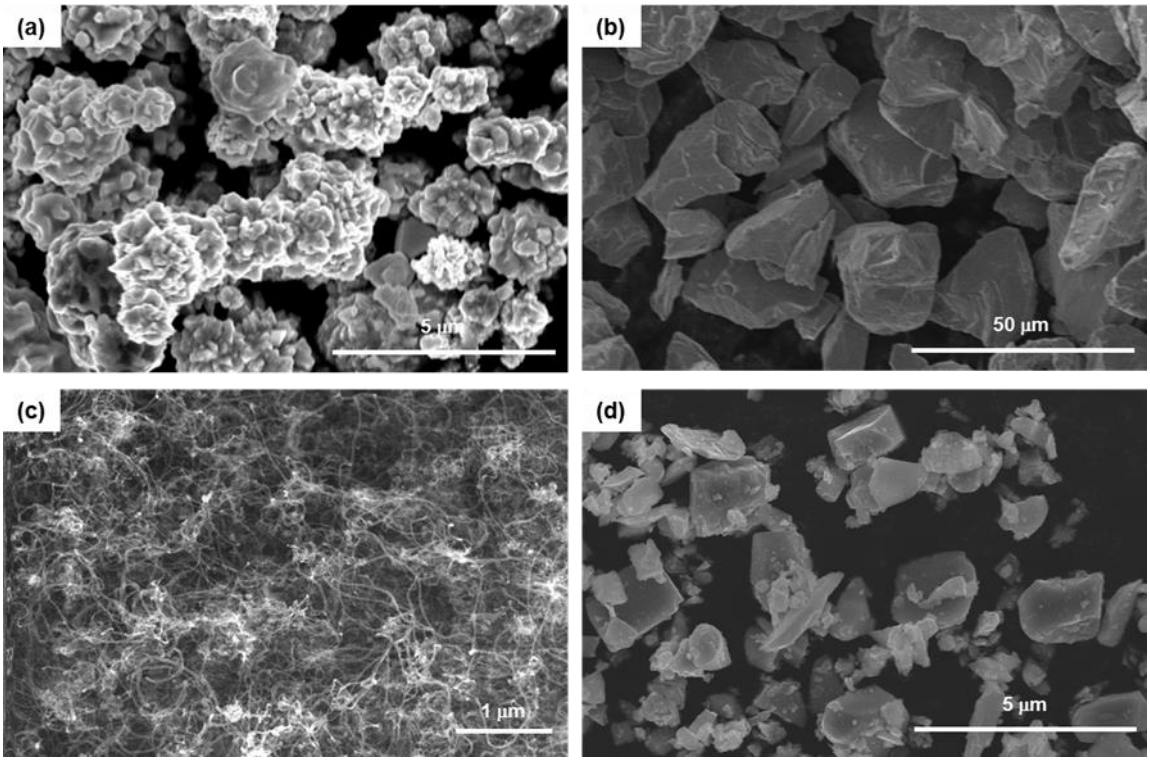

Figure 1-17. SEM micrographs of (a) Ni powder, (b) Ti powder, (c) pristine CNT and (d) TiC powder

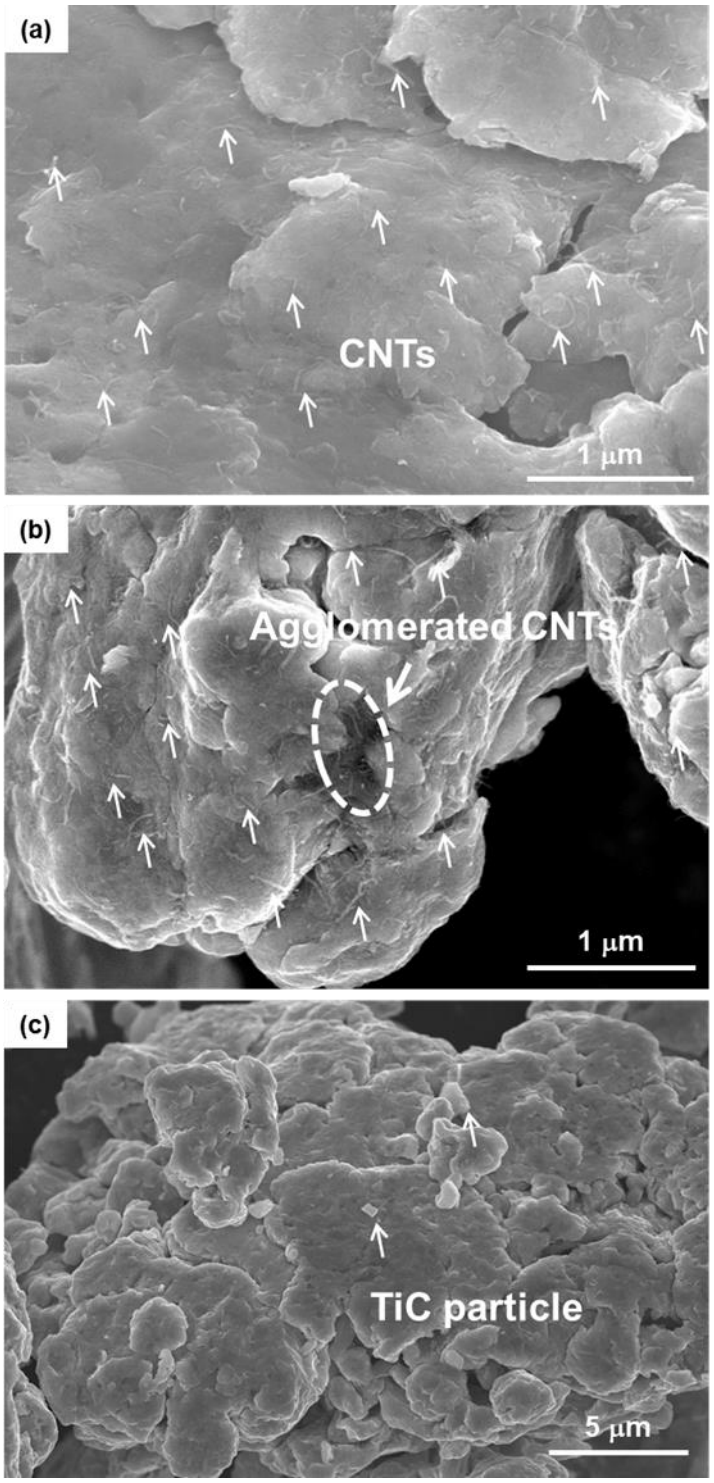

Figure 1-18. SEM micrograph of (a) 0.5 vol.% CNT/NiTi nanocomposite powders, (b) 1vol.% CNT/NiTi nanocomposite powder and (c) 1 vol.% TiC/NiTi composite powder after 2 hrs milling with 100 rpm. Arrows in the figure show dispersed CNTs or TiC particles. CNTs in the circle are agglomerated form.

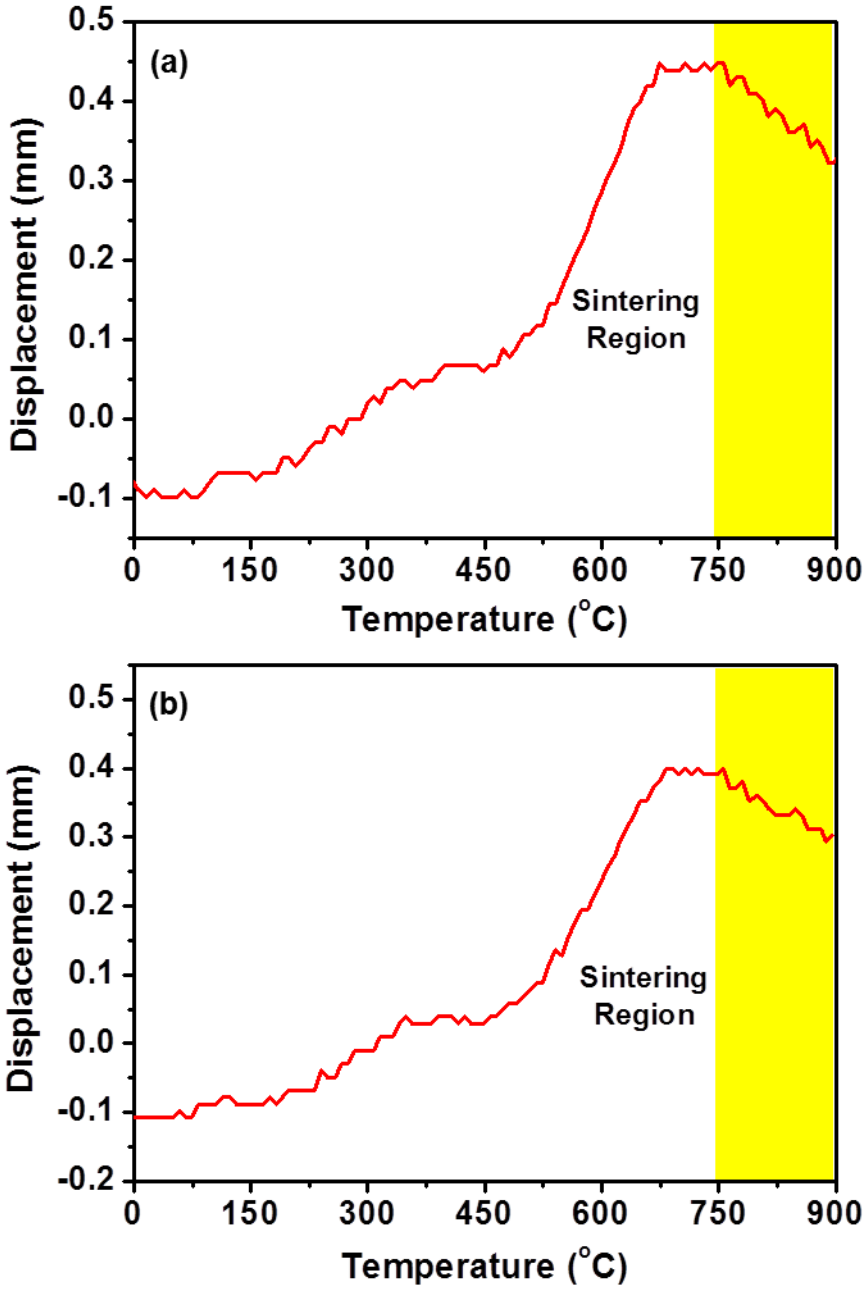

Figure 1-19. Sintering behavior of CNT/NiTi nanocomposite powder and TiC/NiTi composite powder by spark plasma sintering process

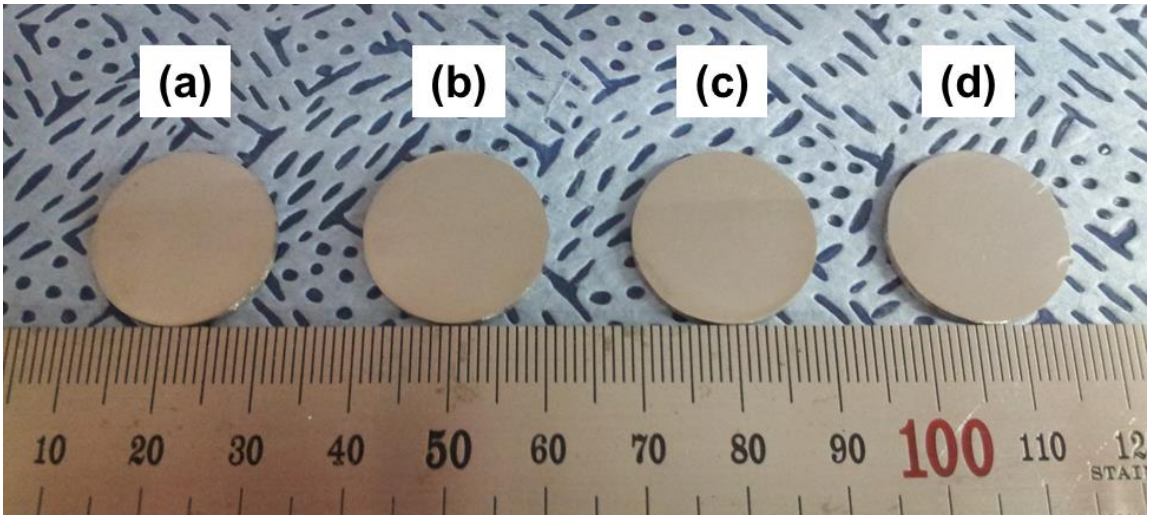

Figure 1-20. (a) NiTi, (b) 0.5 vol.% CNT/NiTi nanocomposite, (c) 1 vol.% CNT/NiTi nanocomposite and (d) TiC/NiTi composite consolidated by spark plasma sintering

Sample	Volume fraction of CNT (%)	Relative density (%)
CNT/NiTi nanocomposites	0	99.7
	0.5	99.3
	1	99.1
TiC/NiTi nanocomposites	1	99.1

Table 1-3. Relative density of NiTi, CNT/NiTi nanocomposite and TiC/NiTi composite with reinforcement content

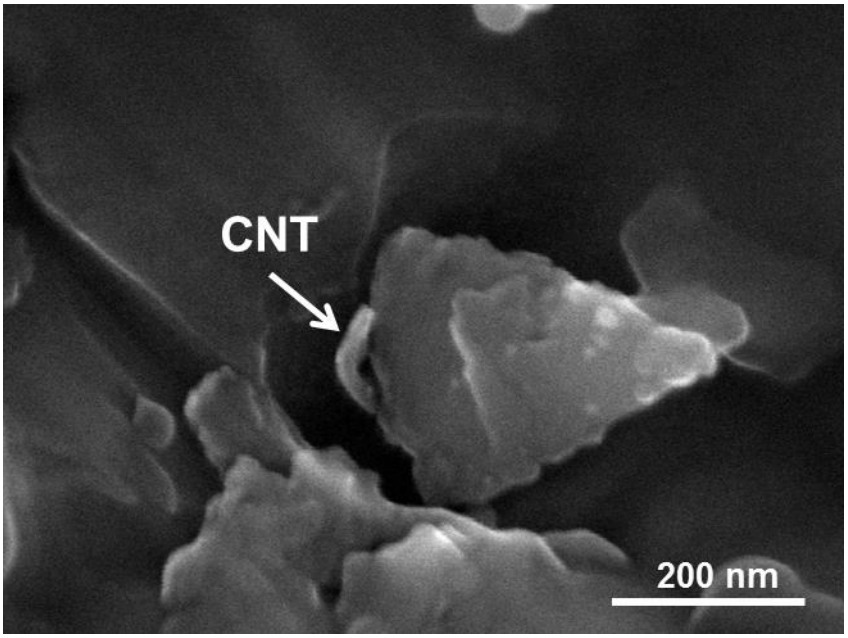

Figure 1-21. SEM micrograph showing dispersed CNT in 0.5 vol.% CNT/NiTi nanocomposite

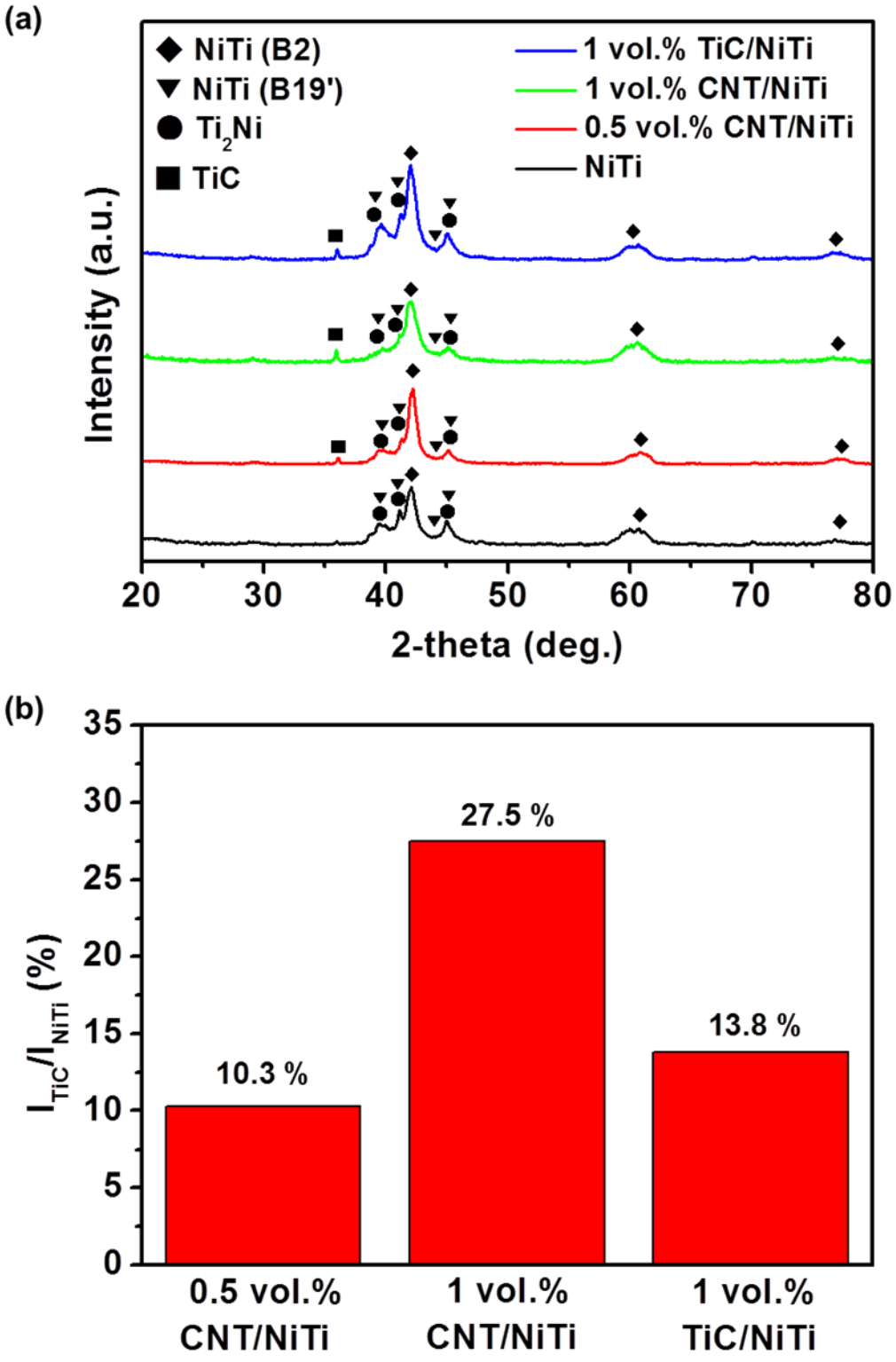

Figure 1-22. (a) XRD pattern of NiTi, CNT/NiTi nanocomposite and TiC/NiTi composite and (b) intensity ratio of TiC peak to NiTi peak in the XRD pattern of each specimen

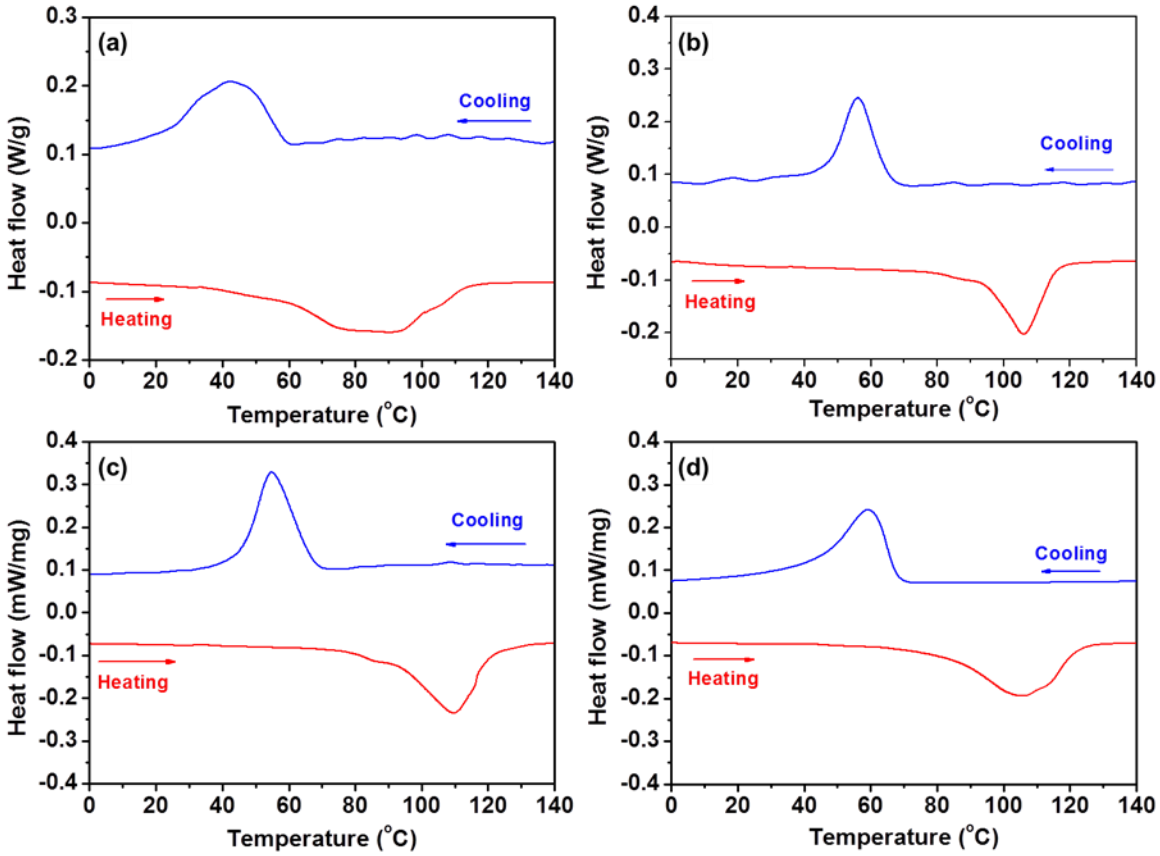

Figure 1-23. Differential scanning calorimetry (DSC) curves of (a) NiTi, (b) 0.5 vol.% CNT/NiTi nanocomposite, (c) 1vol.% CNT/NiTi nanocomposite and (d) 1vol.% TiC/NiTi composite on heating and cooling.

	M_f	M_s	A_s	A_f	Hysteresis (A_f - M_s)
NiTi	21.2	59.1	61.5	108.7	49.6
0.5 vol.% CNT/NiTi	49.5	66.9	89.2	117.4	50.5
1vol.% CNT/NiTi	45.6	67.5	90.7	119.1	51.6
1vol.% TiC/NiTi	44.6	68	83	121.2	53.2

Table 1-4. Phase transformation temperatures and thermal hysteresis of NiTi, CNT/NiTi nanocomposite and 1vol.% TiC/NiTi composite. M_f and M_s mean martensite finish and start, respectively. A_s and A_f mean austenite start and finish, respectively.

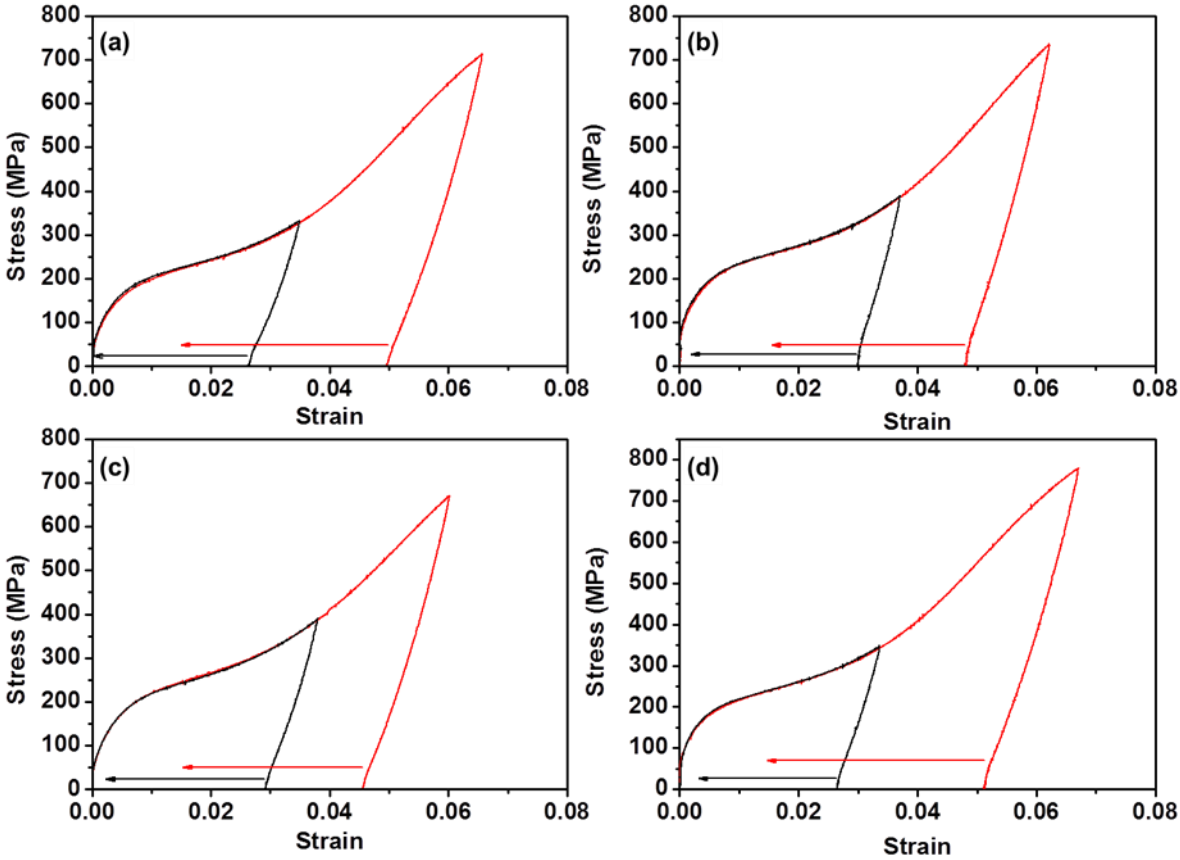

Figure 1-24. The loading-unloading tensile curves at room temperature with various deformation strain; (a) NiTi, (b) 0.5 vol.% CNT/NiTi, (c) 1 vol.% CNT/NiTi and (d) 1vol.% TiC/NiTi. The arrows indicate recovery after heating on A_f.

	Deformation (%)	Recovery (%)	Deformation (%)	Recovery (%)
NiTi	3.5	100	6.56	68.9
0.5 vol.% CNT/NiTi	3.6	94	6.21	67.8
1vol.% CNT/NiTi	3.6	90	6	66
1vol.% TiC/NiTi	3.36	87.5	6.7	71

Table 1-5. Deformation and recovery ratio of NiTi, CNT/NiTi, and TiC/NiTi composite during shape memory test.

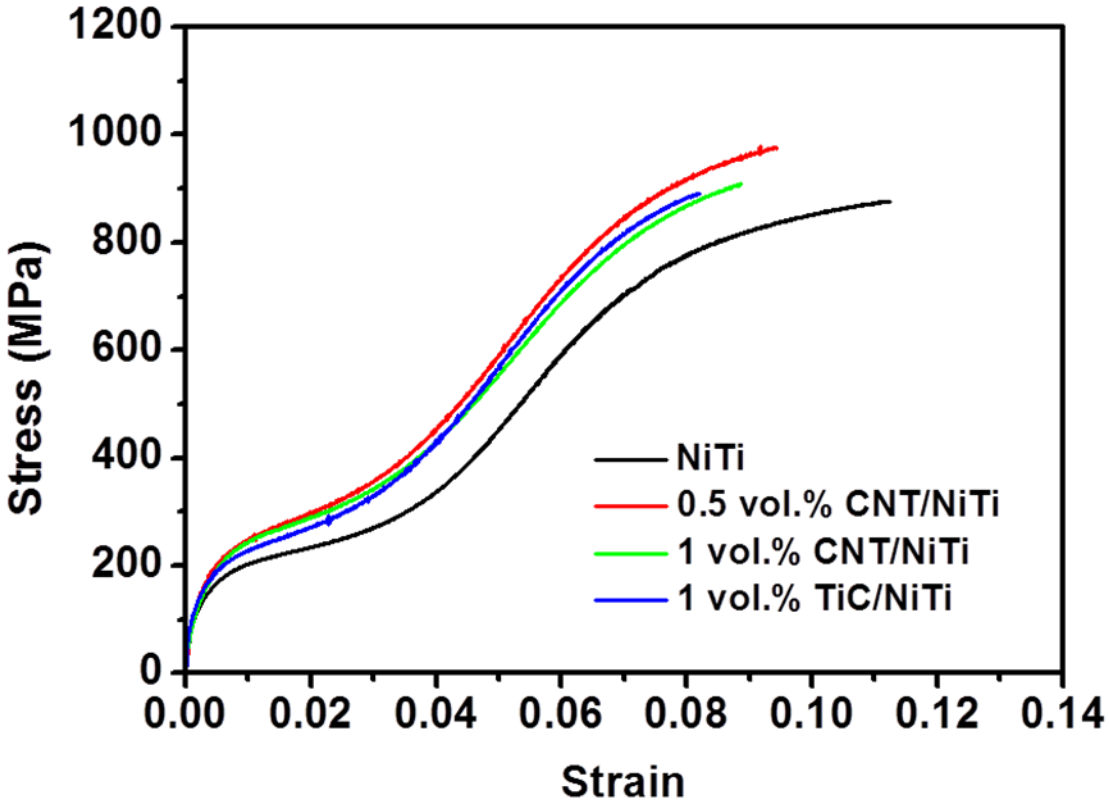

Figure 1-25. Stress-strain curves of the NiTi, CNT/NiTi and TiC/NiTi composites.

	E.M. (GPa)	Y.S.(MPa)	UTS (MPa)	Elongation (%)
NiTi	61	151	876	11.2
0.5 vol.% CNT/NiTi	79 (29%↑)	192 (27%)	975 (11%↑)	9.4 (16%↓)
1vol.% CNT/NiTi	75 (23 % ↑)	185 (22.5 %↑)	907 (3.5%↑)	8.9 (20%↓)
1vol.% TiC/NiTi	77 (26%↑)	177 (17%↑)	891 (1.7%↑)	8.2 (26%↓)

Table 1-6. Mechanical properties of NiTi, CNT/NiTi and 1vol.% TiC/NiTi. Number in parenthesis refers to ratio of increment (↑) or decrement (↓) in comparison with properties of NiTi.

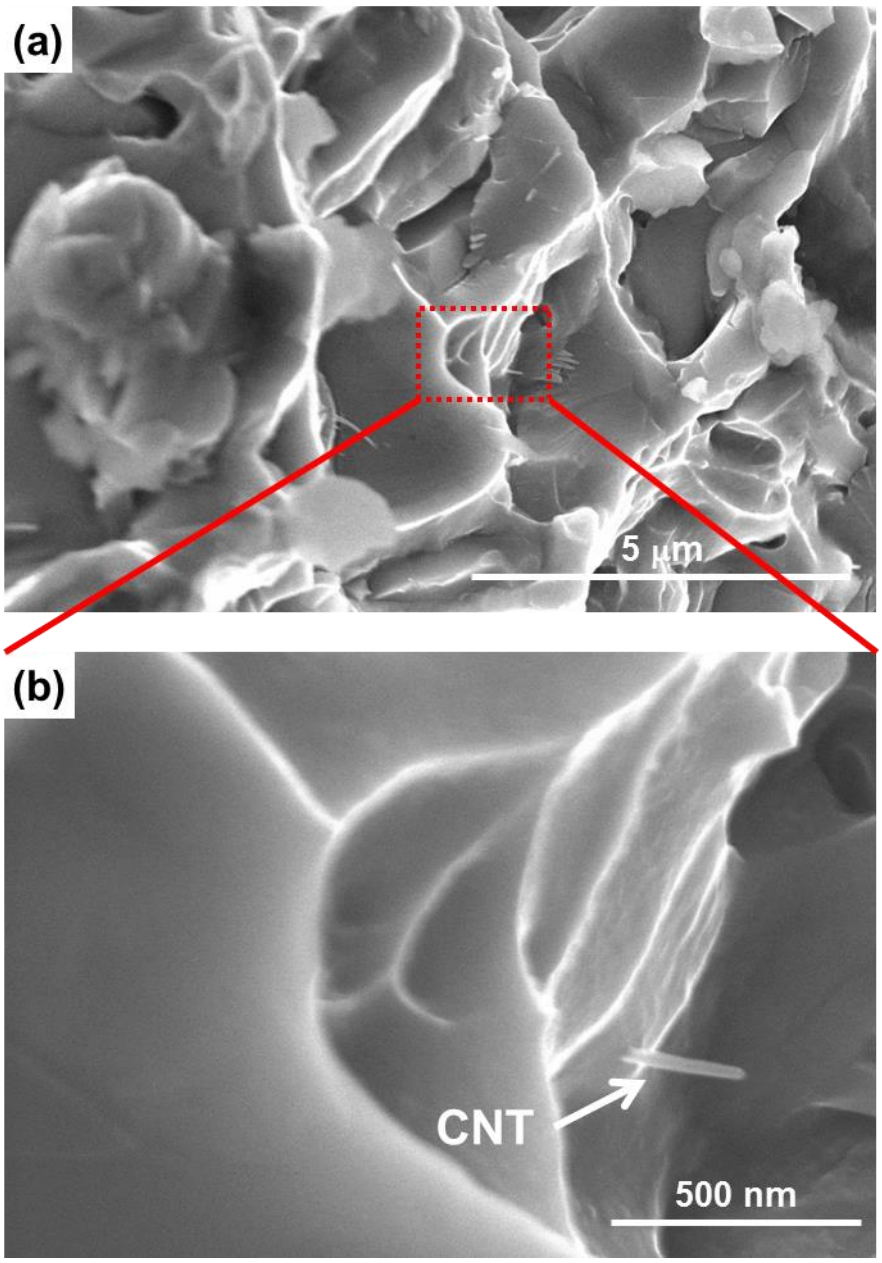

Figure 1-26. SEM micrograph showing CNT on the fracture surface of 0.5 vol.% CNT/NiTi nanocomposite at (a) low magnification and (b) high magnification.

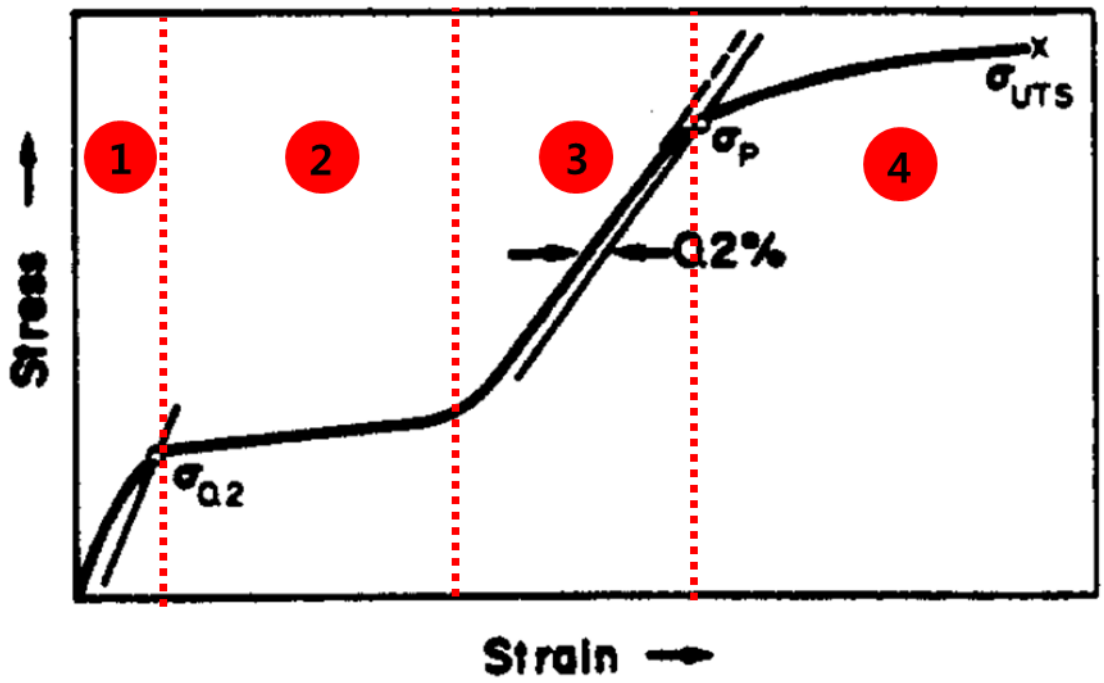

Figure 1-27. Typical stress-strain curve of shape memory alloy

	E.M. (GPa)	Y.S.(MPa)	UTS (MPa)	Elongation (%)
NiTi	61	151	876	11.2
1 vol.% CNT/NiTi (CNT/Ni)	76 (25 %↑)	259 (71.5 %↑)	506 (42 %↓)	2.5 (77 %↓)
1 vol.% CNT/NiTi (CNT/SiO2)	-	-	-	0.14 (98 %↓)
1 vol.% CNT/NiTi (CNT/TiO2)	93 (52 %↑)	219 (45 %↑)	778 (11 %↓)	4.9 (56 %↓)
0.5 vol.% CNT/NiTi (pristine CNTs)	79 (29%↑)	192 (27%)	975 (11%↑)	9.4 (16%↓)
1vol.% CNT/NiTi (pristine CNTs)	75 (23 % ↑)	185 (22.5 %↑)	907 (3.5%↑)	8.9 (20%↓)

Table 1-7. Comparisons of mechanical properties of NiTi, coated CNT/NiTi and uncoated pristine CNT/NiTi nanocomposites

3-2. Fabrication processes and characterization of CNT/Al-Cu nanocomposite

3-2-1. Fabrication process of CNT/Al-Cu nanocomposite

CNT/Al-Cu nanocomposite powders were fabricated by mixing of Al powders and CNT/Cu composite powders which were prepared by molecular level mixing process as can be seen in Figure 2-1. To control the aspect ratio of CNTs, we used two different types of CNTs when fabricating CNT/Cu composite powders. One is acid treated CNT (ATCNT); the other is Poly-vinyl alcohol (PVA) coated CNT (PCNT). The CNT/Al-Cu composite powders were consolidated by both spark plasma sintering (SPS).

3-2-1-1. Fabrication process of CNT/Cu nanocomposite powders by molecular-level mixing process

1) Functionalization of CNTs by acid treatment

Multi-walled carbon nanotubes (Hanwha Nanotech Corporation.), with diameters of 10-15 nm, length of 10-20 μm (Figure 2-2 (a)), and fabricated by thermal chemical vapor deposition, were functionalized by acid treatment. The CNTs were sonicated for 5 hours in a HCl for purification CNTs from metal catalyst and vacuum filtered. The purified CNTs were sonicated for 10 hours in a mixed solution of H_2SO_4 (95 %, Junsei extra pure grade)/HNO_3 (60 %, Junsei extra pure grade) in a 3:1 ratio for in achieving functionalization mainly with carboxylic groups. The functionalized CNTs were centrifuged and filtered with distilled water until the pH reached 7 and then they were finally dried in vacuum at 100 ℃. Figure shows the morphology of CNTs after functionalization by acid treatment. The length of CNTs was reduced to 1-2 μm due to damage during acid treatment. The schematic diagram for functionalization of CNTs by acid treatment is shown in Figure 2-3.

2) Coating of CNTs by PVA

The coating of CNTs by PVA was done by mixing CNTs and PVA aqueous solution by ball milling process. The 0.5 g of PVA was immersed in distilled water of 50 mml with magnetic stirring at 80 ℃. The PVA aqueous solution and 4.5 g of CNTs were mixed by tumbler ball mill with 30 rpm for 48 hours. Zirconia balls, diameter of 5 mm, were used and ball to powder ratio was 10:1. The CNT/PVA mixture was dried in vacuum at 100 ℃. Figure 2-2 (c)

shows the morphology of CNTs after functionalization by PVA. CNTs are well coated by PVA and do not received any damages during process. The length of CNTs is same as pristine CNTs. The schematic diagram for functionalization of CNTs by PVA coating is shown in Figure 2-4.

3) Fabrication of CNT/Cu nanocomposite powders

The functionalized CNTs were dispersed in distilled water by sonication for 3h to form CNT suspension. $Cu(CH_3COO)_2 \cdot H_2O$ (Aldrich) aqueous solution and 2 M NaOH aqueous solution were added to CNT suspension. The volume fraction of CNT in CNT/Cu composite powders was varied with volume fraction of CNTs in CNT/Al nanocomposite for adjusting weight % of Cu in Al matrix as 4 regardless of volume fraction of CNTs. The CNT solution was heated up to 80 ℃ to form CNT/CuO nanocomposite and followed by vacuum filtering and drying at 100 ℃. The schematic diagram for fabrication of CNT/Cu nanocomposite powders is shown in Figure 2-5.

The morphology of CNT/CuO nanocomposite powders is shown in Figure 2-6. CuO particles are not agglomerated and well coated along CNTs. CNT/CuO nanocomposite powders were reduced at 300 ℃ for 6 hours under a hydrogen atmosphere to get CNT/Cu nanocomposite powders. The XRD result in Figure 2-7 clearly shows that CuO were successfully reduced to Cu by reduction process. The morphologies of CNT/Cu nanocomposite powders after reduction process are shown in Figure 2-8. In case of ATCNT/Cu nanocomposite powders, Cu nanoparticles, size of 10-50 nm, are decorated along the surface of CNTs and any agglomeration of Cu nanoparticles are not observed (Figure 2-8 (a)). The morphology of PCNT/Cu nanocomposites powders, shown in Figure 2-8 (b), shows a little different microstructure with ATCNT/Cu nanocomposite powders. The size of Cu nanoparticles is similar with that of ATCNT/Cu nanocomposite powders, but the distribution of Cu nanoparticles on CNTs is less homogeneous than ATCNT/Cu nanocomposite powders. This difference is mainly originated from dispersion of CNTs in water. When CNTs are dissolved in water, ATCNTs form a very stable suspension due to many functional groups on the surface of CNTs such as hydroxyl (-OH), carboxyl (-COOH) group, electrostatic repulsive force between CNTs overcomes the Van der Waals' force. In the case of PCNT, CNTs are dissolved water due to only hydrophilic hydroxyl groups of PVAs and the length of PCNT is larger than that of ATCNT, so dispersion of PCNT in water is harder than ATCNT.

3-2-1-2. Fabrication process of CNT/Al-Cu nanocomposite powders

The CNT/Cu nanocomposite powders and Al powders (Kojundo chemical Laboratory Co. Ltd., 99.9 % purity) with average particle size of 3 μm (Figure 2-9) were mixed into CNT/Al-Cu nanocomposite powders by high energy ball milling process using planetary mill (Fritsch GmbH). The planetary mill was performed by two steps to reduce damage on CNTs. In first step, CNT/Cu nanocomposite powders and Al powders were mixed for 20 hours with 50 rpm under argon atmosphere to distribute CNT/Cu nanocomposite powders on the surface of Al powders. Then, CNTs are homogeneously dispersed in Al matrix and Cu nanoparticles are alloyed in Al to form Al-Cu matrix by high energy milling process for 1 hour with 200 rpm speed (Figure 2-10). Stainless jar and zirconia ball were used and ball to powder ratio was 10:1. Parameters of mechanical alloying process can be pressed as follows:

$$I = \frac{M_b}{M_p} Vf \tag{1}$$

where, I is intensity of milling, M_b is mass of ball, Mp is mass of powders, V is velocity of ball and f is impact frequency. Thus, as the speed and time of milling increase, the damages on CNTs increase and CNTs can be broken and turned into amorphous carbon. As can be seen the Raman spectroscopies and ID/IG values of CNT/Al-Cu nanocomposite powders with high energy milling time in Figure 2-11, CNTs are not as much damaged after 50 rpm milling followed by 1 hours milling with 200 rpm. However, after 18 hours high energy milling with 200 rpm, CNTs are severely damaged due to high impact energy from balls. Figure 2-12 shows the morphology of ATCNT/Al-Cu nanocomposite powders after milling with 50 rpm. The condensed CNT/Cu nanocomposite powders are broken into size of 1-3 μm and dispersed on the surface of Al powders. After 1 hour milling with 200 rpm, CNTs are homogeneously dispersed in Al matrix and Cu nanoparticles are not observed because they are alloyed in Al matrix (Figure 2-13).

3-2-1-3. Fabrication process of CNT/Al-Cu nanocomposite by spark plasma sintering

The CNT/Al-Cu nanocomposite powders were heated up to 200 ℃ and maintained for 12 hours under a nitrogen atmosphere to remove humidity and pre-compacted in a graphite mold under a pressure of 1 MPa. The pre-compacted powders were sintered with full densification by spark plasma sintering system (SPS, Dr. Sinter Lab., Sumitomo) at temperature of 500 ℃ for 5min in vacuum of 10^{-3} torr under a pressure of 50 MPa. The heating rate was 50 ℃/min to sintering temperature. The SPS system can produce high heating rate over 100 ℃/min and

rapid consolidation through high joule heating and spark plasma generated between powders. Figure 2-14 shows the sintering behavior of CNT/Cu nanocomposite powders by spark plasma sintering process. Displacement increases with increasing temperature and over 480 ℃ increase of displacement is stopped and displacement begins to decrease due to full densification and thermal expansion of nanocomposites. Figure 2-15 shows the button type of CNT/Al-Cu nanocomposite sintered by spark plasma sintering process. The relative density of CNT/Al-Cu nanocomposites with content and type of CNT are shown in Table 2-1. Almost nanocomposites show over 99% relative density.

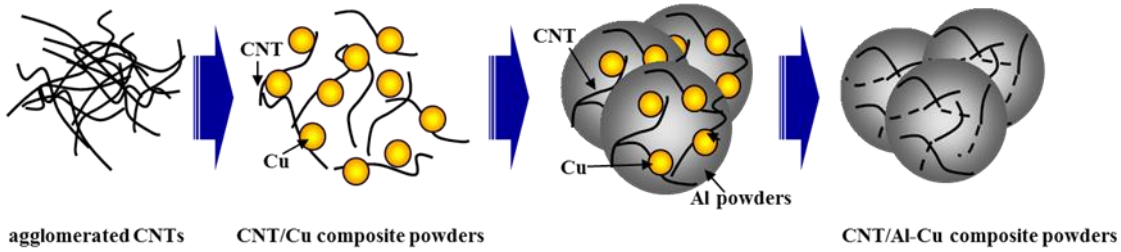

Figure 2-1. Schematic depiction of fabrication process of the CNT/Al-Cu nanocomposite powders.

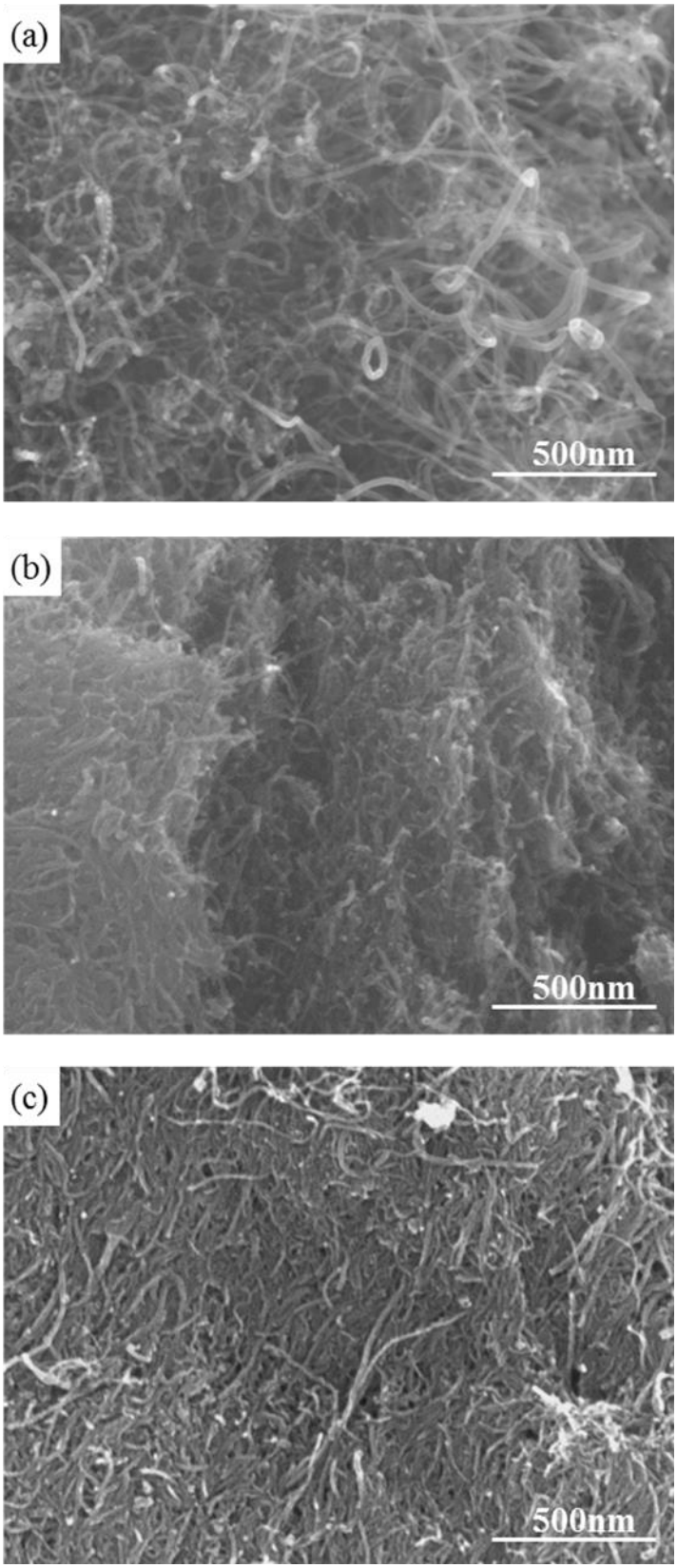

Figure 2-2. SEM micrograph of CNTs (a) pristine CNTs, (b) functionalized CNTs by acid treatment and (c) PVA coated CNTs.

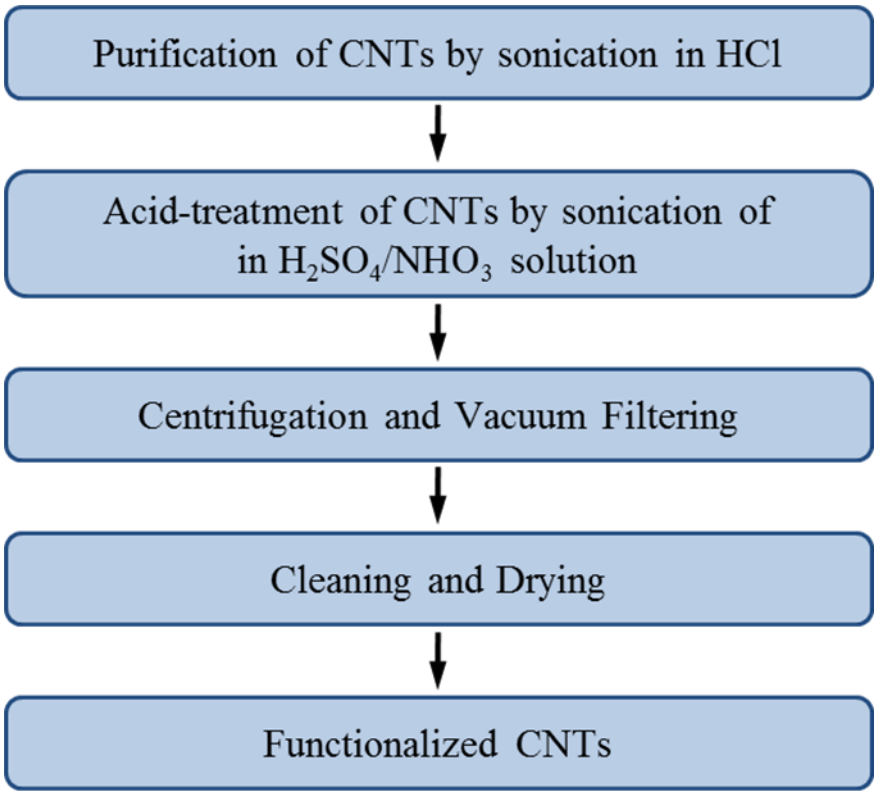

Figure 2-3. Schematic diagram for functionalization of CNTs by acid treatment.

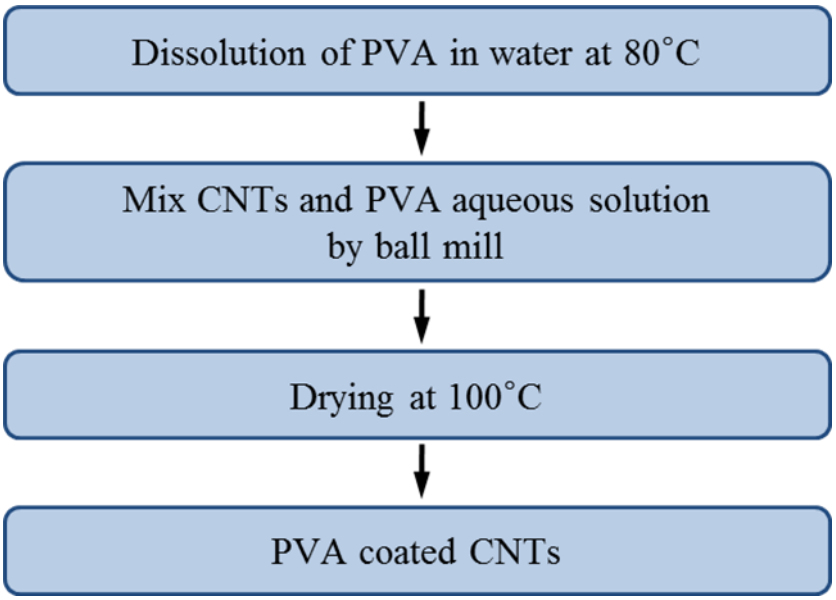

Figure 2-4. Schematic diagram for coating of CNTs by PVA.

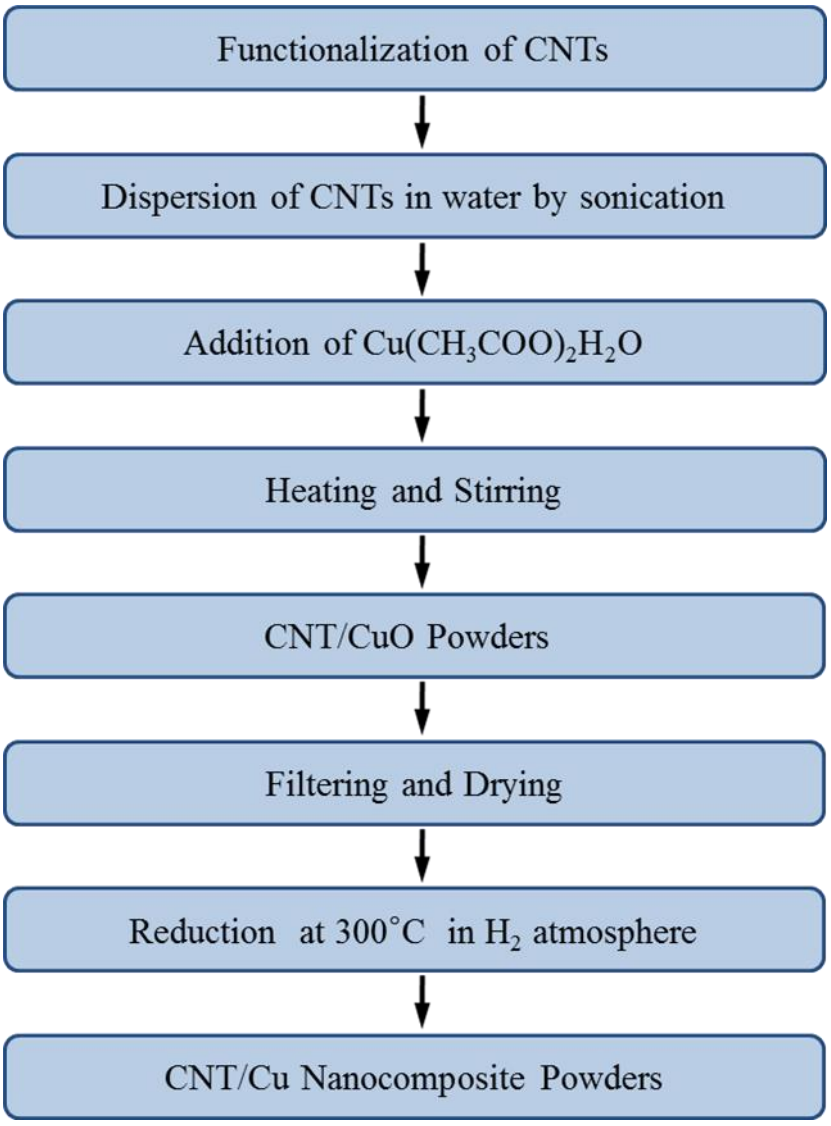

Figure 2-5. Schematic diagram for fabrication process of CNT/Cu nanocomposite powders.

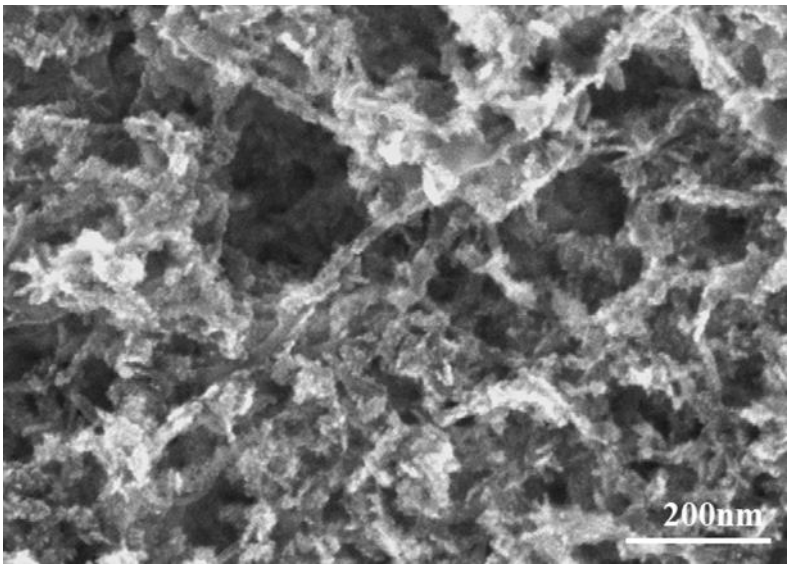

Figure 2-6. SEM micrograph of CNT/CuO nanocomposite powders.

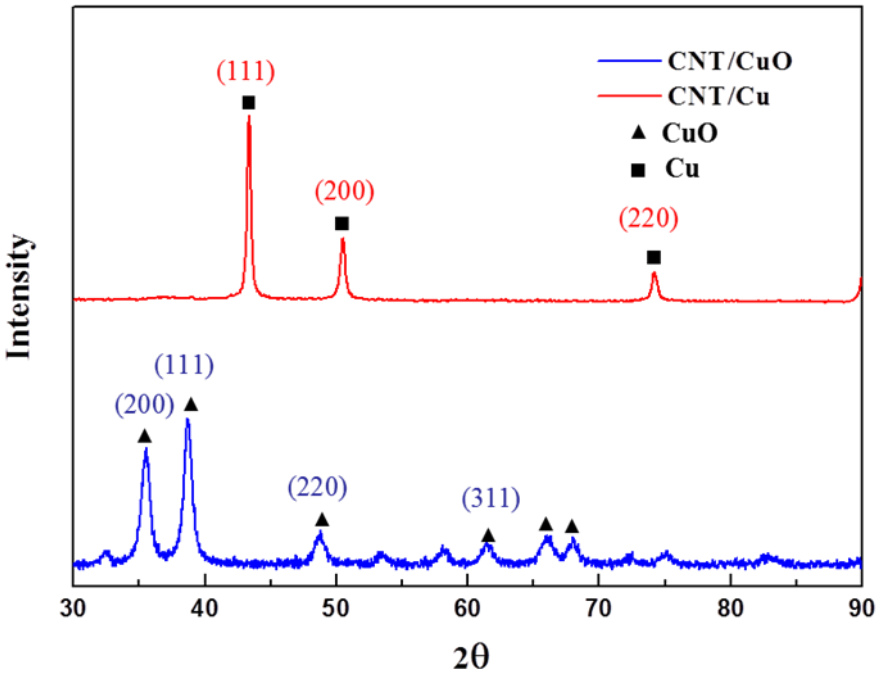

Figure 2-7. XRD of CNT/CuO and CNT/Cu nanocomposite powders.

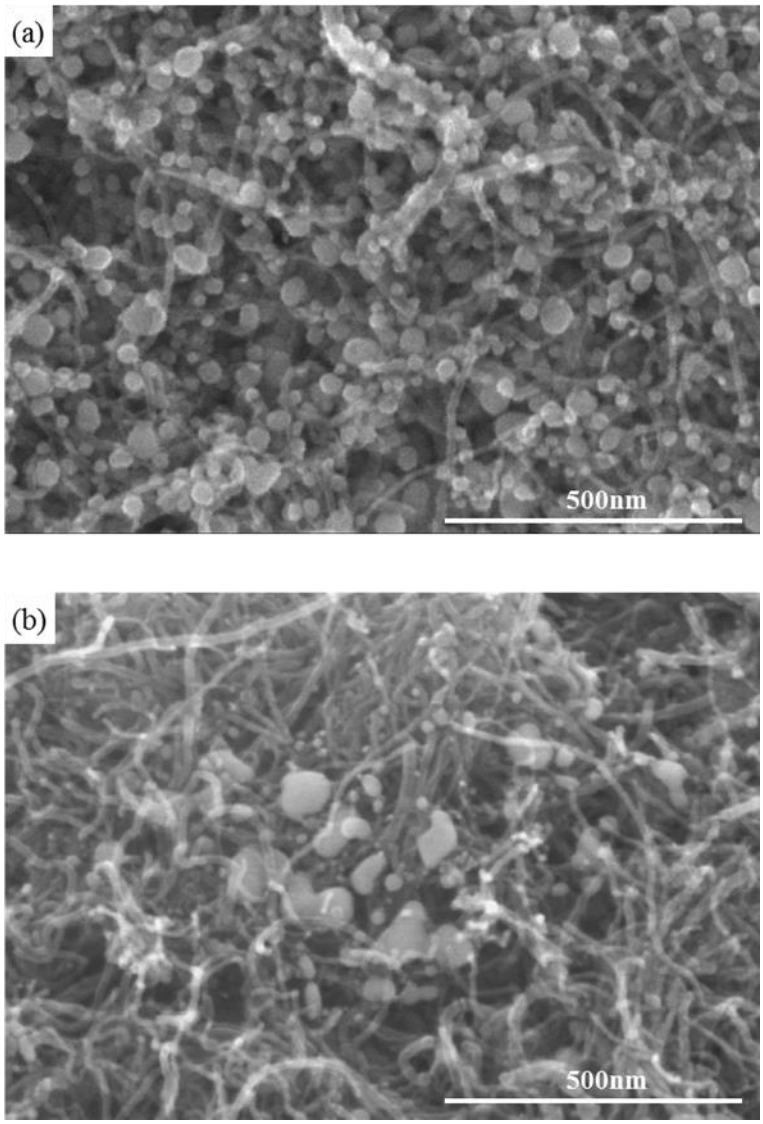

Figure 2-8. SEM micrograph of CNT/Cu nanocomposite powders (a) ATCNT/Cu nanocomposite powders and (b) PCNT/Cu nanocomposite powders.

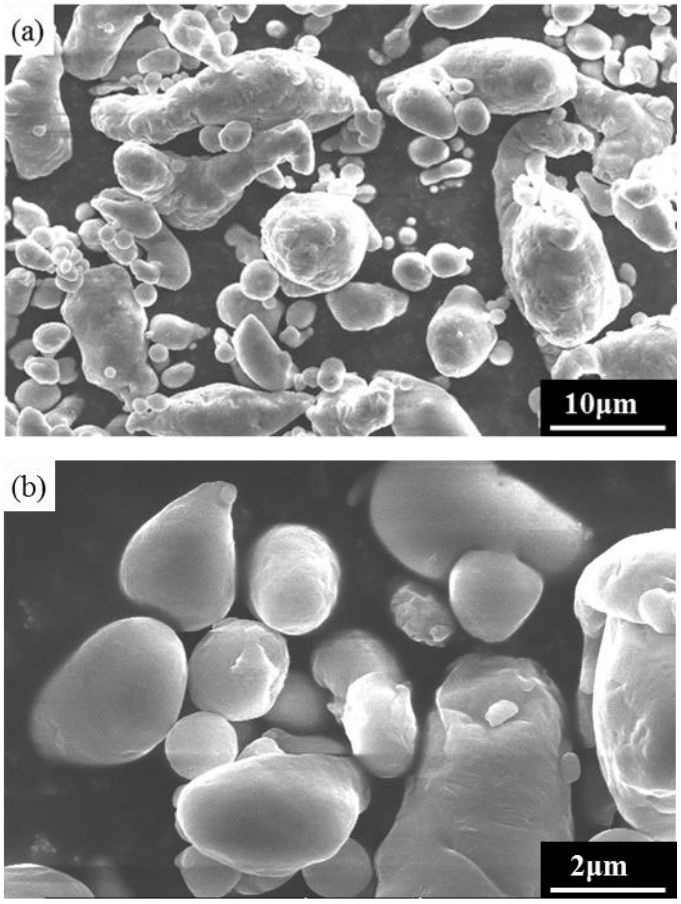

Figure 2-9. SEM micrograph of Al powders (a) Al powders and (b) high magnification image.

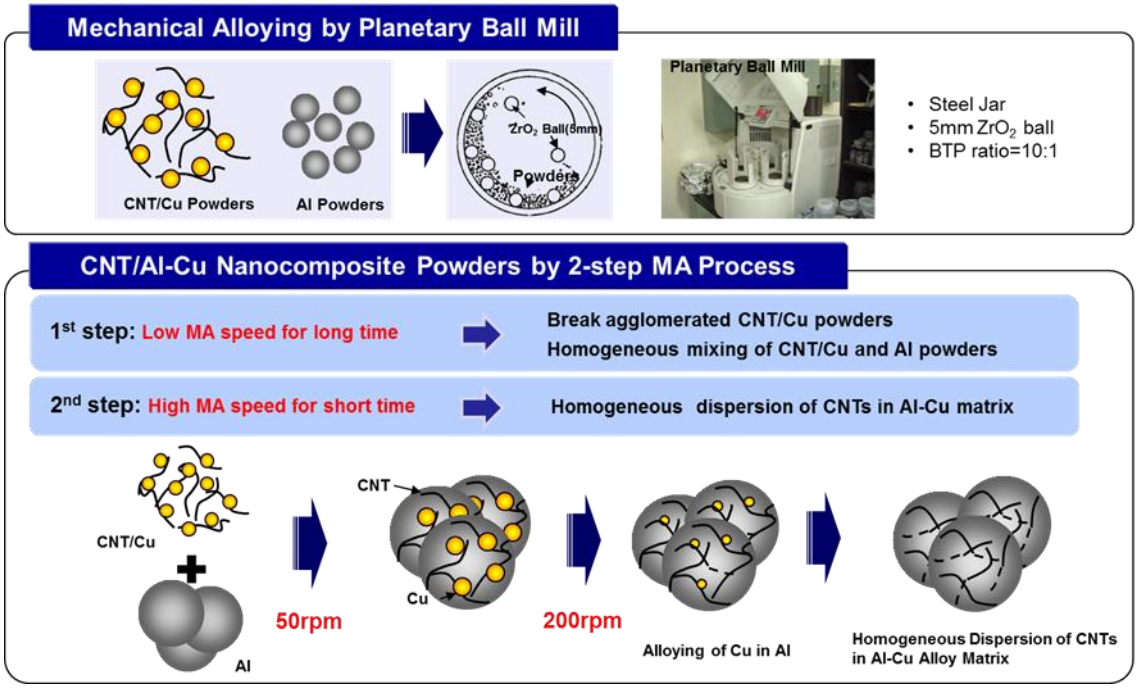

Figure 2-10. Fabrication of CNT/Al-Cu nanocomposite powders by high energy ball milling process.

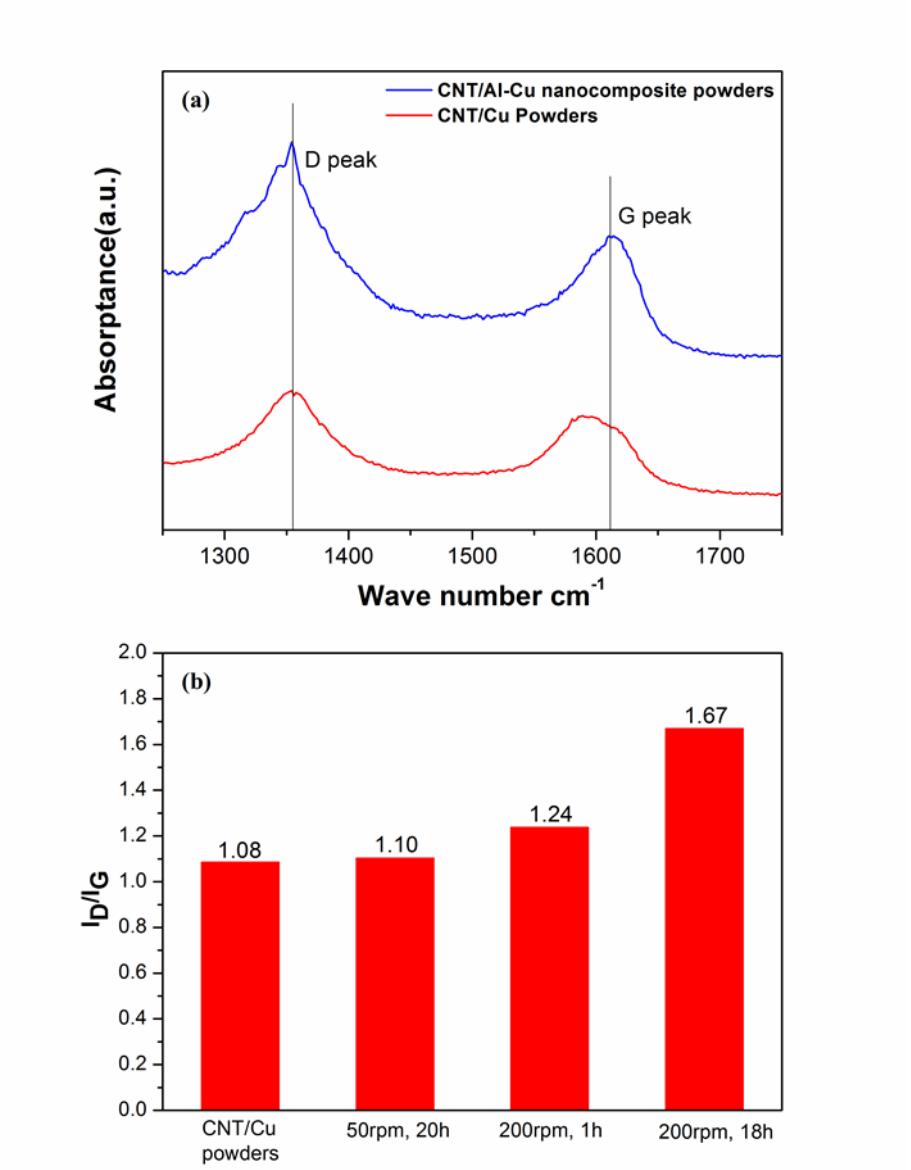

Figure 2-11. (a) Raman spectroscopies of CNT/Cu powders and CNT/Al-Cu nanocomposite powders after 1 hour milling with 200 rpm and (b) I_D/I_G of CNT/Al-Cu nanocomposite powders with high energy milling time.

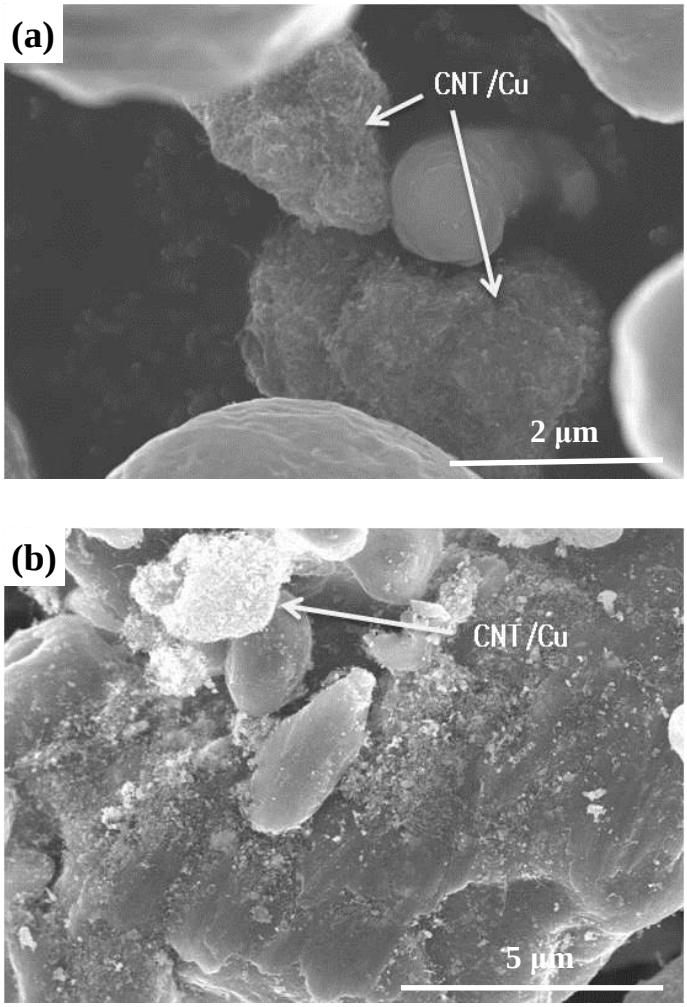

Figure 2-12. SEM micrograph of CNT/Al-Cu nanocomposites powders during high energy ball milling (a) after 1 hours milling with 50 rpm and (b) after 20 hours milling with 50 rpm.

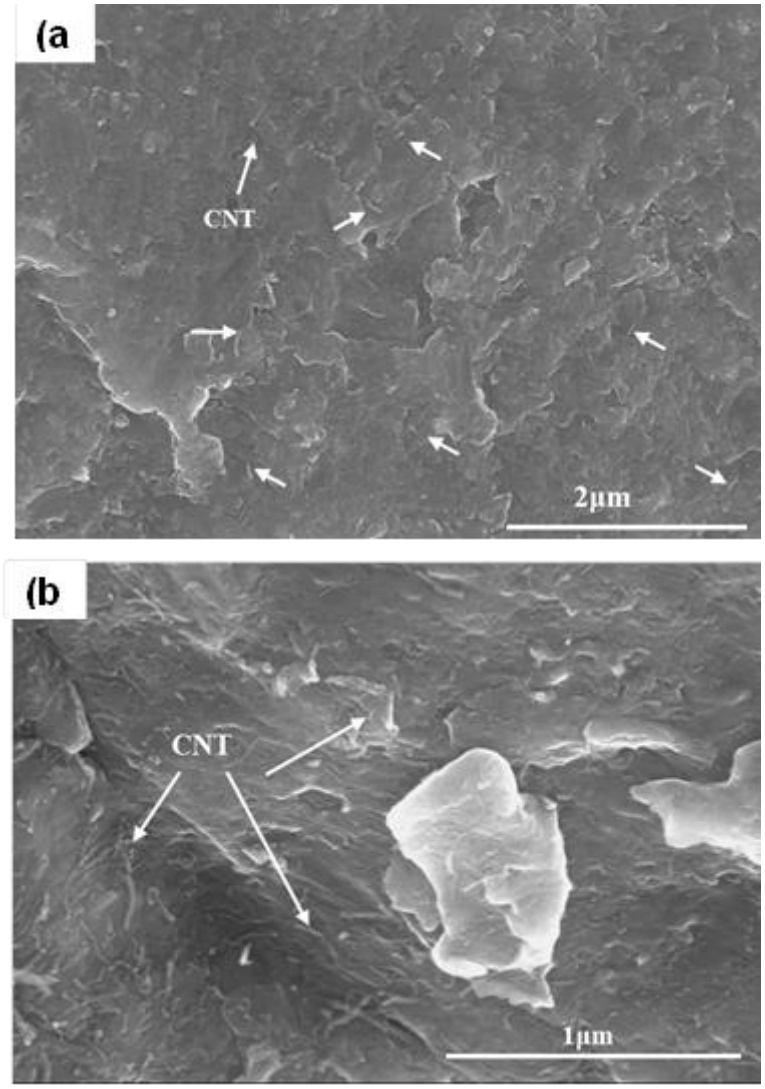

Figure 2-13. SEM micrograph of (a) ATCNT/Al-Cu nanocomposites powders (b) PCNT/Al-Cu nanocomposites powders after 1h milling with 200 rpm.

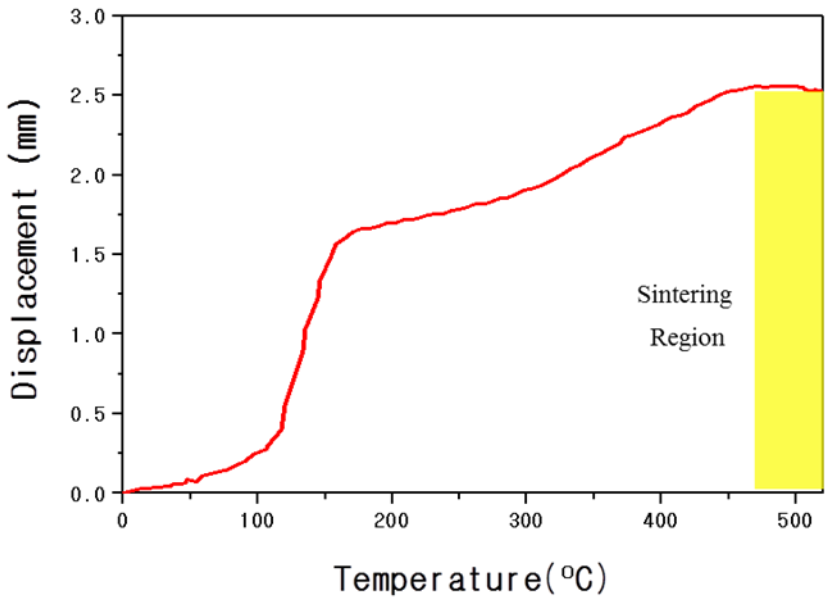

Figure 2-14. Sintering behavior of CNT/Al-Cu nanocomposite powders by spark plasma sintering process.

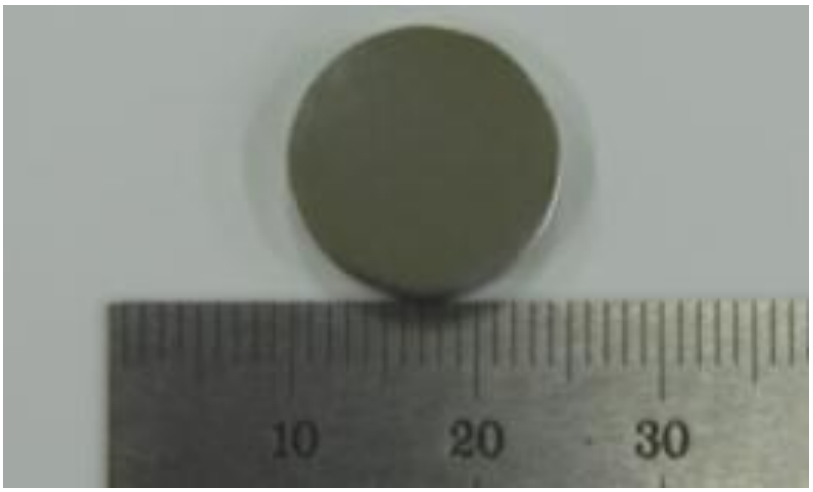

Figure 2-15. CNT/Al-Cu nanocomposite consolidated by spark plasma sintering process.

Sample	Volume fraction of CNT (%)	Relative density (%)
ATCNT/Al-Cu nanocomposites	0	99.2
	2.5	99.4
	4.0	98.1
PCNT/Al-Cu nanocomposites	2.0	99.4
	4.0	99.1

Table 2-1. Relative density of CNT/Al-Cu nanocomposites by spark plasma sintering process.

3-2-2. Characterization of microstructures of CNT/Al-Cu nanocomposite

The microstructures of CNT/Al-Cu nanocomposite were characterized by SEM after mechanical polishing and a chemical etching. As shown in Figure 2-16, CNTs are homogenously dispersed in Al matrix and average grain size of Al matrix was about 60 nm. Figure 2-17 also clearly shows that after sintering at 500 ℃, CNTs survived and did not react with Al matrix to form Al carbide such as Al_4C_3. Particularly the high resolution transmission electron microscope (HRTEM) micrograph of CNT/Al nanocomposite shows that CNT is well embedded in Al matrix and there is no reaction between Al matrix and CNTs (Figure 2-18). The aspect ratio of each type of CNT in the nanocomposites was measured after dissolving the Al-Cu matrix of the CNT/Al-Cu nanocomposites in NaOH, as can be seen in Figure 2-19 (a) & (b). The length of the ATCNTs is about 200 nm, which corresponds with the aspect ratios of 14 to 20 (Figure 2-19 (a)); the length of the PCNT is about 600 nm, which also corresponds with aspect ratios of 40 to 60 (Figure 2-19 (b)). The morphologies of the CNTs also clearly show that although they were shortened after high energy ball milling process, the CNTs do not react to form carbide phase with matrix at the CNT/Al interfaces.

As shown in HRTEM micrograph of Figure 2-18, there is intermetallic compound of Al and Cu revealed as Cu_2Al. The Cu_2Al phase may be formed by precipitation of Cu atoms which are alloyed in Al matrix during high energy ball milling and sintering. This shows possibility of further study about combination of precipitation hardening of Al matrix and strengthening mechanism of CNT. Thus, CNT/Al-Cu nanocomposites with homogenous dispersion of CNTs in Al matrix were successfully fabricated by molecular-level mixing process and high energy ball milling process.

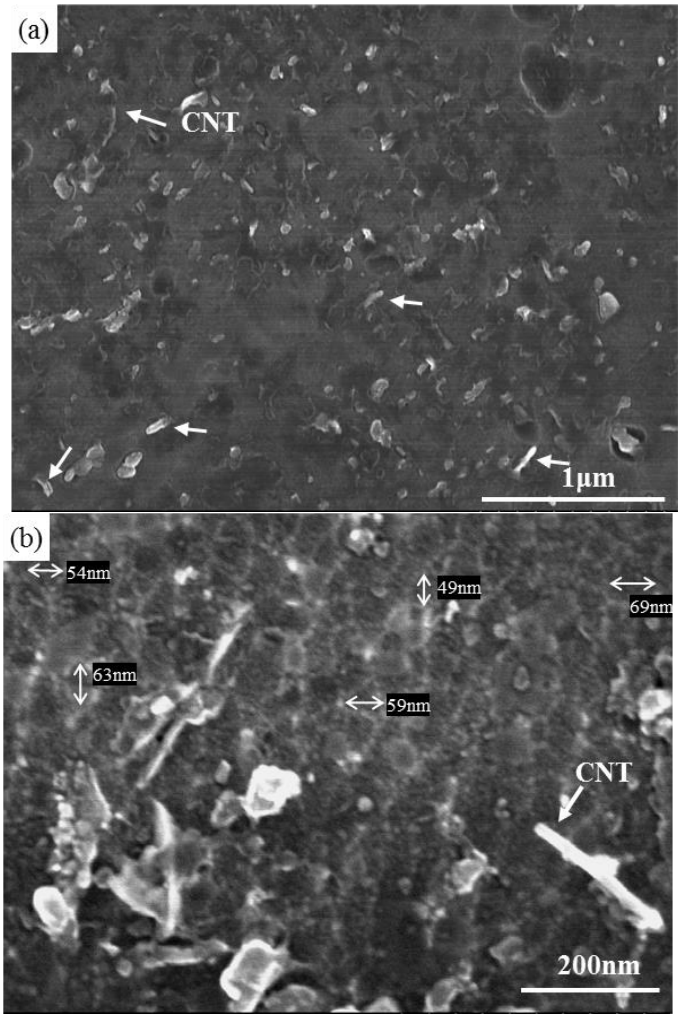

Figure 2-16. SEM micrograph of CNT/Al-Cu nanocomposite by spark plasma sintering process after etching (a) CNT/Al-Cu nanocomposite and (b) high magnification image.

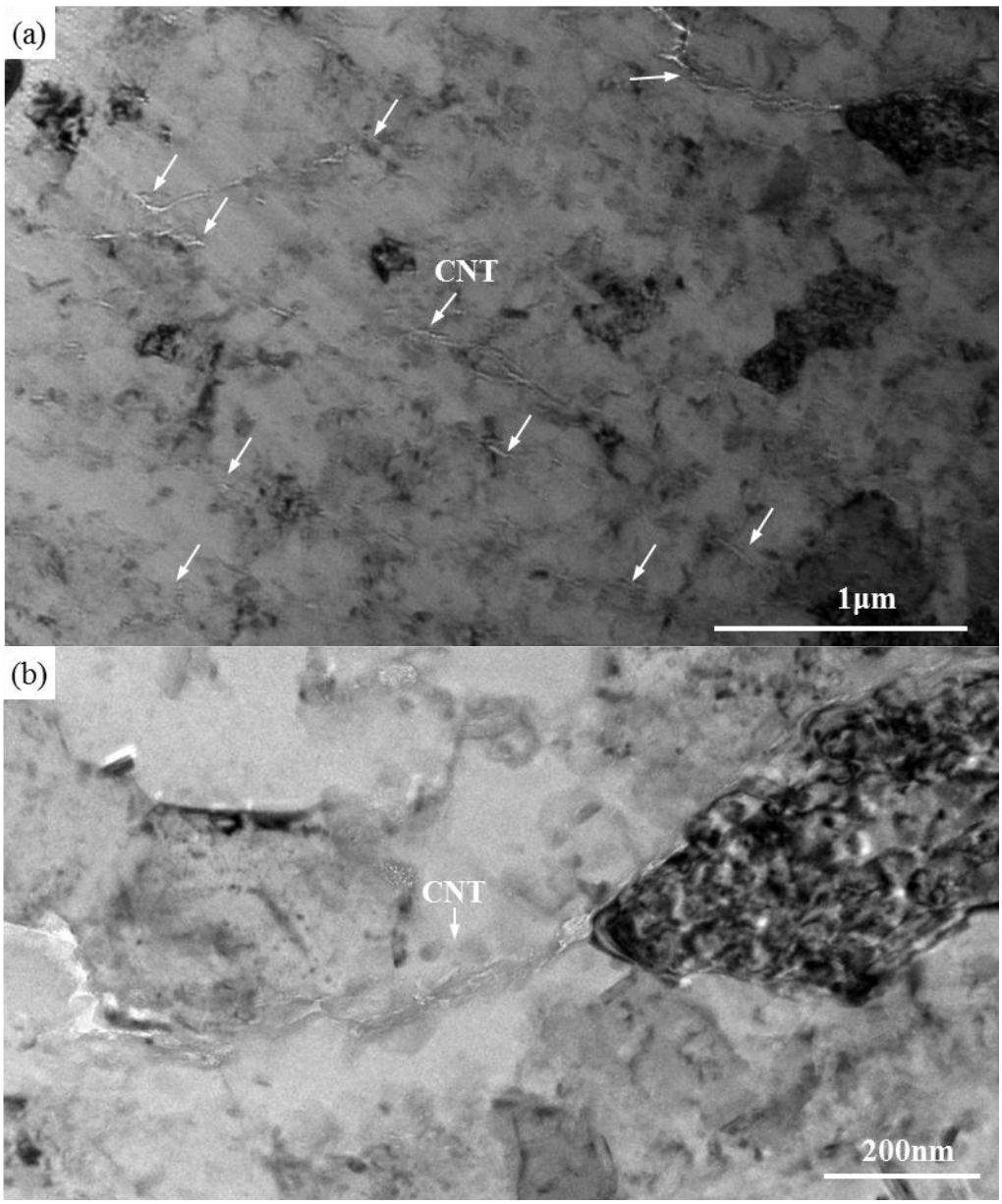

Figure 2-17. TEM micrograph of CNT/Al-Cu nanocomposite by spark plasma sintering process (a) CNT/Al-Cu nanocomposite and (b) high magnification image.

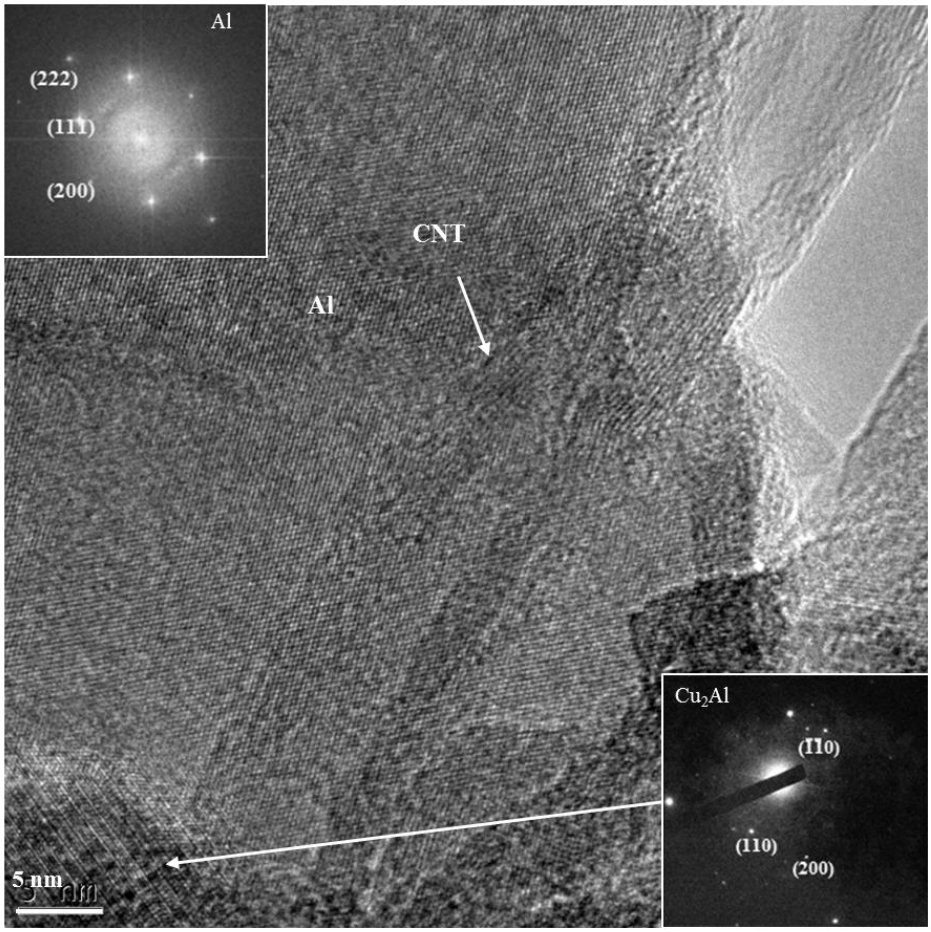

Figure 2-18. HRTEM micrograph of CNT/Al-Cu nanocomposite by spark plasma sintering process.

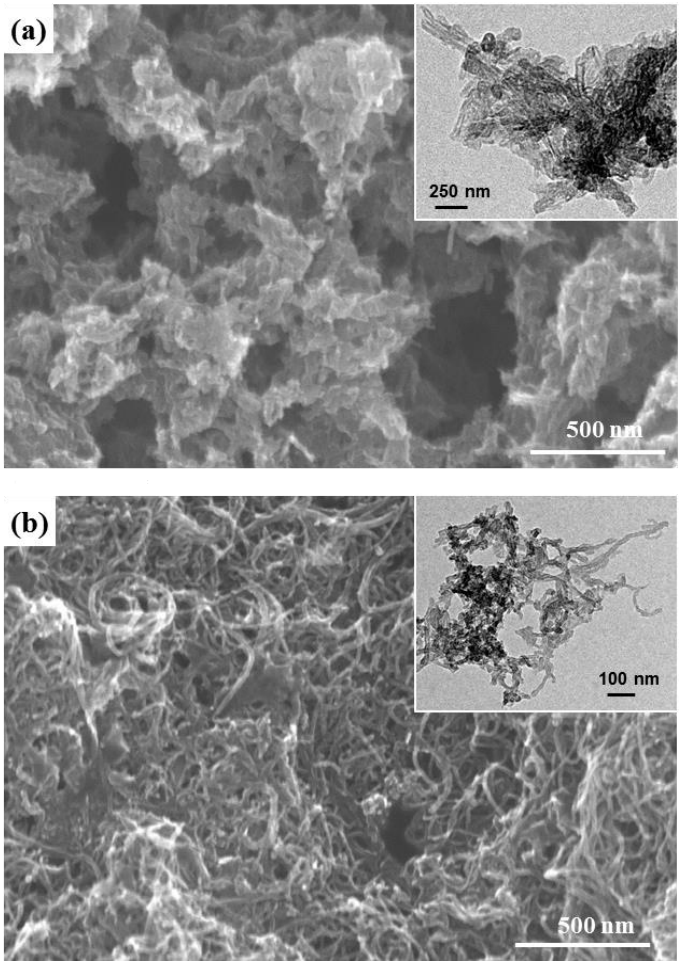

Figure 2-19. Microstructure of the CNTs after dissolving Al-Cu matrix (a) SEM micrograph of CNTs from the ATCNT/Al-Cu nanocomposites, and (b) SEM micrograph CNTs from the PCNT/Al-Cu nanocomposites.

3-2-3. Mechanical properties of CNT/Al-Cu nanocomposite fabricated by spark plasma sintering process

The mechanical properties of CNT/Al-Cu nanocomposite were characterized by tensile test using. Figure 2-20 shows the stress-strain curves of CNT/Al-Cu nanocomposite with content and type of CNT. The strength of nanocomposites increases with increasing content of CNT and elongation decreases. As can be seen Figure 2-21 of fracture surface micrograph, some CNTs were pulled out after tensile test.

The yield strength of CNT/Al-Cu nanocomposite from stress-strain curves and elastic moduli are shown in Figure 2-20 (a), (b) and Table 2-2. The yield strength of 4 vol.% ATCNT/Al-Cu nanocomposites increases 3.4 times (from 110 MPa of Al-Cu to 376 MPa) and ultimate tensile strength also increases 2 times (from 237 MPa to 494 MPa) of Al-Cu, which was fabricated by same process without addition of CNTs. PCNT/Al-Cu nanocomposites show similar tendency with ATCNT/Cu nanocomposites. The yield strength and ultimate tensile strength increase 3.5 times and 2 times of Al-Cu. It is very interesting result that the strengthening effect of CNT is same regardless of CNT type (ATCNT, PCNT). However, elastic moduli of CNT/Al-Cu nanocomposite show different increase with type of CNT. At PCNT/Al nanocomposite, elastic modulus increases by 30% with 4 vol.% CNT (93 GPA compared to 73 GPa), but in case ATCNT/Al nanocomposite, the increase of elastic modulus with increasing content of CNTs is less than that of PCNT/Al.

The grain sizes of CNT/Al-Cu composite were controlled by variation of additional heat treatment time (Figure 2-22). The stress-strain curves of the Al-Cu matrix and the PCNT/Al-Cu nanocomposites with different grain sizes are shown in Figure 2-23 and in Table 2-3. The yield strength of both the Al-Cu matrix and the PCNT/Al-Cu nanocomposites increased with decreasing Al-Cu matrix grain size. This result reveals that the CNT/Al-Cu nanocomposites are hardened by the addition of CNTs accompanied with grain refinement of the Al-Cu matrix, like other CNT reinforced metal matrix composites.

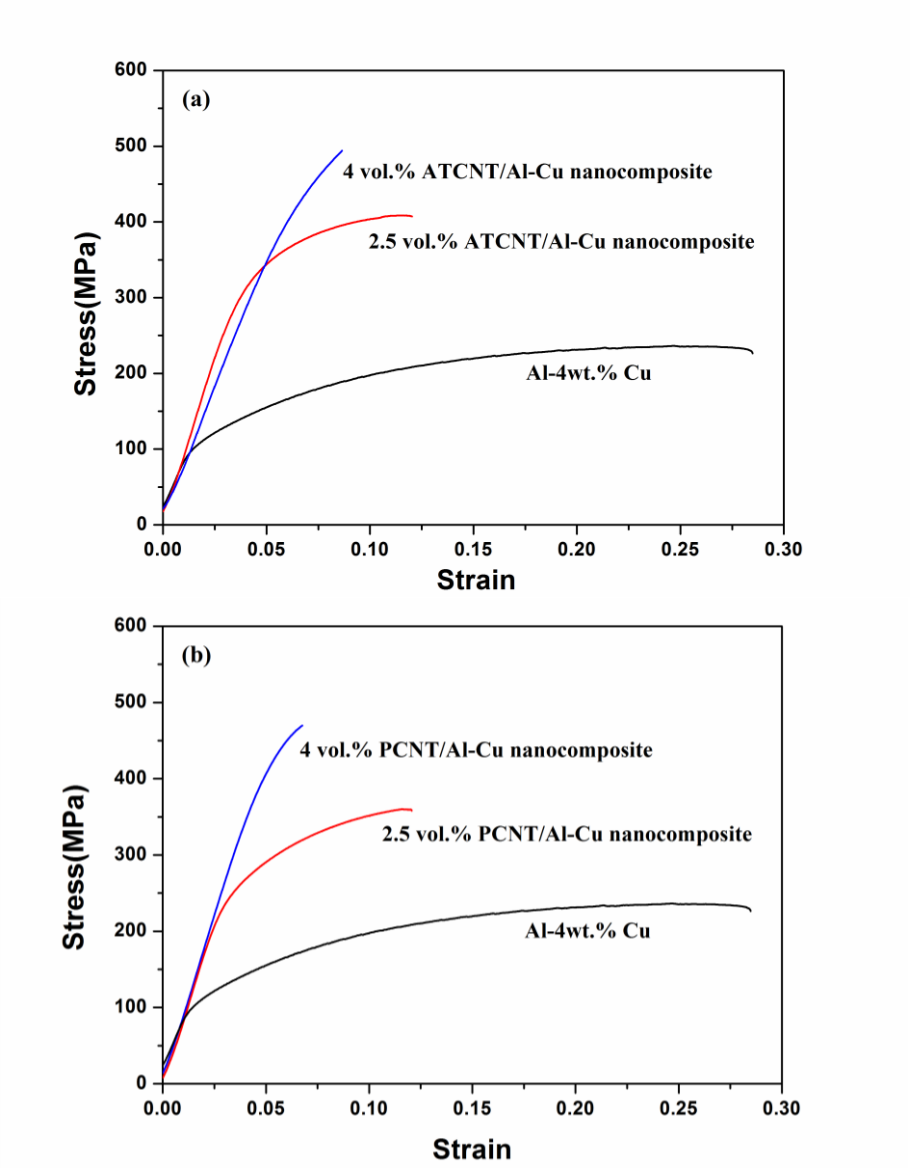

Figure 2-20. Mechanical properties of the CNT/Al-Cu nanocomposites. (a) stress-strain curves of the ATCNT/Al-Cu nanocomposites, (b) stress-strain curves of the PCNT/Al-Cu nanocomposites.

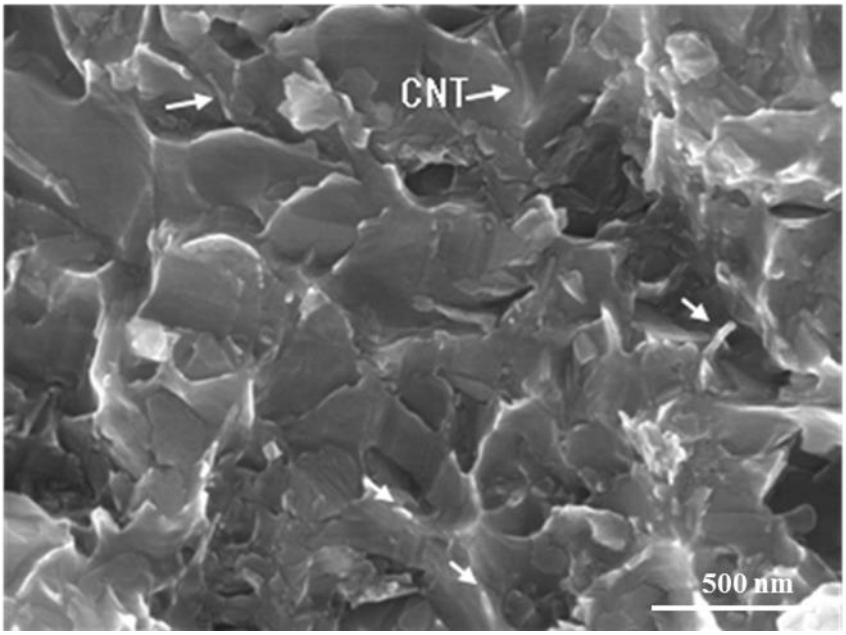

Figure 2-21. Fracture surface of CNT/Al-Cu nanocomposites. Some CNTs are pulled out after tensile test.

CNT	Vol % of CNTs	Relative Density (%)	Yield Strength (MPa)	Ultimate Tensile Strength (MPa)	Elastic Modulus (GPa)
	0	99.2	110 ± 7	237 ± 15	73 ± 1.2
ATCNT	2.5	99.8	301 ± 3	409 ± 22	80 ± 2.1
	4	98.1	376 ± 11	494 ± 14	79 ± 1.9
PCNT	2.5	99.3	255 ± 11	365 ± 9	84 ± 1.3
	4	99.1	384 ± 6	470 ± 13	93 ± 0.8

Table 2-2. The relative density and the mechanical properties of the CNT/Al-Cu nanocomposites.

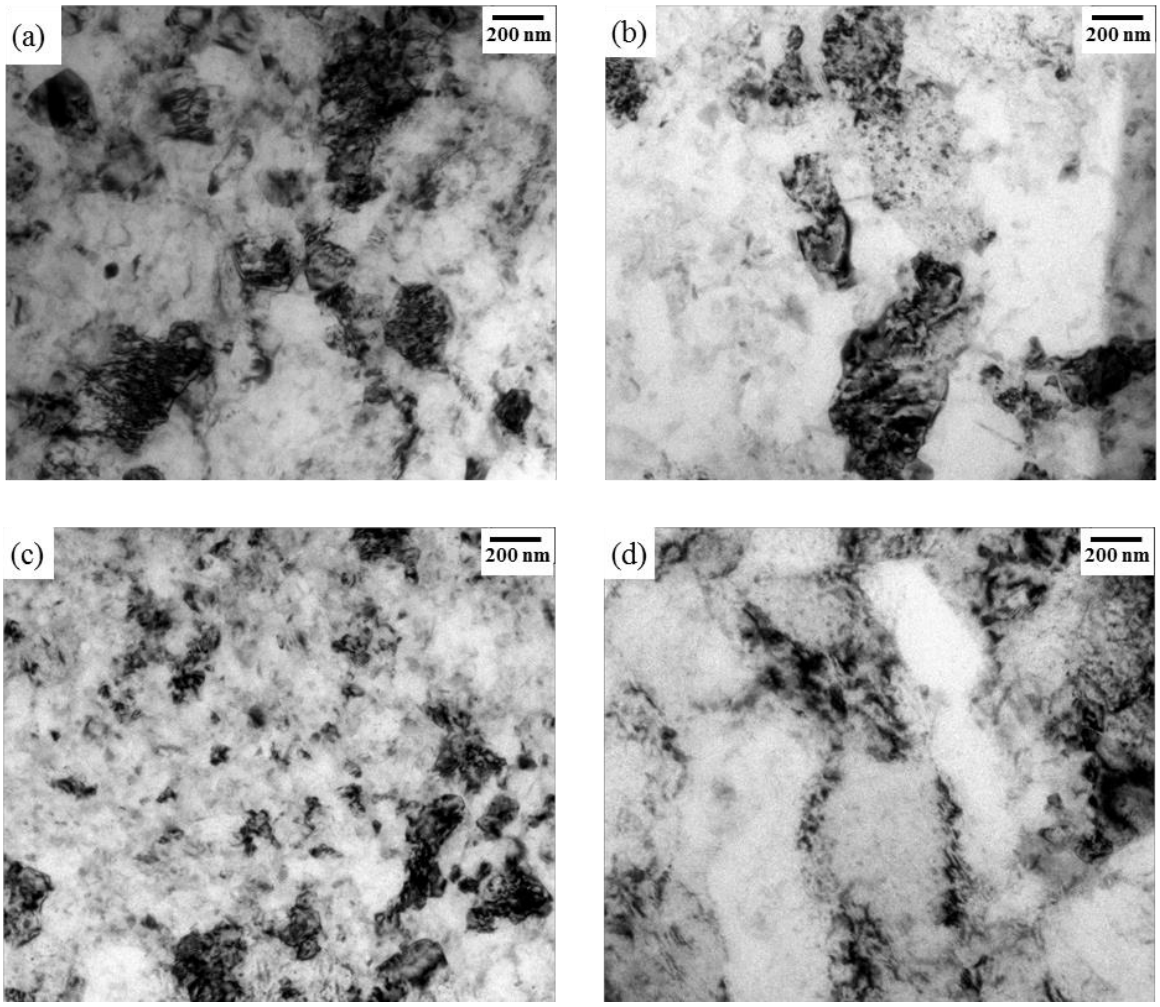

Figure 2-22. TEM micrographs of the PCNT/Al-Cu nanocomposites. (a) 2 vol.% PCNT/Al-Cu nanocomposite after heat treated at 500 ℃ for 2 hours, (b) 2 vol.% PCNT/Al-Cu nanocomposite after heat treated at 500 ℃ for 48 hours, (c) 4 vol.% PCNT/Al-Cu nanocomposite after heat treated at 500 ℃ for 2 hours and (d) 4 vol.% PCNT/Al-Cu nanocomposite after heat treated at 500 ℃ for 48 hours.

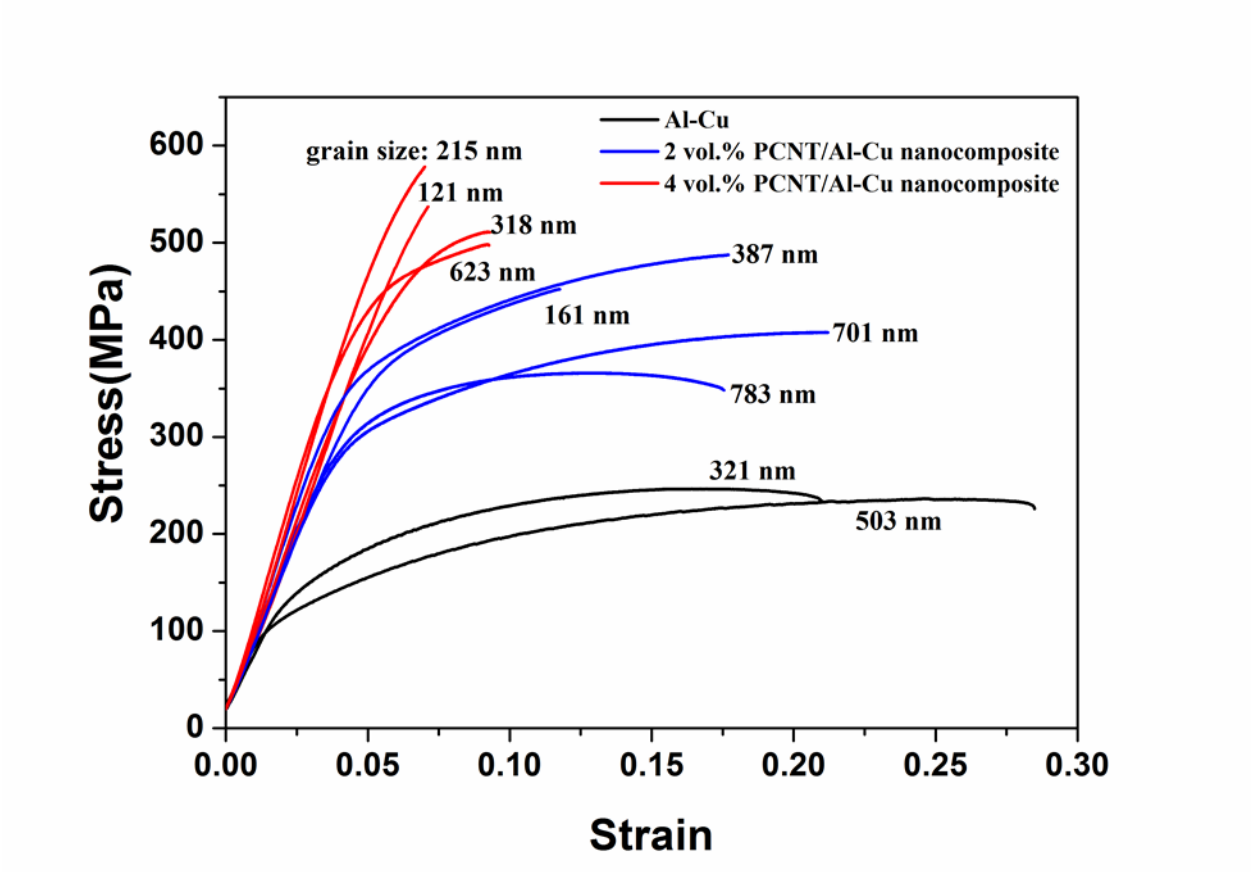

Figure 2-23. Stress-strain curves of Al-Cu matrix and PCNT/Al-Cu composites with different grain sizes.

Sample	Heat Treatment Time (h)	Average Grain Size (nm)	Yield Strength (MPa)
Al-Cu	-	747 ± 73	110
	-	312 ± 57	143
2 vol.% PCNT/Al-Cu	48	783 ± 107	270
	24	701 ± 62	279
	12	386 ± 96	306
	2	161 ± 52	346
4 vol.% PCNT/Al-Cu	48	624 ± 84	364
	24	318 ± 64	389
	12	215 ± 41	446
	2	122 ± 39	485

Table 2-3. The grain size and the yield strength of the CNT/Al-Cu nanocomposites.

3-2-4. Characterization of precipitation hardened CNT/Al-Cu nanocomposite

3-2-4-1. Precipitation hardening behavior of CNT/Al-Cu nanocomposite

Most Al alloys are used for structural applications after heat treatment and for further working processes in industry. Thus, more understanding of the effect of CNTs on the microstructure and mechanical properties of Al alloys during heat treatment is needed in order to apply CNT/Al-Cu nanocomposites to structural applications. In precipitation hardened Al-Cu alloys, five sequential structures can be identified: supersaturated solid solution, GP1 zones, GP2 zones (θ″phase), θ′ phase, θ phase ($CuAl_2$). The general sequence of precipitation in binary Al-Cu alloys can be presented by Supersaturated solid solution → GP1 zones → GP2 zones (θ″phase) → θ′ phase → θ phase ($CuAl_2$) [103]

In this research, the effect of CNTs on the precipitation hardening behavior of Al-Cu alloys during aging heat treatment was investigated. Analyses of the mechanical properties and microstructure of the CNT/Al-Cu composites, with heat treatment and content of CNTs, were carried out in order to discuss the effect of CNTs. Figure 2-24 is a phase diagram of Al-Cu binary system. The CNT/Al-Cu nanocomposites were solution heat treated at 550 ℃ for 12 hours and quenched in a water bath at room temperature. They were then cold rolled to achieve 5% plastic deformation. The CNT/Al-Cu composites were aged at 130 ℃ for 0 to 24 hours.

The hardness of the CNT/Al-Cu nanocomposites with aging time measured by Vickers hardness test is shown in Figure 2-25. The hardness of Al-Cu alloy increase gradually and reaches a maximum value after 9 h aging. After 9 h aging, the hardness decreases with increasing aging time. However, the hardness of the CNT/Al-Cu nanocomposites increases during the early stages of aging. The maximum hardness of the CNT/Al-Cu nanocomposites was obtained after 3 hours aging, compared to 9 hours of aging for Al-Cu. As can be seen in Figure 2-25, the hardness of CNT/Al-Cu nanocomposites increased with increasing volume fraction of the CNTs both before and after the aging. The hardness of the 4 vol.% CNT/Al-Cu nanocomposites is two times higher than the value of the Al-Cu alloy (181.2 HV compared to 79.8 HV). After aging, the hardness also increased from 102.9 to 193.8 HV. From these results, it can be seen that the addition of CNTs increases the hardness and accelerates the precipitation hardening behavior of the Al-Cu matrix.

Figure 2-26 shows the TEM microstructure of the CNT/Al-Cu nanocomposites and the Al-Cu alloy with aging time. In the case of the Al-Cu alloy (as shown in Figure 2-26 (a)), θ″

precipitates (disk shape) were observed after 3 hours aging and the volume fraction and the size of the θ″ precipitates increased with increasing aging time until 24 hours. After 72 hours aging, θ′ precipitates were observed and θ″ precipitates were found to have disappeared. However, 2 vol.% CNT/Al-Cu nanocomposites show different behavior as can be seen in Figure 2-26 (b). The volume fraction of θ″ precipitates rapidly increased after 12 hours aging and θ″ precipitates were observed after 24 hours aging. In Figure 2-26 (c), the 4 vol.% CNT/Al-Cu nanocomposites can be seen to have a more accelerated precipitation behavior. After 12 hours aging, θ″ precipitates were observed. This accelerated precipitation behavior mainly results in a different hardening behavior for the CNT/Al-Cu nanocomposites compared to that of the Al-Cu alloy matrix. In general, particle or whisker type reinforcements can affect the precipitation behavior of the matrix. This is because of the mismatch in the coefficient of thermal expansion (Δα) between the reinforcement and the matrix. During the solution heat treatment and quenching process, many excess dislocations are generated due to the mismatch in the Δα; these excess dislocations can act as heterogeneous nucleation sites of precipitates and as a diffusion path of the Cu atoms. The excess dislocation density ρ generated due to the Δα between the reinforcement and the matrix can be calculated by the theoretical model proposed by Arsenalult & Shi, as follows,

$$\rho = \frac{BV_f \Delta\alpha \Delta T}{b(1-V_f)} \frac{1}{t} \tag{2}$$

where B is a geometric constant (B=10 for fibers), V_f is the volume fraction of reinforcement, ΔT is the temperature variation, b is the length of the Burgers vector and t is the smallest dimension of the reinforcement. The coefficient of thermal expansion of the CNTs is ~10^{-6}·K^{-1} and that of Al is 23.6 ×10^{-6}·K^{-1}. Thus, the calculated excess dislocation density generations are 4.3×10^{14} m^{-2} and 8.7×10^{14} m^{-2} in 2 vol.% and 4 vol.% CNT/Al-Cu nanocomposites, respectively. Figure 2-27 shows a comparison of dislocation density between the Al-Cu alloy and the CNT/Al-Cu nanocomposites. It can be seen that the dislocation density of the CNT/Al-Cu nanocomposites is much higher than that of the Al-Cu alloy and precipitates have formed on these dislocations. These generated dislocations affect the age-hardening behavior in the CNT/Al-Cu nanocomposites.

3-2-4-2. Mechanical properties of precipitation hardened CNT/Al-Cu nanocomposite

The yield strength and tensile strength of the Al-Cu alloy and CNT/Al-Cu nanocomposites with volume fraction of CNTs and aging are shown in Figure 2-28 and Table 2-4. The aging

condition is confirmed as the factor that determines when the hardness values reach a maximum (Al-Cu is 9 hours and that for CNT/Al-Cu composites is 3 hours). From the mechanical properties of the CNT/Al-Cu nanocomposites, we can obviously see the strengthening effect of CNT addition. The yield strength increased from 110 MPa to 384 MPa in 4 vol.% CNT/Al-Cu nanocomposites and the tensile strength also increased by two times. The mechanical properties of the CNT/Al-Cu nanocomposites, after aging, show a similar increase to the one that occurred before aging. The yield strength increased from 201 MPa to 450 MPa and the tensile strength increased by two times. This result means that the strengthening of the CNT/Al-Cu nanocomposites is mainly due to the addition of CNTs and the precipitation hardening of the Al-Cu alloy matrix.

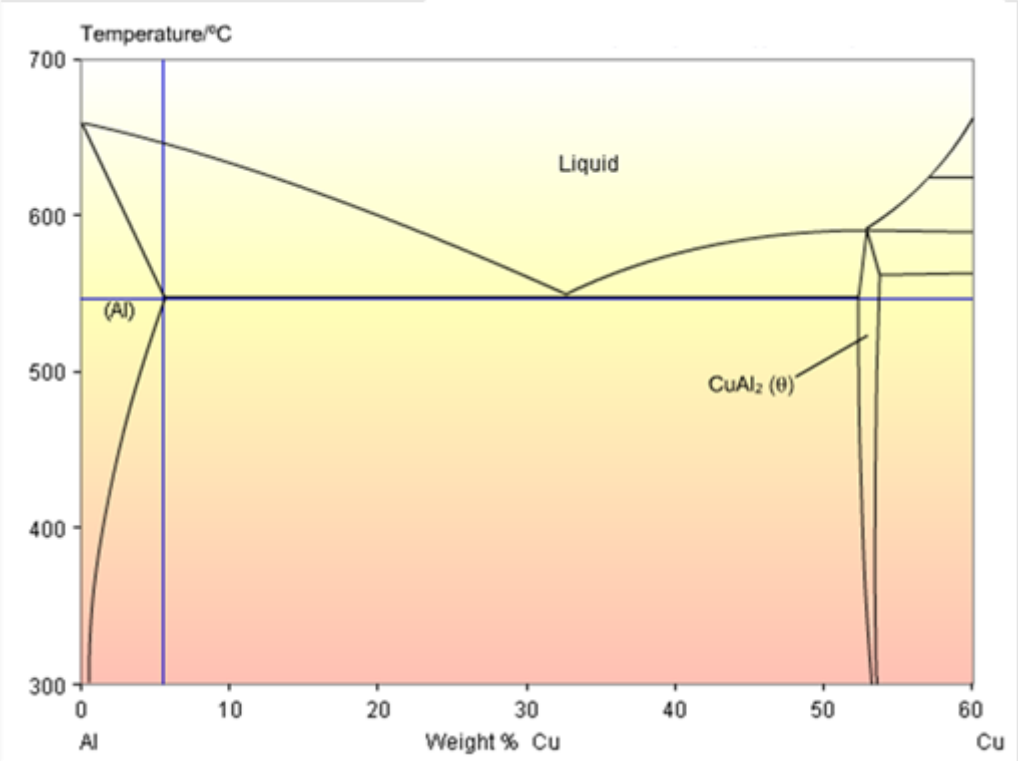

Figure 2-24. Phase diagram of Al-Cu binary system.

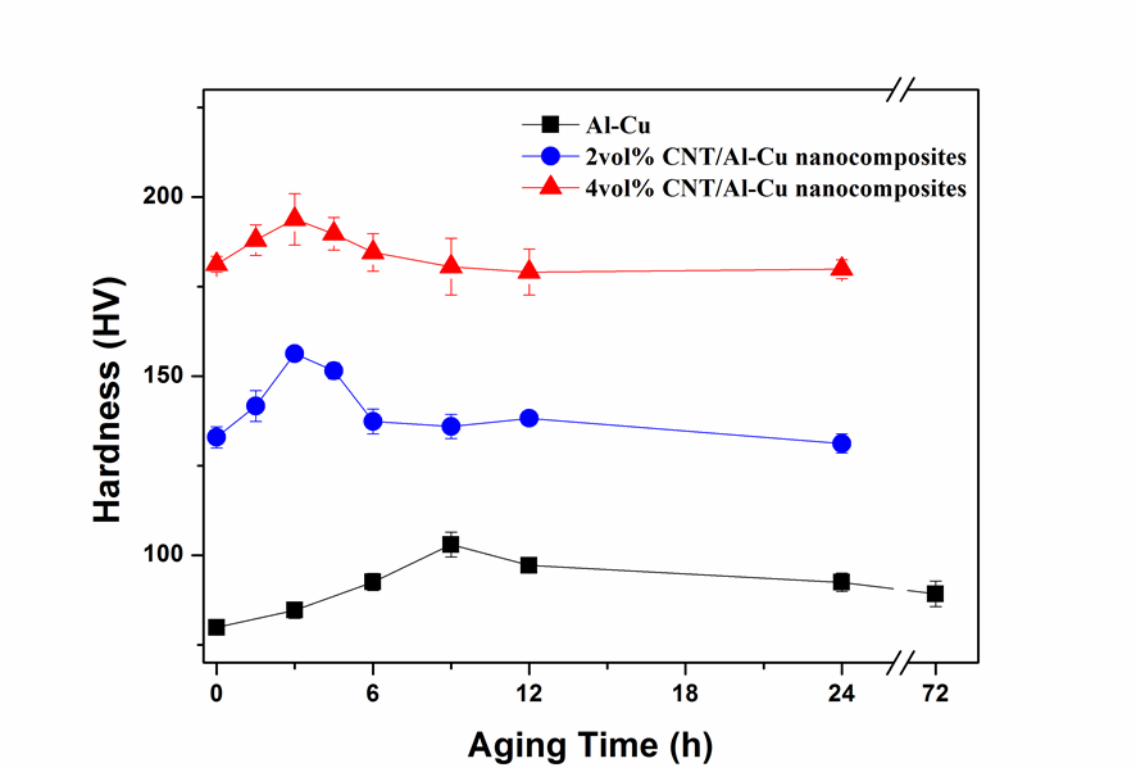

Figure 2-25. Aging behavior of the Al-Cu alloy and CNT/Al-Cu composites with varying of aging time.

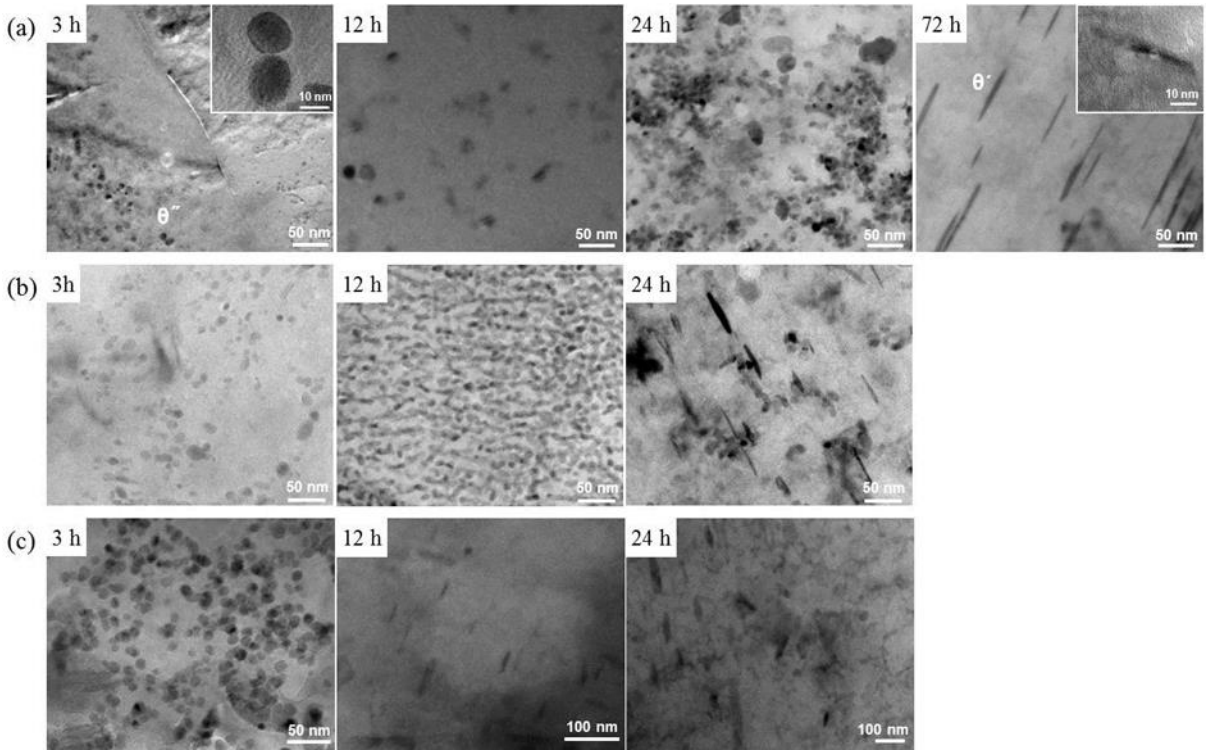

Figure 2-26. TEM micrograph of precipitates with aging time (a) Al-Cu alloy, (b) 2 vol.% CNT/Al-Cu nanocomposites, and (c) 4 vol.% CNT/Al-Cu nanocomposites.

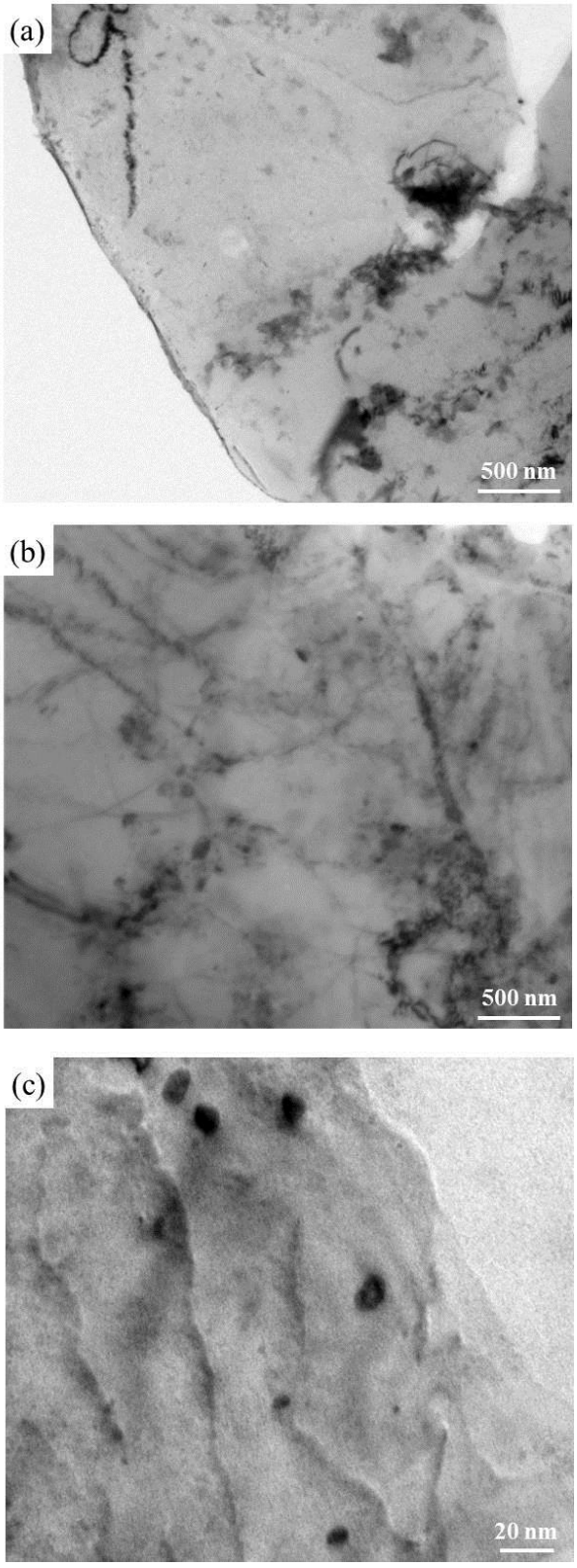

Figure 2-27. TEM micrograph comparing dislocation density of the Al-Cu alloy and that of the CNT/Al-Cu nanocomposites (a) Al-Cu alloy, (b) 2 vol.% CNT/Al-Cu nanocomposites, and (c) high magnification image of (b).

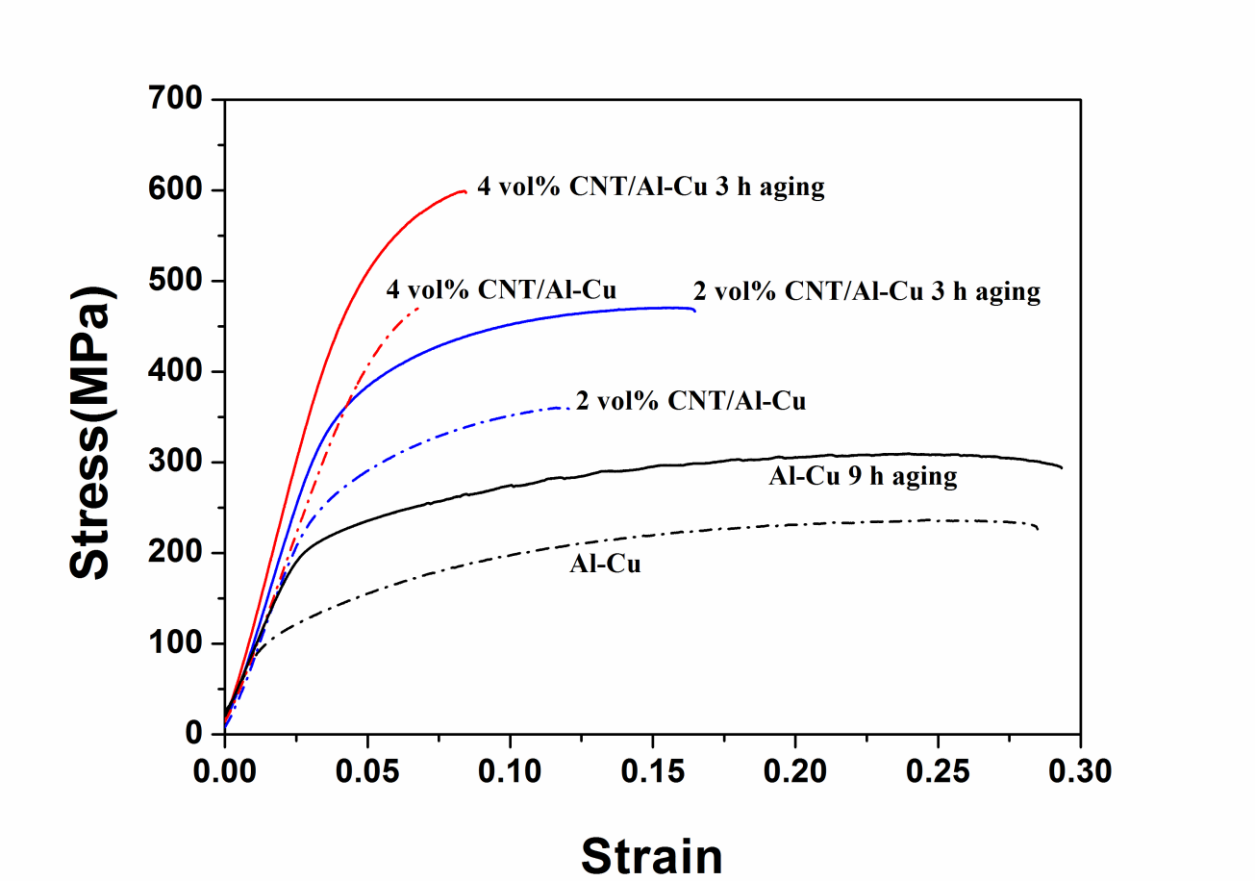

Figure 2-28. Stress-strain curves of CNT/Al-Cu nanocomposites after aging.

Vol % of CNTs	Heat Treatment	Hardness (HV)	Yield Strength (MPa)	Ultimate Tensile Strength (MPa)
0	-	79.8 ± 2.1	110 ± 7	237 ± 15
0	9 h aging	102.9 ± 3.5	201 ± 11	309 ± 16
2	-	132.9 ± 3.0	255 ± 11	365 ± 9
2	3 h aging	156.3 ± 1.8	337 ± 9	461 ± 13
4	-	181.2 ± 2.2	384 ± 6	470 ± 13
4	3 h aging	193.8 ± 7.1	450 ± 21	601 ± 15

Table 2-4. The mechanical properties of the CNT/Al-Cu nanocomposites after aging.

3-2-5. Analysis of mechanical behavior of CNT/Al-Cu nanocomposite

3-2-5-1. Effect of CNTs on elastic modulus of CNT/Al-Cu nanocomposite

The elastic modulus of CNT reinforced nanocomposites can be calculated by the shear-lag model, which is derived from the load-transfer theory between a matrix and misaligned fiber reinforcements under assumption of perfect bonding at interface, as follows:

$$E_c = V_f E_f \left(1 - \frac{\tanh(nS_{eff})}{ns}\right) + (1 - V_f) E_m \tag{3}$$

$$n = \sqrt{\frac{2E_m}{E_f (1+\nu_m) \ln(1/V_f)}} \tag{4}$$

$$S_{eff} = S\cos^2\theta + \left(\frac{3\pi - 4}{3\pi}\right)\left(1 + \frac{1}{S}\right)\sin^2\theta \tag{5}$$

where, V_f is the volume fraction of CNTs, E_f is the elastic modulus of CNTs (E_f=800 GPa), E_m is the elastic modulus of the Al-Cu matrix, θ is the misorientation angle between the longitudinal axis of the CNTs and the loading axis of the tensile test, S is the aspect ratio of the CNTs and S_{eff} is the effective aspect ratio of the CNTs. The effective aspect ratio of CNTs is half of the aspect ratio of the CNTs, when CNTs are randomly distributed (S_{eff}=1/2S). The comparison between the measured and the calculated mechanical properties of CNT/Al-Cu nanocomposite is shown in Figure 2-29. The estimated elastic moduli of PCNT/Al nanocomposite match with measured value of nanocomposites, when effective aspect ratio of CNT is 30. These estimated aspect ratios are well match with real aspect ratio of CNTs in nanocomposites, as shown in previous microstructure of CNTs after dissolving Al matrix of CNT/Al nanocomposite by NaOH. From this good agreement between the estimated and measured values, it is considered that the increase of the elastic modulus is mainly due to an efficient load transfer from the Al-Cu matrix to the CNTs. However, in case of ATCNT/Al-Cu nanocomposites, load transfer from the Al-Cu matrix to the CNTs did not occur because of low aspect ratio of ATCNT. Thus, it is considered that there is a critical aspect ratio of CNT for effective load transfer.

3-2-5-2. Strengthening by addition of CNTs

As discussed previous chapter, the yield strengths of the CNT/Al-Cu nanocomposites are almost the same regardless of the aspect ratio of the CNTs. This indicates that the strengthening mechanism of the CNT/Al-Cu nanocomposites varied with the aspect ratio of

the CNTs and the increase of yield strength can be contributed to not only the load transfer from the Al-Cu matrix to the CNTs, but also to a dislocation related strengthening mechanism such as Orowan looping or thermal mismatch between CNTs and the Al-Cu matrix. The dispersion strengthening is expected as a dominant strengthening mechanism for the ATCNT/Al-Cu nanocomposites, because the ATCNTs have low aspect ratio and behave as dispersed particles rather than load transfer constituents. In the case of the PCNT/Al-Cu nanocomposites, load transfer is the more dominant strengthening mechanism. It is considered that the major strengthening mechanism of CNT/Al-Cu nanocomposites has changed from dispersion strengthening to a load transfer mechanism with increasing the aspect ratio of the CNTs. This is a very important result for understanding the strengthening mechanism of CNT/Metal nanocomposites. The yield strength of the fiber reinforced composites can be estimated with the shear-lag model based on the load transfer theory as follows,

$$\sigma_c = \sigma_m(1 + S_{eff}V_f) \tag{6}$$

where σ_c is the yield strength of composites and σ_m is the yield strength of matrix. The increase of yield strength by dispersion strengthening can be expressed as follows,

$$\Delta\sigma = \frac{0.13GbV_f^{1/2}}{r}\ln(\frac{2r}{r_0}) \tag{7}$$

where *b* is Bugers vector, r_0 is the core radius of dislocation, r is the volume equivalent radius of CNTs and G is modulus of rigidity of matrix. By comparing the measured yield strength with the calculated yield strength, we can estimate which mechanism is dominant.

3-2-5-3. Strengthening by grain refinement of Al-Cu matrix

In general, yield strength of polycrystalline metal is dependent on its grain size; it is known as Hall-Petch relation as follows,

$$\sigma_m = \sigma_0 + kd_m^{-1/2} \tag{8}$$

where σ_m is the yield strength of the matrix, σ_0 is the frictional stress, k is a strengthening coefficient and d_m is the grain size of the matrix. The yield strength increase of the CNT/Al-Cu nanocomposites is thought to originate from a combination of CNT addition effect and grain refinement of the Al-Cu matrix; the effect of CNT addition on the increase yield strength is much higher than that of the grain refinement predicted from the Hall-Petch relationship. One interesting thing is that the k values (slopes in Figure 2-30) of the

PCNT/Al-Cu nanocomposites increase with increasing CNT content. From Equations (6) and (8),

$$\sigma_c = \sigma_0' + k' d_m^{-1/2} = \left(\sigma_0 + k d_m^{-1/2}\right)\left(1 + \frac{S_{eff}}{2} V_f\right) \quad (9)$$

$$\sigma_0' = \sigma_0\left(1 + \frac{S_{eff}}{2} V_f\right) \quad (10)$$

$$k' = k\left(1 + \frac{S_{eff}}{2} V_f\right) \quad (11)$$

Thus, σ_0 and k depend on the volume fraction and the aspect ratio of the reinforcement. In CNT/Al-Cu nanocomposites, both σ_0 and k values increase with the volume fraction of CNTs, as can be seen in Table 2-5. This indicates that the addition of CNTs increased the effect of grain refinement due to the load transfer from the Al-Cu matrix to the CNTs.

3-2-5-4. Strengthening by precipitation hardening of Al-Cu matrix

Figure 2-31 shows a comparison of the yield strength with the volume fraction of CNTs and aging. Both the yield strength of the Al-Cu alloy and that of the CNT/Al-Cu nanocomposites increased after aging and the increase rate of yield strength with volume fraction of CNTs after aging is almost the same as that before aging. After precipitation heat treatment, distance between the CNTs is larger than distance between the precipitates. Thus, we can ignore the dispersion strengthening by CNTs and the yield strength of composite materials can be calculated by the generalized shear-lag model. Equation (10) can be expressed as follows,

$$\sigma_c/\sigma_m - 1 = V_f S_{eff} \quad (12)$$

From equation (12), we can calculate the S_{eff} from the slope of the graph of σ_m/σ_m-1 vs V_f. From Figure 2-32, the S_{eff} can be seen to correspond to a value of 31, which is almost the same as the actual aspect ratio of CNTs as determined in the microstructural analysis in our previous result. Thus, it can be thought that the CNT/Al-Cu nanocomposites were strengthened by both the load transfer from the Al-Cu matrix to the CNTs and by precipitation hardening of the Al-Cu matrix.

3-2-5-5. Strengthening mechanisms of CNT/Al-Cu nanocomposite

The strengthening effect of CNTs in Al-Cu nanocomposites was clearly confirmed in this research and it is thought that CNT/Al-Cu nanocomposites were strengthened by various

strengthening mechanisms such as load transfer from Al-Cu matrix to CNTs, dispersion strengthening, grain refinement associated strengthening and precipitation strengthening. The details are summarized as follows,

1) Strengthening by load transfer mechanism

The enhancement of elastic modulus of CNT/Al-Cu nanocomposites was analyzed by shear-lag model, which is based on load transfer theory, considering the aspect ratio of CNTs. From good agreement between the estimated and measured elastic modulus, it is confirmed that the mechanical properties of CNT/Al-Cu nanocomposites are enhanced because CNTs are sharing the load transferred from Al-Cu matrix. However, when the aspect ratio of CNT is less than some critical value, efficient load transfer from the Al-Cu matrix to the CNTs did not occur.

2) Dispersion strengthening mechanism

In this mechanism, CNTs inhibit the dislocation movement and increase the Al-Cu matrix. The dispersion strengthening expected as a dominant strengthening mechanism when aspect ratio of CNT is small. CNTs with small aspect ratio could behave as dispersed particles rather than load transfer constituents.

3) Grain refinement strengthening

It is confirmed that the strength of CNT/Al-Cu nanocomposites is deeply related to the addition of CNTs and grain size refinement of Al-Cu matrix. As Al-Cu matrix grain size decreased, the strength of CNT/Al-Cu nanocomposites increased according to the Hall-Petch relationship. It is thought that the addition of CNTs increased the effect of grain refinement due to the load transfer from the Al-Cu matrix to the CNTs

4) Precipitation strengthening

The CNT/Al-Cu nanocomposites, after aging heat treatment, showed significant increase of strength due to precipitation strengthening of Al-Cu matrix. Precipitates, which are formed during aging heat treatment, resist dislocation penetration considerably and increase the strength of matrix. The increase rate of the yield strength with volume fraction of CNTs is similar to that which occurred before aging. It is thought that the CNT/Al-Cu nanocomposites were strengthened by the addition of CNTs and by precipitation strengthening of the Al-Cu matrix.

As a result, the strengthening mechanism of the CNT/Al–Cu nanocomposites is a

synergistic effect of load transfer from matrix to the CNTs, dispersion strengthening mechanism, grain refinement strengthening of the Al–Cu matrix and precipitation strengthening mechanism. From the comparison between the measured yield strength and the calculated yield strength of CNT/Al-Cu nanocomposites, as can be seen in Table 2-6 and the summary of strengthening mechanism in Figure 2-33, it is considered that the major strengthening mechanism of CNT/Al-Cu nanocomposites is to a load transfer mechanism.

In summary, CNTs were homogeneously dispersed in CNT/Al-Cu nanocomposite and CNT showed strong reinforcing effect in Al-Cu matrix. Moreover, mechanical properties of CNT/Al-Cu nanocomposite were further increased by precipitation hardening. Therefore, since Al is a lightweight material, CNT/Al-Cu nanocomposite is expected to be applied in body of airplane or cars, which requires high strength and lightweight.

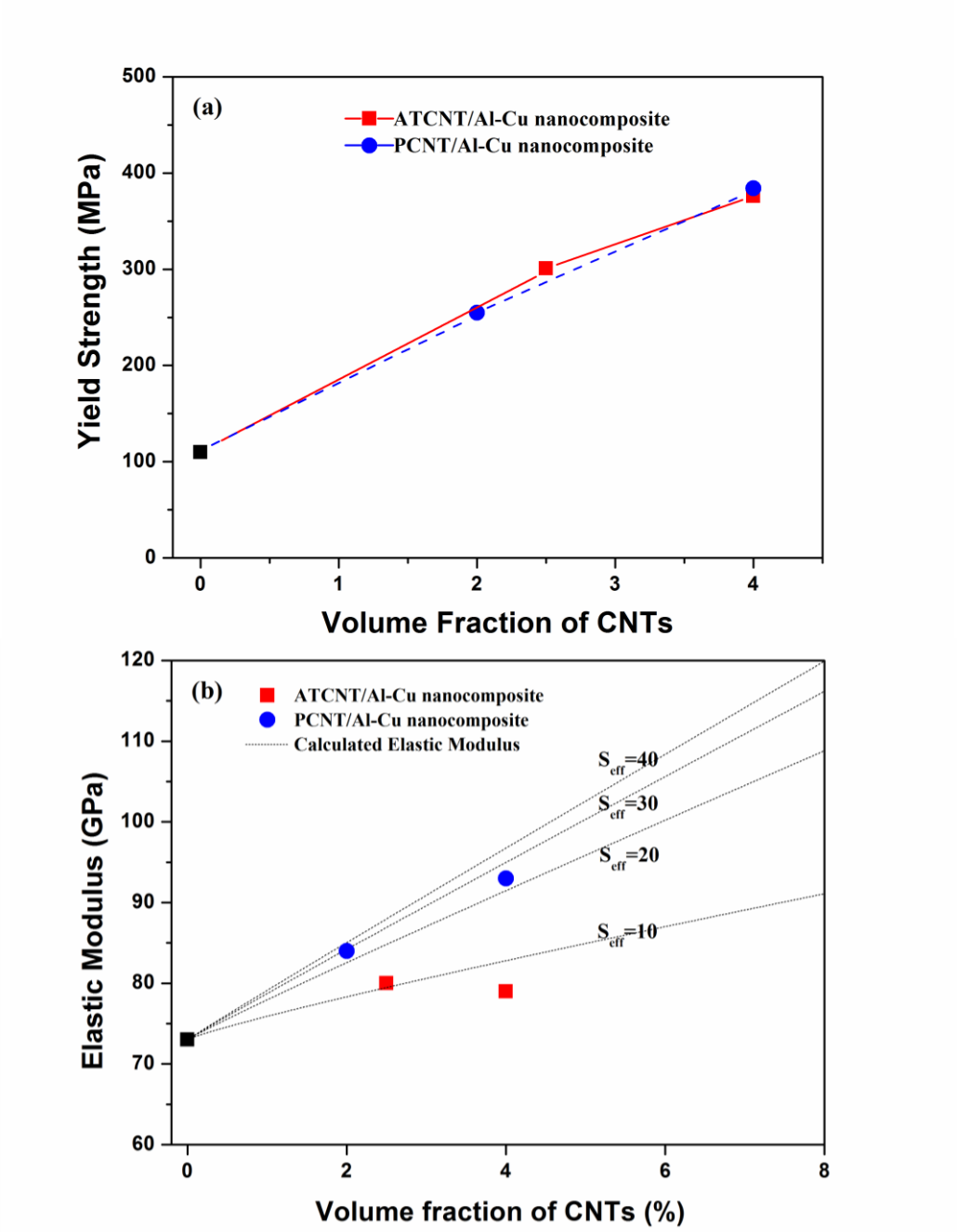

Figure 2-29. Mechanical properties of the CNT/Al-Cu nanocomposites. (a) yield strength of PCNT/Al-Cu and ATCNT/Al-Cu nanocomposites with volume fraction of CNTs, (b) elastic modulus of PCNT/Al-Cu and ATCNT/Al-Cu nanocomposites with volume fraction of CNTs and comparison with the calculated elastic modulus.

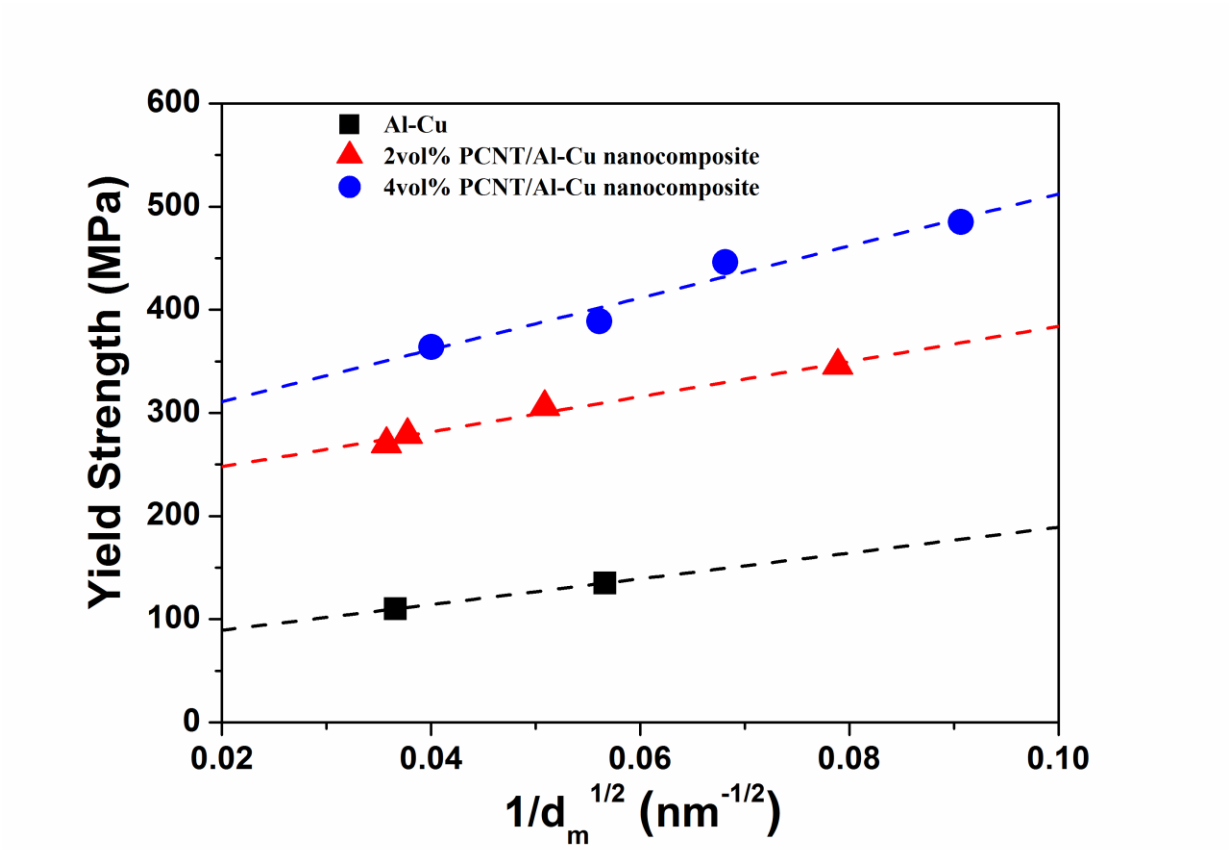

Figure 2-30. Hall-Petch relationship of Al-Cu and PCNT/Al-Cu nanocomposites.

Sample	Measured σ_0 (MPa)	Calculated σ_0 (MPa)	Measured k (MPa $m^{1/2}$)	Calculated k (MPa $m^{1/2}$)
Al-Cu	64.4	64	0.040	0.040
2 vol.% PCNT/Al-Cu	214	84	0.054	0.052
4 vol.% PCNT/Al-Cu	261	103	0.079	0.065

Table 2-5. The comparison between the measured and the calculated frictional stress and strengthening coefficient of the PCNT/Al-Cu nanocomposites

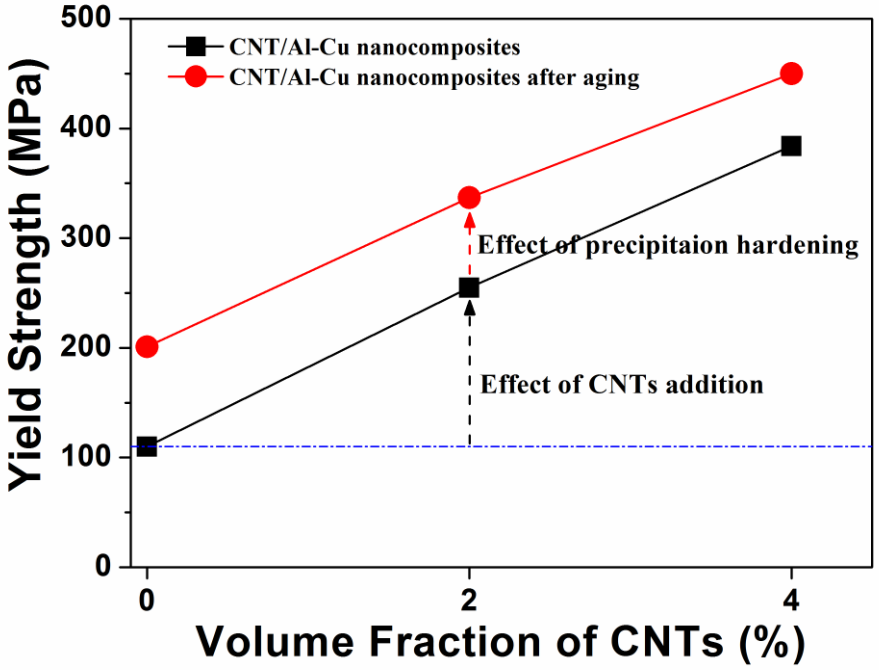

Figure 2-31. Yield strength of CNT/Al-Cu nanocomposites with volume fraction of CNTs and aging

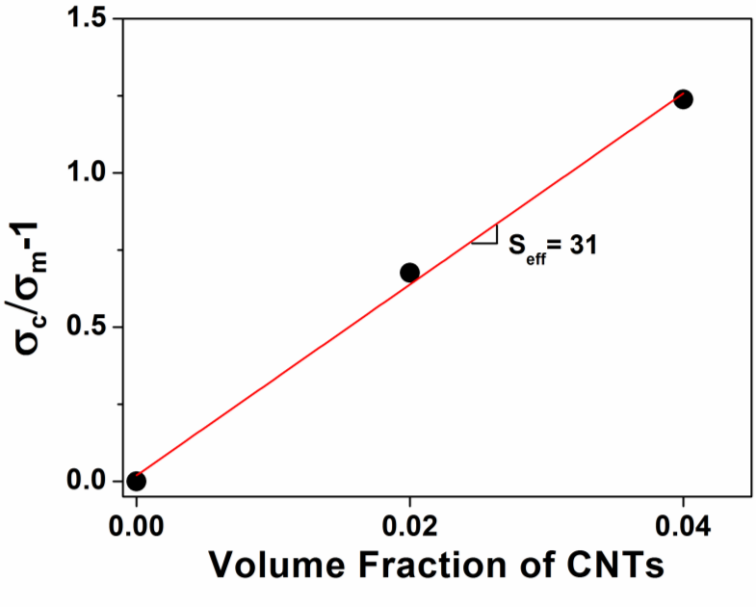

Figure 2-32. The effective aspect ratio of CNT/Al-Cu nanocomposites (slope of graph) after aging heat treatment derived from generalized shear-lag model

Sample	Measured Y.S. (MPa)	Calculated Y.S. (MPa)				
		Load Transfer	Dispersion Strengthening	Grain Refinement	Precipitation Hardening	Total
Al-Cu (aging)	201 (+91)	-	-	46	58	104
2 vol.% PCNT/Al-Cu (aging)	337 (+227)	55	28	51	78	212
4 vol.% PCNT/Al-Cu (aging)	450 (+340)	110	40	63	66	279

Table 2-6. The comparison between the measured and the calculated yield strength of PCNT/Al-Cu nanocomposites

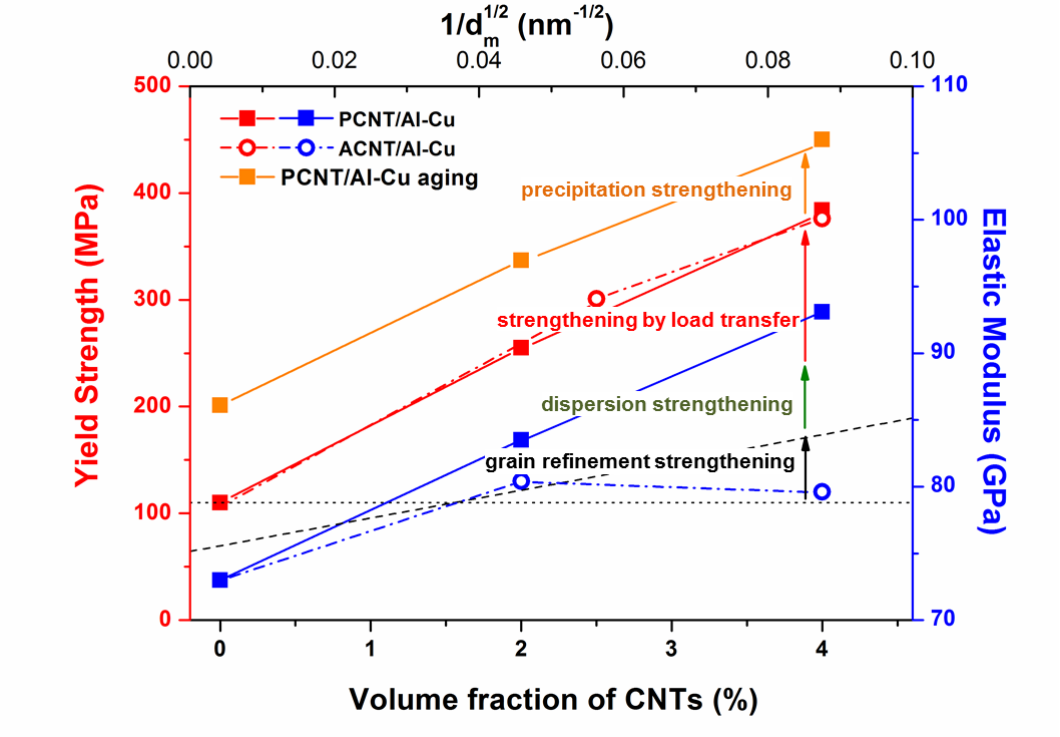

Figure 2-33. Strengthening mechanism of CNT/Al-Cu nanocomposite.

4. Summary

Fabrication process and consolidation of CNT/Cu and CNT/Ni nanocomposite powders were investigated in the 1st year of research. A novel process for the fabrication of CNT/Cu and CNT/Ni nanocomposite powders with homogeneous dispersion of CNTs, named as "molecular level mixing process", was developed. The phases, morphologies, distributions and interfaces have been characterized for the CNT/Cu and CNT/Ni nanocomposite powders fabricated by molecular level mixing process and sintered nanocomposites. The processing conditions to fabricate the CNT/Metal nanocomposites were optimized and established.

The 2nd year of research focusses on the microstructure and mechanical properties of CNT/Cu and CNT/Ni nanocomposite. An analysis on the strengthening mechanisms of CNT/Cu and CNT/Ni nanocomposites was also performed. The microstructures of the nanocomposites revealed that CNTs were homogeneously dispersed in Cu and Ni matrices. The mechanical properties of CNT/Cu and CNT/Ni nanocomposites were improved with higher CNT content. Also, fabrication process and microstructures of CNT/NiTi nanocomposite powders were investigated for possibility of CNT as reinforcement in NiTi shape memory alloy.

In the 3rd year of research, matrix systems were further extended to NiTi and Al-Cu systems by combining molecular level mixing process with high energy milling process. For the CNT/NiTi nanocomposite, both coated and uncoated CNTs were used for fabrication of CNT/NiTi nanocomposite powders and followed by spark plasma sintering. For the CNT/Al-Cu nanocomposite, CNTs were functionalized by acid treatment and PVA coating to investigate the effect of aspect ratio on mechanical properties of CNT/Al-Cu nanocomposite. CNT/Cu nanocomposite powders were fabricated by two types of CNTs: ACNT and PCNT, and were followed by high energy milling process with Al powders for fabrication of CNT/Al-Cu nanocomposite. The microstructure and mechanical properties of CNT/NiTi and CNT/Al-Cu nanocomposites were characterized and analyzed.

The major achievements of 1st, 2nd and 3rd year of research are summarized as follows.

4-1. Summary of the 1st year research

4-1-1. Fabrication process and analysis of microstructures of CNT/Cu nanocomposite powders

- Homogeneous CNT/Cu nanocomposite powders were fabricated by molecular level mixing process and controlled oxidation process.
- CNTs were uniformly dispersed in Cu matrix of CNT/Cu nanocomposite powders fabricated by molecular level mixing process and controlled oxidation process.
- CNT/Cu nanocomposite powders, which were fabricated by controlled oxidation process, showed lower oxygen contents, more uniform size and shape than those fabricated by molecular level mixing process.

4-1-2. Fabrication process and analysis of microstructure of CNT/Ni nanocomposite powders

- Homogeneous CNT/Ni nanocomposite powders were fabricated by direct reduction process.
- It was possible to obtain CNT/Ni nanocomposite powders without CNT/Ni-oxide intermediate state because of good wettability between CNT and Ni.
- It was observed that CNTs restricted the growth of particle size during the reduction process.

4-1-3. Consolidation process of CNT/Cu nanocomposite powders and analysis of microstructure of CNT/Cu nanocomposite

- CNT/Cu nanocomposite powders were fully densified by spark plasma sintering process at 550^{o}C under 50MPa.
- CNTs were uniformly dispersed and resulted in a formation of 3-dimensional network in Cu matrix of sintered CNT/Cu nanocomposite.
- Oxygen atoms, observed at interfaces between CNT and Cu matrix, could increase the interfacial bonding and enhance the load transfer by forming oxygen rich interphase at CNT/Cu interfaces.

4-1-4. Consolidation process of CNT/Ni nanocomposite powders and analysis of microstructure of CNT/Ni nanocomposite

- CNT/Ni nanocomposite powders were fully densified by spark plasma sintering at 800^{o}C under 50MPa.
- CNTs were homogeneously dispersed and resulted in a formation of 3-dimensional network in Ni matrix.
- Ni nanocrystals, located at interfaces between CNT and Ni matrix, increased the interfacial bonding and enhanced the load transfer from matrix to CNTs.

4-2. Summary of the 2nd year research

4-2-1. Characterization of microstructures and mechanical properties of CNT/Cu nanocomposite powders

- CNTs were uniformly dispersed and resulted in a formation of 3-dimensional network in Cu matrix of sintered CNT/Cu nanocomposite.
- The 10 vol.% CNT/Cu nanocomposite showed outstanding yield strength of 485 MPa and elastic modulus of 135 GPa which are 3 and 1.7 times higher than those of Cu, respectively.
- The CNTs were analyzed as the most effective strengthening reinforcement compared to other types of reinforcements: 8 times higher than that of SiC particles and 3 times higher than that of SiC whisker.

4-2-2. Characterization of microstructures and mechanical properties of CNT/Ni nanocomposite powders

- CNTs were homogeneously dispersed and resulted in a formation of 3-dimensional network in Ni matrix of CNT/Ni nanocomposite.
- The 10 vol.% CNT/Ni nanocomposite showed extraordinary yield strength of 700 MPa and elastic modulus of 238 GPa which are 4 and 1.5 times higher than those of Ni, respectively.
- Strengthening mechanisms of CNT/Ni nanocomposite are identified as composite strengthening by CNTs and grain refinement strengthening of Ni matrix.

4-2-3. Fabrication process and characterization of CNT/NiTi nanocomposite powders by using CNT/Ni nanocomposite powder

- A new fabrication process, i.e. molecular level mixing and high energy milling process, was developed for fabrication of CNT/NiTi nanocomposite powders with homogeneous dispersion of CNTs.
- CNTs were homogeneously dispersed in CNT/NiTi nanocomposite powders fabricated by high energy milling process of CNT/Ni nanocomposite powders, which were prepared by molecular level mixing process.
- CNTs were partially agglomerated in CNT/NiTi nanocomposite powders fabricated by high energy milling process of pristine CNTs and NiTi powders.

4-3. Summary of 3rd year research

4-3-1. Fabrication process and characterization of CNT/NiTi nanocomposite

- CNTs need to remain undamaged during fabrication process for effective strengthening effect as reinforcement in nanocomposite.
- Effects of coating of Ni, SiO_2 & TiO_2 on CNTs have been investigated to control the unwanted severe reaction between CNT with Ti.

4-3-1-1. Fabrication process and characterization of CNT/NiTi nanocomposite by using CNT/Ni nanocomposite powder

- CNT/NiTi nanocomposite powders, which was fabricated by a new fabrication process developed in 2nd year research, were consolidated by spark plasma sintering.
- TiC was formed by reaction of CNTs with Ti and reaction of Ni coating layer with NiTi matrix formed brittle Ni-rich phase (Ni_4Ti_3) during consolidation of CNT/NiTi nanocomposite powders by spark plasma sintering, resulting in a reduction of elongation.

4-3-1-2. Fabrication process and characterization of CNT/NiTi nanocomposite fabricated by using CNT/SiO_2 nanocomposite powder

- CNTs were uniformly coated by SiO_2 layer with thickness of 15-20 nm by sol-gel process.
- TiC was formed by reaction of CNTs with Ti and SiO_2 layer reacted with NiTi matrix, resulting in a formation of brittle silicide ($Ni_{16}Ti_6Si_7$) phase during spark plasma sintering of CNT/NiTi nanocomposite powder, which was fabricated by using

CNT/SiO_2 nanocomposite powder.

4-3-1-3. Fabrication process and characterization of CNT/NiTi nanocomposite fabricated by using CNT/TiO_2 nanocomposite powder

- CNTs were uniformly coated by TiO_2 layer with thickness of 10-15 nm by sol-gel process.
- TiC, formed by reaction between CNTs with Ti, and TiO_2 phase in CNT/TiO_2 nanocomposite powders reduced the elongation of CNT/NiTi nanocomposite to 4.9%.

4-3-1-4. Fabrication process and characterization of CNT/NiTi nanocomposite fabricated by using pristine CNT

- CNTs were homogeneously dispersed in CNT/NiTi nanocomposite powders by high energy milling process of pristine CNTs, Ni and Ti powders.
- CNT/NiTi nanocomposite powders were fully densified after consolidation by spark plasma sintering at 900°C for 5 mins under a pressure of 50 MPa.
- The 0.5 vol.% CNT/NiTi nanocomposite showed yield strength of 192 MPa and elastic modulus of 79 GPa, which are 1.3 times higher, compared to those of the NiTi.
- The 1 vol.% TiC/NiTi composite showed yield strength of 177 MPa and elastic modulus of 77 GPa, which is 7.8 % and 2.5 % lower, respectively, compared to those of the 0.5 vol.% CNT/NiTi nanocomposite, which indicates that CNTs showed excellent strengthening effect in NiTi matrix compared to TiC.

4-3-2. Fabrication processes and characterization of CNT/Al-Cu nanocomposite

4-3-2-1. Fabrication process of CNT/Al-Cu nanocomposite

- CNT/Al-Cu nanocomposite powders were fabricated by molecular level mixing process, and followed by high energy milling process with Al powders for homogeneous dispersion of CNTs.
- CNT/Al-Cu nanocomposite powders were fully consolidated above 99% of relative density by spark plasma sintering process at 500°C for 5 min under pressure of 50 MPa.
- CNT/Al-Cu nanocomposites were aged at 130°C for 3 hrs to investigate effect of CNTs on precipitation hardening after spark plasma sintering.

4-3-2-2. Characterization of microstructures and mechanical properties of CNT/Al-Cu nanocomposite

- The CNTs were homogeneously dispersed in Al-Cu matrix in spark plasma sintered CNT/Al-Cu nanocomposite.
- Aluminium carbide (Al_4C_3) was not formed due to a reduced damage of CNTs by controlling ball milling process for CNT/Al-Cu nanocomposite.
- The aged 4 vol.% PCNT/Al-Cu nanocomposite showed yield strength of 450 MPa and ultimate tensile strength of 601 MPa, which are 4.1 and 2.5 times higher than those of precipitation hardened Al-Cu.
- The addition of CNTs accelerated the precipitation due to excess dislocations, which were generated by a mismatch of the coefficients of thermal expansion between the CNTs and the matrix.

4-3-2-3. Strengthening mechanisms of CNT/Al-Cu nanocomposite

- Elastic modulus of PCNT/Al-Cu nanocomposite was higher than that of ATCNT/Al-Cu nanocomposite, which indicates that elastic modulus increases as aspect ratio of reinforcement increases.
- Strengthening behavior by CNTs in CNT/Al-Cu nanocomposite was shown independent regardless of grain size effect or precipitation strengthening of Al-Cu matrix.
- The strengthening of the CNT/Al-cu nanocomposites was found to be originated by a synergistic effects of loads transfer, dispersion strengthening, grain refinement strengthening and precipitation hardening mechanisms.

5. List of Publications

5-1. Papers published in peer-reviewed journals

1) B. K. Lim, J. W. Hwang, D. J. Lee, S. H. Suh, S. H. Hong, "Fabrication processes and multi-functional applications of carbon nanotube nanocomposites", Journal of Composite Materials, 46, 2012, pp. 1731-1737.

2) Dong. H. Nam, Seung I. Cha, Byung K. Lim, Hoon M. Park, Do S. Han, Soon H. Hong, "Synergistic strengthening by load transfer mechanism and grain refinement of CNT/Al-Cu composites", Carbon, 50, 2012, pp. 2417-2423

3) Dong. H. Nam, Yun K. Kim, Seung I. Cha, Soon H. Hong, "Effect of CNTs on precipitation hardening behavior of CNT/Al-Cu composites", Carbon, 50, 2012, pp. 4809-4814.

4) J. Y. Hwang, B.K. Lim, J. Tiley, R. Banerjee, S.H. Hong,. "Interface analysis of ultra-high strength carbon nanotube/nickel composites processed by molecular level mixing", Carbon, 57, 2013, pp. 282-287.

5) Walid M. Daoush and Soon H. Hong, "Synthesis of multi-walled carbon nanotube/silver nanocomposite powders by chemical reduction in aqueous solution", Journal of Experimental Nanoscience, 8, 2013, pp. 578-587.

5-2. Conference presentations without papers

1) K.T. Kim, B. K. Lim, S. H. Hong, “The role of interfacial structure in the thermal properties of carbon canotube/Cu nanocomposites”, Spring Meeting of The Korean Powder Metallurgy Institute, April, 7-8, 2011, Ulsan, Korea.

2) K. T. Kim, J. Eckert and S. H. Hong, “Interfacial characteristics and properties of carbon nanotube reinforced metal matrix nanocomposites”, THERMEC 2011, International Conference on Processing & Manufacturing of Advanced Materials, August 1-5, 2011, Quebec, Canada.

3) S. H. Hong, B. K. Lim, D. H. Nam, Y. K. Kim, "Development and applications of carbon nanotube nanocomposites", The 18th International Conference on Composite Materials(ICCM 18), August 21-26, 2011, Jeju, Korea.

4) K. T. Kim, B. K. Lim, S. H. Hong, "Enhanced mechanical property of carbon nanotube/Ni nanocomposites fabricated by molecular-level mixing and direct reduction process", 8th Korea-Japan Joint Symposium on Composite Materials, Nov 17, 2011, Changwon, Korea.

5) K. T. Kim, J. Eckert, S. H. Hong, "Influence of carbon nanotubes on the thermal properties of Cu matrix nanocomposites", The 10th International Nanotech Symposium & Nano-Convergence Expo (NANO KOREA 2012), Aug 16-18, 2012, Seoul, Korea.

6) S. H. Hong, "Fabrication processes and structural applications of nanocomposites", The 9th International Conference on Fracture & Strength of Solids (FEOFS 2013), June 9-13, 2013, Jeju, Korea.

7) Dong H. Nam, Jae W. Kim, Hyun D. Park, Soon H. Hong, "Hardness and wear resistance of carbon nanotube reinforced aluminum matrix composites", The 11th international Nanotech Symposium & Nano-Convergence Expo (NANO KOREA 2013), July 10-12, 2013, Seoul, Korea.

8) S. H. Hong, "Fabrication and applications of multi-functional nanocomposites", THERMEC 2013, International Conference on Processing & Manufacturing of Advanced Materials, Dec. 2-6, 2013, Las Vegas, USA.

5-3. Manuscripts submitted but not yet published

1) Dong H. Nam, Jae W. Kim, Hyun D. Park, Soon H. Hong, "Hardness and wear resistance of carbon nanotube reinforced aluminium matrix composites", Journal of Nanoscience and Nanotechnology, Submitted, 2013.